Scientific Research

International Journal of Communications, Network and System Sciences

ISSN: 1913-3715
Volume 3, Number 6, June 2010

ISSN: 1913-3715

www.scirp.org/journal/ijcns/

JOURNAL EDITORIAL BOARD

ISSN 1913-3715 (Print) ISSN 1913-3723 (Online)
http://www.scirp.org/journal/ijcns/

Editors-in-Chief

Prof. Huaibei Zhou	Wuhan University, China
Prof. Tom Hou	Virginia Tech, USA

Editorial Board

Prof. Dharma P. Agrawal	University of Cincinnati, USA
Prof. Mohamed B. El_Mashade	Al_Azhar University, Egypt
Prof. Eduardo Alberto Castro	National University of La Plata, Argentina
Prof. Hengda Cheng	Utah State University, USA
Prof. Ko Chi Chung	National University of Singapore, Singapore
Dr. Franca Delmastro	Italian National Research Council, Italy
Dr. Klaus Doppler	Nokia Corporation, Finland
Dr. Li Huang	Stiching IMEC Nederland, Netherlands
Prof. Hiroaki Ishii	Kwansei Gakuin University, Japan
Prof. Chun Chi Lee	Shu-Te University, Taiwan (China)
Prof. Mengchi Liu	Carleton University, Canada
Prof. Jaime Lloret Mauri	Polytechnic University of Valencia, Spain
Dr. Lim Nguyen	University of Nebraska-Lincoln, USA
Prof. Yi Pan	Georgia State University, USA
Dr. Petar Popovski	Aalborg University, Denmark
Dr. Kosai Raoof	University of Joseph Fourier, France
Prof. Bimal Roy	Indian Statistical Institute, India
Prof. Heung-Gyoon Ryu	Chungbuk National University, Korea (South)
Prof. Shaharuddin Salleh	University Technology Malaysia, Malaysia
Prof. Rainer Schoenen	RWTH Aachen University, Germany
Dr. Lingyang Song	University Graduate Center, Norway
Prof. Boris S. Verkhovsky	New Jersey Institute of Technology, USA
Prof. Hassan Yaghoobi	Intel Corporation, USA
Prof. Shi Ying	Wuhan University, China

Editorial Assistant

Vivian QI	Scientific Research Publishing, USA. Email: ijcns@scirp.org

Int. J. Communications, Network and System Sciences, **2010, 3, 495-577**
Published Online June 2010 in SciRes (http://www.SciRP.org/journal/ijcns/)

TABLE OF CONTENTS

Volume 3 Number 6 June 2010

Performances of Chaos Coded Modulation Schemes Based on Mod-MAP Mapping and High Dimensional LDPC Based Mod-MAP Mapping with Belief Propagation Decoding

N. Khodor, J. P. Cances, V. Meghdadi, R. Quere.....495

Efficiency Improvement of Space Time Block Codes

Z. A. Baloch, M. U. Baloch, N. Hussain.....507

An Empirical Examination of Routing Protocols in Mobile Ad Hoc Networks

K. Sahadevaiah, O. B. V. Ramanaiah.....511

Nonlinear Blind Equalizers: NCMA and NMCMA

D. Wang, S. Chandana.....523

A Multi-Objective QoS Optimization with Fuzzy Based Parameter Setting for Real-Time Multicasting

S. C. Rai, B. B. Misra, A. K. Nayak, R. Mall, S. K. Pradhan.....530

Uplink Performance Evaluation of CDMA Communication System with RAKE Receiver and Multiple Access Interference Cancellation

A. J. Bamisaye, M. O. Kolawole.....540

Magnetization Performance of LDPC Reduced-Complexity Decoding Algorithms

M. Abdelhedi, O. Hamdi, A. Bouallegue.....548

Performance of Multirate Multicast in Distributed Network

S. Kanrar, M. Siraj.....554

Design and Simulation of Intelligent Optical WDM Switching Node Based on Erlang Traffic Model

M. K. Dutta, V. K. Chaubey.....563

Flocking Control of a Group of Agents Using a Fuzzy-Logic-Based Attractive/Repulsive Function

H. Yu, J. G. Jian, Y. J. Shen.....569

Copyright © 2010 SciRes.

International Journal of Communications, Network and System Sciences (IJCNS)

Journal Information

SUBSCRIPTIONS

The *International Journal of Communications, Network and System Sciences* **(**Online at Scientific Research Publishing, www.SciRP.org) is published monthly by Scientific Research Publishing, Inc., USA.

Subscription rates:

Print: $50 per issue.
To subscribe, please contact Journals Subscriptions Department, E-mail: sub@scirp.org

SERVICES

Advertisements
Advertisement Sales Department, E-mail: service@scirp.org

Reprints (minimum quantity 100 copies)
Reprints Co-ordinator, Scientific Research Publishing, Inc., USA.
E-mail: sub@scirp.org

COPYRIGHT

Copyright©2010 Scientific Research Publishing, Inc.

All Rights Reserved. No part of this publication may be reproduced, stored in a retrieval system, or transmitted, in any form or by any means, electronic, mechanical, photocopying, recording, scanning or otherwise, except as described below, without the permission in writing of the Publisher.

Copying of articles is not permitted except for personal and internal use, to the extent permitted by national copyright law, or under the terms of a license issued by the national Reproduction Rights Organization.

Requests for permission for other kinds of copying, such as copying for general distribution, for advertising or promotional purposes, for creating new collective works or for resale, and other enquiries should be addressed to the Publisher.

Statements and opinions expressed in the articles and communications are those of the individual contributors and not the statements and opinion of Scientific Research Publishing, Inc. We assumes no responsibility or liability for any damage or injury to persons or property arising out of the use of any materials, instructions, methods or ideas contained herein. We expressly disclaim any implied warranties of merchantability or fitness for a particular purpose. If expert assistance is required, the services of a competent professional person should be sought.

PRODUCTION INFORMATION

For manuscripts that have been accepted for publication, please contact:
E-mail: ijcns@scirp.org

Int. J. Communications, Network and System Sciences, **2010, 3, 495-506**
doi:10.4236/ijcns.2010.36067 Published Online June 2010 (http://www.SciRP.org/journal/ijcns/).

Scientific Research

Performances of Chaos Coded Modulation Schemes Based on Mod-MAP Mapping and High Dimensional LDPC Based Mod-MAP Mapping with Belief Propagation Decoding

Naim Khodor, Jean-Pierre Cances, Vahid Meghdadi, Raymond Quere
University of Limoges, *XLIM-Department*, *Limoges*, *France*
E-mail: {*naim.khodor*, *cances*, *frmeghdadi*, *raymond.quere*}*@ensil.unilim.fr*
Received February 5, 2010; *revised March* 11, 2010; *accepted April* 15, 2010

Abstract

In this paper, we propose to generalize the coding schemes first proposed by Kozic *et al*. to high spectral efficient modulation schemes. We study at first Chaos Coded Modulation based on the use of small dimensional modulo-MAP encoding process and we give a solution to study the distance spectrum of such coding schemes to accurately predict their performances. However, the obtained performances are quite poor. To improve them, we use then a high dimensional modulo-MAP mapping process similar to the low-density generator-matrix codes (LDGM) introduced by Kozic *et al*. The main difference with their work is that we use an encoding and decoding process on GF (2^m) which enables to obtain better performances while preserving a quite simple decoding algorithm when we use the Extended Min-Sum (EMS) algorithm of Declercq & Fossorier.

Keywords: Chaos Coded Modulation, Expectation Maximization, Gaussian or Rayleigh Mixtures, Low-Density Parity-Check (LDPC), Low-Density Generator-Matrix (LDGM), Factor Graph, Extended Min-Sum (EMS)

1. Introduction

Since the pioneering work of Frey in 1993 [1], chaotic communications has been an important topic in digital communications. Due to their extreme sensitivity to initial conditions which, for example, facilitates theoretically the separation of merging paths in a trellis based code, these systems have also been considered as good potential candidates for channel encoding [2-7]. This explains why chaotic modulations and channel encoders derived from chaotic systems have been extensively studied in the open literature. According to us, there are mainly two types of chaos based channel encoders depending on the size of the transmitted alphabet. The first kind of chaos based channel encoders includes non-linear generators which transmit binary messages and benefit from the correlation between successive transmitted bits to obtain some coding gain. Due to the poor spectral efficiency, it is rather easy to optimize this kind of codes to obtain a non-null free distance and to obtain reasonable good performances, *i.e.*, codes that outperform un-coded systems [8-12]. Some authors have even used these binary non-linear constituent encoders to build parallel concatenated schemes just like turbo-codes which perform quite closely to the theoretical bounds provided that the interleave size is big enough [13,14]. The second kind of chaos based channel encoders includes those which transmit a complex quasi-continuous alphabet, *i.e.*, those which are inherently chaotic in all their characteristics. These channel encoders exhibit a high spectral efficiency and can be compared to Trellis Coded Modulation (TCM) schemes. Many works deal with the optimization of such coders and, among them, perhaps the most famous ones were those named Chaos Coded Modulation (CCM) schemes. However, the weakness of such transceiver was their poor BER performance since they did not have even better performances than un-coded systems such as Binary Phase Shift Keying (BPSK) [15-17]. This was particularly the case for the systems which use CSK (Chaos Shift Keying) Modulation [18-20]. Nevertheless, some recent studies have stressed the fact that Chaos Coded Modulation (CCM) systems,

Copyright © 2010 SciRes.

working at a joint waveform and coding level, can be efficient in additive white Gaussian noise channels [21-23]. These promising works on the AWGN channel have been recently further extended by Escribano & al in the case of Rayleigh flat fading channels [24].

In this work, we use Chaos Coded Modulation designs of S. Kozic [25,26] and we optimize them using the distance spectrum. We find that the distance spectrum distribution can be good approximated by Rayleigh probability distribution function (pdf). Using this optimization step, we can optimize their structures. Furthermore we show that using a high dimensional modulo-MAP mapping process we are able to considerably improve the performances of this kind of schemes and to obtain performing codes. This principle is related to the former work of Kozic & Hasler in [27]. In their work, low-density generator-matrix (LDGM) codes are used as natural interleave in front of mappings to signal constellation. That is why this kind of code can be assumed as particular kind of BICM. However, the chaotic map is used as joint coding (interleaving) and modulation, and thus, the complete system is a single code. The framework of iterative decoding is based on factor graphs, which is a graphical representation of codes. LDPC and LDGM linear block codes have a very simple graphical representation called Tanner graph. However, for nonlinear codes, the graphical representation is not so simple, and this may be the reason why the large potential of nonlinear codes is not yet exploited. The main difference with their work is that we use an encoding and decoding process on GF (2^m) which enables to obtain better performances while preserving a relative simple decoding algorithm when we use the Extended Min-Sum (EMS) algorithm of Declercq & Fossorier [28]. The contributions of our paper are thus the following ones.

Detailed study of the distance spectra of the chaos based encoders and characterization of their distribution.

New encoding and decoding process based on the use of graph factorization and the use of Belief Propagation (BP) algorithm over high order Galois fields GF (2^m).

The rest of the paper is organized as follows. In Section 2, we give the basic principles for the chaos coded modulation schemes proposed by S. Kozic. We propose to approximate the distance distribution with some usual laws such as the Rayleigh one. In Section 3, we show the high dimensional coding process based on LDPC over GF(2^m); simulation results are provided which demonstrate the outstanding performances of these structures. Concluding remarks are eventually given in Section 4.

2. Chaos Coded Modulation Scheme, Distance Spectrum Study

2.1. Chaotic Coder Structure

We consider the Chaos-Coded modulation scheme of **Figure 1**. This scheme was originally given by S. Kozic in his PhD works [26]. The scheme of **Figure 1**. can be represented by means of a convolutional coder of rate $\eta = 1/(n.(Q+1))$, where at each time step k, one bit b_k enters the coder and a vector of $(Q+1)$ bits $\mathrm{v} = [\mathrm{v}_Q, \mathrm{v}_{Q-1}, \ldots, \mathrm{v}_0]^T$ is produced. The signal constellation is realized by a weighted sum of vectors 2^{-i}. $\boldsymbol{A}^{(Q-i+1)}$ *mod* (1) where $\boldsymbol{A}$ is some matrix which optimizes the distance spectrum of the code. This mapping, due to the modulus operation, is a highly non-linear operation and serves as a chaos generator. Henceforth, we have a system which combines a convolutional coder with a multi-dimensional mapping in the same way as Multi-level Trellis Coded Modulation (M-TCM). The corresponding convolutional coder is classically described by:

$$h_i(D) = \frac{\mathrm{v}_i(D)}{b(D)} = t_{i,Q} + t_{i,Q-1}.D + \ldots + t_{i,0}.D^Q \qquad (1)$$

S. Kozic defines several possible matrices $\boldsymbol{T} = \{t_{i,j}\}$ in his work which give good performances:

$$\boldsymbol{T}_{shift} = \begin{bmatrix} 1 & 0 & 0 \\ 0 & 1 & 0 \\ 0 & 0 & \end{bmatrix} \quad \boldsymbol{T}_{e-shift} = \begin{bmatrix} 1 & 0 & 1 \\ 0 & 1 & 0 \\ 0 & 0 & \end{bmatrix}$$

$$\boldsymbol{T}_{tent} = \begin{bmatrix} 1 & 0 & 0 \\ 1 & 1 & 0 \\ 1 & 1 & \end{bmatrix}$$

Concerning, the choice of the matrix $\boldsymbol{A}$, we can write the transmitted vector at the output of the modulator:

$$x_k = \sum_{i=0}^{Q_a} 2^{-(i+1)} A^{Q_a - i} v_i(D) + \sum_{i=Q_a+1}^{Q} 2^{-(i+1)} v_i(D) \bmod (1) \quad (2)$$

Before transmitting $\boldsymbol{x}_k$ on the channel propagation medium, we modulate each of its components in NRZ-BPSK, *i.e.*, : $\boldsymbol{x}_k \rightarrow 2\,\boldsymbol{x}_k$ -1.

Rather than a global optimization algorithm which should look for the convolutional coder together with the mapping process, we choose to fix a convolutional coder structure and then we work on the mapping process by using a particular form of matrix $\boldsymbol{A}$. We found that the choice $\boldsymbol{T}_{i,j} = \boldsymbol{T}_{shift}$ for $i = j$ and $\boldsymbol{T}_{i,j} = \boldsymbol{T}_{tent}$ for $i \neq j$ enables to obtain a large set of performing non-linear mapping with $\boldsymbol{A}$. For example, in the case $n = 2$, using this choice for matrices $\boldsymbol{T}$, we are looking for matrices $\boldsymbol{A}$ with the following structure:

$$\boldsymbol{A} = \begin{pmatrix} 1 & -1 \\ a_{21} & 1 \end{pmatrix}.$$

and we optimize the choice of a_{21} using the distance spectrum. In the case, $n = 3$, we use matrix form:

$$\boldsymbol{A} = \begin{pmatrix} 1 & 1 & 1 \\ a_{21} & 1 & 1 \\ a_{31} & a_{32} & 1 \end{pmatrix}.$$

Copyright © 2010 SciRes.

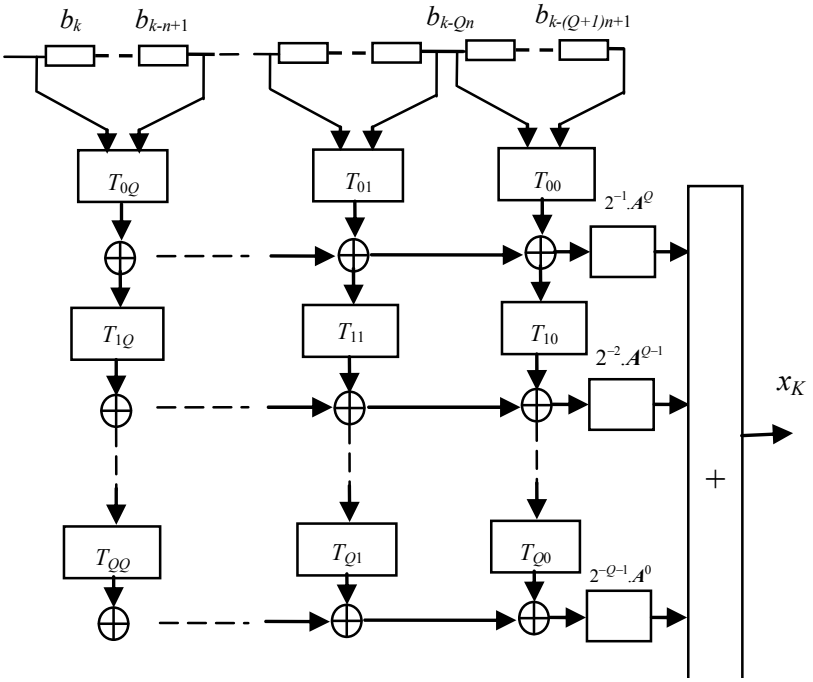

Figure 1. Trellis chaos-coded modulation encoder.

The choice of the remaining parameters $a_{i,j}$ is done using the distance spectrum of the code. The state of the coder is defined by vector $\boldsymbol{S}_k$:

$$\boldsymbol{S}_k = [b_k,\ldots,b_{k-n},\ldots b_{k-Qn},\ldots,b_{k-(Q+1).n+1}]^T \qquad (3)$$

Concerning the choice of Q, it's clear that the Viterbi decoding algorithm is rapidly limited by the complexity in the number of states which is equal to $2^{n.(Q+1)}$. Practically, the number $n(Q + 1)$ should not exceed 12 which correspond to 4096 states. For $n = 2$, this gives a maximum value of Q equal to 5, and for $n = 3$, this gives a maximum value of Q equal to 3. The choice of Q_a, is more complicated and is related to the chaotic behaviour of the coder.

2.2. Spectrum Distance Analysis

In order to optimize the coders, we study their distance spectrum. To do this, we have to determine the trajectories in the trellis which start with a common state $\boldsymbol{S}_i = \boldsymbol{S}_i^*$ and evolve in disjoint paths for (L-1) time steps and then merge again into the same state $\boldsymbol{S}_k = \boldsymbol{S}_k^*$ not necessarily equal to $\boldsymbol{S}_i$. This kind of trajectory in the trellis defines a loop and the loop is characterized by its initial state $\boldsymbol{S}_i$, its final state $\boldsymbol{S}_k$ and its length L. The distance of corresponding codewords belonging to the two competing paths in the loop is:

$$d^2_{L,S_i,S_k} = \sum_{m=1}^{L-1} \left\| \boldsymbol{x}_m - \boldsymbol{x}_m^* \right\|^2 \qquad (4)$$

The problem of the computation of (4) is that, unlike linear codes when we can choose a reference path equal to a all zero sequence, due to the non-linear mapping, we have to test all the possible transmitted sequence for a given loop length together with all the possible starting states. Hence, the distance spectrum computation problem is of non polynomial complexity and in straightforward manner requires the inspection of all possible initial conditions and all possible controlled trajectories. For example, there are $2^{n.(Q+1)}.2^{nL}$ different controlled trajectories of length L. In order to compute the distance spectrum with a reasonable complexity while keeping a sufficient accuracy, we form all the possible pair of sequences starting from a given state and both converging towards an other state after L steps with L belonging to the interval $[Qn + 1, n.(Q + m)]$, *i.e.* the length of the loop varies from Qn+1 (the constraint length of the code plus one) to to $n.(Q + m)$ (we limit practically the search to $m = 2$ or 3 in our case due to the computation burden). We have partitioned the distance spectrum into subsets by distinguishing error events which entail one error bit, error events which entail two error bits, error events which entail three error bits and so on. In practice, we limit our search to error events which entail five maximum error bits since simulation results evidenced that it was sufficient to obtain accurate upper bounds for the BER.

We obtain for example with matrices: $\boldsymbol{T}_{i,j} = \boldsymbol{T}_{shift}$ for $i = j$ and $\boldsymbol{T}_{i,j} = \boldsymbol{T}_{tent}$ (*i.e.* $n = 2$) for $i \neq j$ and $a_{21} = 8$, $Q = Q_a = 3$, the distance spectrum illustrated on **Figure 2**.

In fact, we found that, in a majority of cases, the shape of the distance spectrum is close to a Rayleigh distribu-

Copyright © 2010 SciRes.

tion with the following probability density function:

$$f_C(x) = \frac{(x-\mu_j)}{\sigma_j^2}.e^{-(x-\mu_j)^2/2.\sigma_j^2} \quad x \geq \mu_j$$
$$x < \mu_j \qquad (5)$$
$$f_C(x) = 0$$

For example, with the distance spectrum plotted on **Figure 2**, we calculate parameters μ_j and σ_j^2 to obtain the best fitting between the pdf of the distance spectrum and $f_c(x,m_j,\sigma_j^2)$ we obtain with classical MMSE technique: $\mu_j \cong \sigma_j^2 \cong 6.7$. This corresponds to a minimum free distance of the coder equal to $d_{free} \cong 6.7$. We have developed an original EM (Expectation-Maximization) algorithm to obtain the approximated Rayleigh distribution of the distance spectrum as a mixture of Rayleigh laws. The mixture of Rayleigh laws can be written as:

$$f_C(x) = \sum_{n=1}^{J} \pi_n . \frac{(x-\mu_n)}{\sigma_n^2}.e^{-(x-\mu_n)^2/2.\sigma_n^2}$$
$$= \sum_{n=1}^{J} \pi_n . \mathcal{R}(\mu_n, \sigma_n^2) \qquad (6)$$

where $\mathcal{R}(\mu_n,\sigma_n^2)$ represents a Rayleigh law of parameters: μ_n and σ_n^2. The Maximum Likelihood (ML) research algorithm to find: π_n, μ_n, σ_n^2 can be summarized as:

$$\hat{\boldsymbol{\theta}} = \arg \max_{\boldsymbol{\theta}: \sum_{j=1}^{J} \pi_j = 1} \log p_{\boldsymbol{\theta}}(\Xi)$$
$$= \arg \max_{\boldsymbol{\theta}: \sum_{j=1}^{J} \pi_j = 1} \sum_{i=1}^{n} \log \sum_{j=1}^{J} \pi_j . \psi(\xi_i; \mu_j, \sigma_j^2) \qquad (7)$$

where $\psi(x,\mu,\sigma^2)$ denotes the value of a Rayleigh law of parameters μ,σ^2 at x. For a fixed number of mixtures J, based on the observations: $\Xi \equiv \{\xi, i = 1,\ldots,n\}$, the parameters $\boldsymbol{\theta} \equiv \{\pi_j, m_j, \sigma_j, j=1,\ldots,J\}$ can be estimated using the EM (Expectation Maximization) algorithm. The algorithm proceeds in two steps:

E-step: Compute

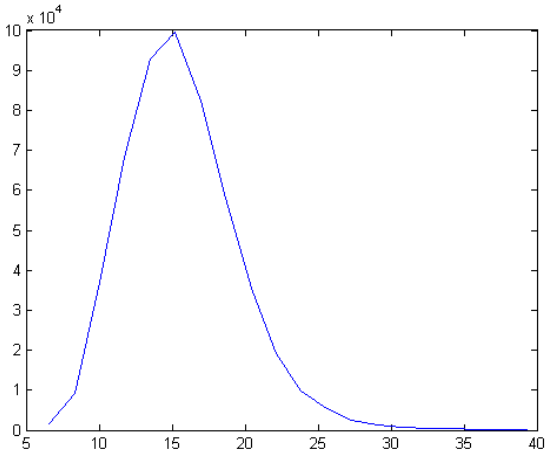

Figure 2. Distance spectrum of the chaos coded modulation.

$$Q(\boldsymbol{\theta} \mid \boldsymbol{\theta}^{(i)}) = E_{\boldsymbol{\theta}^{(i)}} \{\log p_{\boldsymbol{\theta}}(\boldsymbol{X}) \mid \Xi\} \qquad (8)$$

M-step: solve

$$\boldsymbol{\theta}^{(i+1)} = \arg\max_{\boldsymbol{\theta}} Q(\boldsymbol{\theta} \mid \boldsymbol{\theta}^{(i)}) \qquad (9)$$

Define the following hidden data $\boldsymbol{Z} = \{z_i, i = 1,\ldots, n\}$ where z_i is a J-dimensional indicator vectoring such that:

$$z_{i,j} = \begin{cases} 1, \textit{ if } \xi_i \cong R(m_j, \sigma_j^2) \\ 0, \textit{ otherwise} \end{cases} \qquad (10)$$

The complete data is then $\boldsymbol{X} \cong (\Xi,\boldsymbol{Z})$, we have :

$$p_{\boldsymbol{\theta}}(\Xi, \boldsymbol{Z}) = \prod_{i=1}^{n} \prod_{j=1}^{J} \left[\pi_j . R(\xi_i; m_j, \sigma_j^2)\right]^{z_{i,j}} \qquad (11)$$

The log-likelihood function of the complete data is then given by:

$$\log p_{\theta}(\Xi, Z) = \sum_{i=1}^{n} \sum_{j=1}^{J} z_{i,j} . \log \pi_j +$$
$$\sum_{i=1}^{n} \sum_{j=1}^{J} z_{i,j} . \left[\log(\xi_i - \mu_j) - \log(\sigma_j^2) - \frac{(\xi_i - \mu_j)^2}{2\sigma_j^2}\right] + C \qquad (12)$$

where C is a constant. The E-step can then be calculated as follows:

$$Q(\boldsymbol{\theta} \mid \boldsymbol{\theta}') = E_{\boldsymbol{\theta}}' \{\log p_{\boldsymbol{\theta}}(\Xi, \boldsymbol{Z}) \mid \Xi\}$$
$$Q(\boldsymbol{\theta} \mid \boldsymbol{\theta}') =$$
$$\sum_{i=1}^{n} \sum_{j=1}^{J} \hat{z}_{i,j} . \left[\log \pi_j + \log(\xi_i - \mu_j) - 2\log(\sigma_j) - \frac{(\xi_i - \mu_j)^2}{2\sigma_j^2}\right] + C$$

We have:

$$\hat{z}_{i,j} = E_{\boldsymbol{\theta}}' \{z_{i,j} \mid \Xi, \boldsymbol{\theta}'\} = P_{\boldsymbol{\theta}}' \{z_{i,j} = 1 \mid \xi_i\}$$
$$= \frac{\psi(\xi_i; m_j', \sigma_j'^2).\pi_j'}{\sum_{l=1}^{J} \psi(\xi_i; m_l', \sigma_l'^2).\pi_l'} \qquad (13)$$

The M-step is calculated as follows. To obtain $\{\pi_j\}$, we have:

$$\frac{\partial Q(\boldsymbol{\theta}, \boldsymbol{\theta}')}{\partial \pi_j} = 0 \Rightarrow \pi_j = \frac{1}{n} . \sum_{i=1}^{n} \hat{z}_{i,j}, \quad j = 1,\ldots,J \qquad (14)$$

To obtain $\{\mu_j\}$, we have:

$$\frac{\partial Q(\boldsymbol{\theta}, \boldsymbol{\theta}')}{\partial m_j} = 0 \Rightarrow$$
$$\sum_{i=1}^{n} \hat{z}_{i,j} . \left[-\frac{1}{\xi_i - m_j} + \frac{(\xi_i - m_j)}{\sigma_j^2}\right] = 0, \quad j = 1,\ldots,J$$
$$\sum_{i=1}^{n} \hat{z}_{i,j} . \left[\frac{-\sigma_j^2 + (\xi_i - m_j)^2}{\sigma_j^2 . (\xi_i - m_j)^2}\right] = 0, \quad j = 1,\ldots,J$$

Copyright © 2010 SciRes.

$$\sum_{i=1}^{n}\hat{z}_{i,j}.\sigma_j^2=\sum_{i=1}^{n}\hat{z}_{i,j}.(\xi_i^2-2.m_j.\xi_i+m_j^2),\quad j=1,...,J$$

$$\sum_{i=1}^{n}\hat{z}_{i,j}.\xi_i^2-2.m_j.\sum_{i=1}^{n}\hat{z}_{i,j}.\xi_i+ \tag{15}$$

$$m_j^2.\sum_{i=1}^{n}\hat{z}_{i,j}=\sum_{i=1}^{n}\hat{z}_{i,j}.\sigma_j^2,\quad j=1,...,J$$

To obtain $\{\sigma_j\}$ we have the set of equations:

$$\frac{\partial Q(\boldsymbol{\theta},\boldsymbol{\theta}')}{\partial \sigma_j}=0$$

$$\sum_{i=1}^{n}\hat{z}_{i,j}.[-\frac{2}{\sigma_j}+\frac{(\xi_i-m_j)^2}{\sigma_j^3}]=0,\quad j=1,...,J$$

$$\Rightarrow 2.\sigma_j^2.\sum_{i=1}^{n}\hat{z}_{i,j}=\sum_{i=1}^{n}\hat{z}_{i,j}.(\xi_i-m_j)^2,\quad j=1,...,J \tag{16}$$

$$\sigma_j^2=\frac{\sum_{i=1}^{n}\hat{z}_{i,j}.(\xi_i-m_j)^2}{2.\sum_{i=1}^{n}\hat{z}_{i,j}},\quad j=1,...,J \tag{17}$$

The set of Equations (16) and (17) is a set of coupled non-linear equations and we use the optimization toolbox with the function *fsolve* to solve (16-17) at each maximization step.

2.3. Performances over AWGN Channels

To end this part, we give some BER results on AWGN channels, using the optimization obtained by the distance spectrum computation to find good modulation parameters. Due to a lack of place we only give simulation results. For $n = 2$, we obtain the following result on **Figure 3**.

The chaotic coder outperforms un-coded BPSK at high SNR's due to good asymptotic properties with a moderate high free distance. The weakness of this kind of code is their poor coding rate. There are several solutions to improve this. The first is to make input bits enter the coder by groups of k bits. In this case, the coding rate becomes equal to: $k/n.(Q+1)$.

However, this considerably reduces the correlation degree between consecutive states and renders the trellis non-binary. We found that the penalty encountered by this method too much important (using $k = 2$ results in 4 dB losses compared to $k = 1$) so we prefer using puncturing to increase the coding rate of our proposed coders. We added the case of punctured codes on **Figure 4** with the best puncturing patterns we found for rate 8/7 and 4/3.

The conclusions are nearly the same, considering the case $n = 3$ as it is illustrated on **Figure 4**.

With a free distance equal to 13 for the optimized code

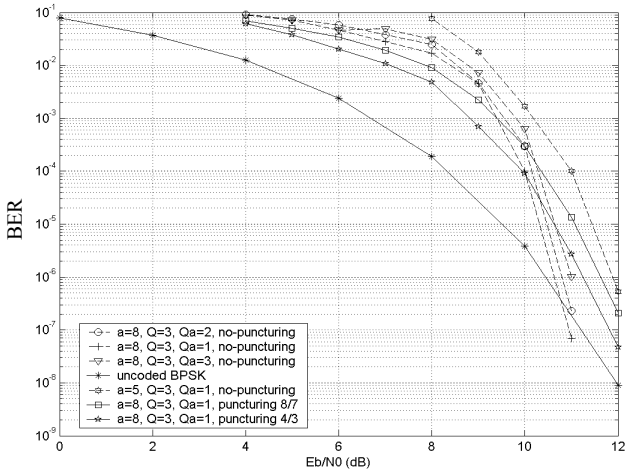

Figure 3. Performances of Trellis Chaos-Coded Modulation over AWGN channels for $n = 2$, $Q = 3$.

with rate 1/9, the punctured codes (9/7) are able to out perform un-coded BPSK at high SNR's. To complete this overview of BER performances over AWGN channels, it is important to say that using the approximate pdf's of the distance spectrum, we are able to accurately predict the BER at high's SNR's. To complete the results, we give on **Figure 12** the best performances we found with $n = 3$, $Q = 3$ (*i.e.* the number of states is 4096).

In fact, as it is expected, increasing the quantization level for a given dimensionality n, entails some losses. Compared to **Figure 4**, the loss in terms of SNR for a BER of 10^{-4}, 10^{-5} is approximately 1 dB on **Figure 5** and punctured codes are unable to outperform un-coded BPSK.

It is clear that the obtained performances remain poor.

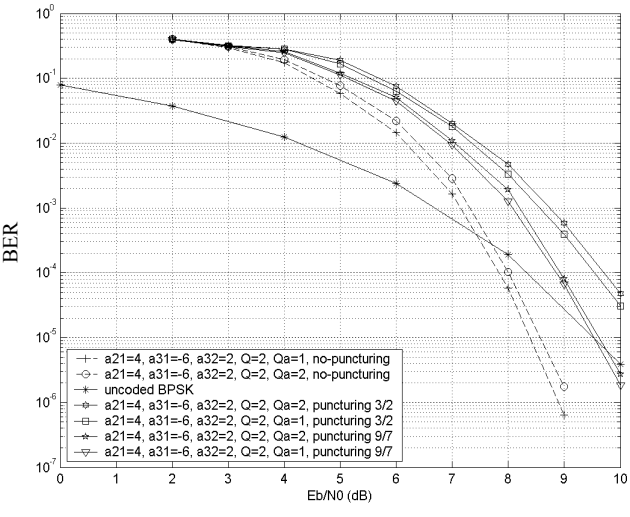

Figure 4. Performances of Trellis Chaos-Coded Modulation over AWGN channels for $n = 3$, $Q = 2$.

Copyright © 2010 SciRes.

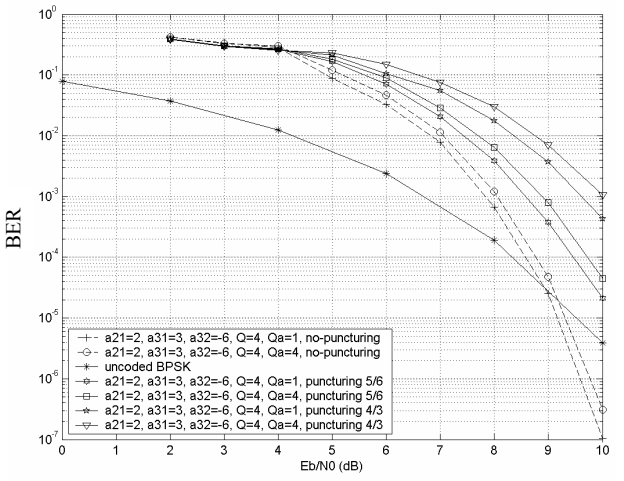

Figure 5. Performances of optimized Trellis Chaos-Coded Modulation over AWGN channels for n = 3, Q = 3 (4096 states).

To increase them, we propose to generalize the non-linear output mapping to matrices $\boldsymbol{A}$ of high-dimension.

3. High Dimensional LDPC Based Mod-MAP Mapping with B.P Decoding

3.1. The Encoding Process

The generalized mod-MAP function is written as:

$$\boldsymbol{x}_{k+1} = 2.\boldsymbol{A}.\boldsymbol{x}_k \bmod q \tag{18}$$

where $\boldsymbol{x}_k$ is the input vector of size n and $\boldsymbol{A}$ is a $n \times n$ matrix with elements belonging to alphabet: A = (0, 1,…, q-1) with $q = 2^m$ since we take here: $q = 2^m$ for the considered Galois-field $GF(q)$. The encoding scheme is drawn on **Figure 6**. The binary streams $\boldsymbol{b} = (\boldsymbol{b}_1, \boldsymbol{b}_2,\ldots, \boldsymbol{b}_k,\ldots)$ are grouped into vector vector $\boldsymbol{b}_{k+i-Q}$ of size: $n_{.m} = n.m$ with m denoting the spectral efficiency we want to use in the encoding-decoding process. Hence, we can write: $\boldsymbol{b}_{k+i-Q} = (\boldsymbol{b}_{k+i-Q}^{(1)}, \boldsymbol{b}_{k+i-Q}^{(2)},\ldots, \boldsymbol{b}_{k+i-Q}^{(nm-1)}, \boldsymbol{b}_{k+i-Q}^{(nm)})^T$. A binary/$q$-ary converter is then used to obtain vectors $\boldsymbol{d}_{k+i-Q} = (\boldsymbol{d}_{k+i-Q}^{(1)}, \boldsymbol{d}_{k+i-Q}^{(2)},\ldots, \boldsymbol{d}_{k+i-Q}^{(n-1)}, \boldsymbol{d}_{k+i-Q}^{(n)})^T$ of q-ary symbols: $\boldsymbol{d}_i^{(p)}$, p = 1,2,…,n belonging to the alphabet: A = (0,1,…,q-1). Each obtained vector $\boldsymbol{d}_{k+i-Q}$ is then multiplied by a sparse low-density based matrix $\boldsymbol{A}^{Q-I}$ and weighted by a factor $2^{-(i+1)}$ then, the new resulting encoding vectors are added to obtain the vector:

$$\boldsymbol{z}_k = \sum_{i=0}^{Q} 2^{-(i+1)}.\boldsymbol{A}^{Q-i}.\boldsymbol{d}_{k+i-Q} \bmod(q).$$

Finally, to obtain a chaotic trajectory we add the vector: $\mathbf{2}^{-(\boldsymbol{Q}+1)}.(\boldsymbol{A}-\boldsymbol{I}).\boldsymbol{e}$ with: $\boldsymbol{e}$ **[1, 1,…, 1]**^{T}. This yields to the following equation:

$$\boldsymbol{x}_k = \sum_{i=0}^{Q} 2^{-(i+1)}.\boldsymbol{A}^{Q-i}.\boldsymbol{d}_{k+i-Q} + \frac{2^{-Q}}{2}.\boldsymbol{p} \bmod q \tag{19}$$

With: $\boldsymbol{p}=\mathbf{2}^{-\boldsymbol{Q}}.(\boldsymbol{A}-\boldsymbol{I}).\boldsymbol{e}=\boldsymbol{K}.(\boldsymbol{A}-\boldsymbol{I}).\boldsymbol{e}$.

The coding sequence at the output of the modulator is then equal to: $\boldsymbol{x}$ = ($\boldsymbol{x}_1$, $\boldsymbol{x}_2$,…, $\boldsymbol{x}_k$,…).The relation (19) is called the high-dimensional expansion associated with the chaotic system (18). Another way to represent the encoding rule is to use the following equation:

$$\boldsymbol{x}_{k+1} = 2.\boldsymbol{A}.\boldsymbol{x}_k \bmod q + 2^{-Q}.(\boldsymbol{d}_{k+1} - 1/2.\boldsymbol{e}) \bmod q \tag{20}$$

The relation (20) is simpler than (19) to better understand the encoding algorithm; however Equation (19) is more suitable for the factorization of the factor graph. The rule (20) represents a dynamical system controlled with stochastic perturbations of small amplitudes $2^{-\boldsymbol{Q}}$ which constitute the input signal. It is obvious that as: $Q \rightarrow +\infty$, the small amplitudes vanish and the output signal vector becomes the chaotic state.

It is important to note that the decoding of a LDPC over $GF(q)$ implies that we use a systematic form for the encoding process. It's the case here since $\boldsymbol{b}$ = ($\boldsymbol{b}_1$, $\boldsymbol{b}_2$,…, $\boldsymbol{b}_k$,…) is the systematic part and $\boldsymbol{x}$ = ($\boldsymbol{x}_1$, $\boldsymbol{x}_2$,…, $\boldsymbol{x}_k$,…) is the redundancy check part. We have of course a overall coding rate of 0.5 because the systematic part and the redundancy check part have the same dimension.

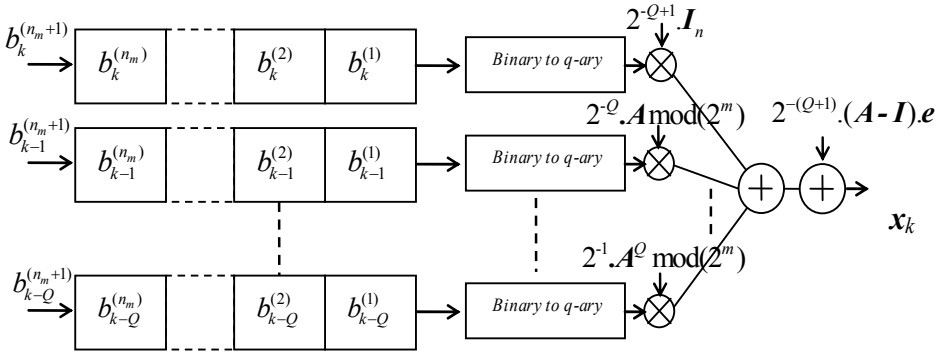

Figure 6. Coding Scheme with high dimensional LDPC based Mod-MAP mapping.

Copyright © 2010 SciRes.

3.2. Factor Graphs

To explain how the factorization can be efficiently implemented it is convenient to represent a function with a factor graph. Once a factor graph has been found it is straightforward to use the BP (Belief Propagation) algorithm to determine the marginal of a multivariate function. For linear block codes the factor graph of the code becomes a Tanner graph. Of course, in our case due to the use of a non-linear encoding process, finding this graph is a much more complicated task. In fact as Kozic demonstrated in [27], there are mainly two possible solutions to obtain it here. The first one consists in using the party-check equation given by Equation (20). The second one is the consequence of the high-dimensional expansion associated with Equation (19). The first solution is not appropriate since it would imply to obtain information about $\boldsymbol{b}_k$ from the soft information about the states $\boldsymbol{x}_k$ which constitute the graph of variable and check nodes and $\boldsymbol{d}_k$ is multiplied by a small value: 2^{-Q}. Hence the reliability about information concerning $\boldsymbol{b}_k$ would be small in this case. Hence, the second solution is the only tractable one. However, it is important to avoid the use of successive power of $\boldsymbol{A}$ in the graph factorization. This is due to the fact that short cycles of length four appear when we use for example $\boldsymbol{A}^2$ in a factor graph even if $\boldsymbol{A}$ does not exhibit short length cycles.

The graph factorization may be expressed in the following way: it comprises mainly three steps. The first one is related directly to the scheme of **Figure 6** and concerns the computation of $\boldsymbol{x}_k$ given $\boldsymbol{d}_{k+i-Q}$ it will be named high-order expansion graph. The second one concerns the LDPC code contained in each matrix $\boldsymbol{A}$, it will be named $GF(q)$ LDPC graph and finally the third one concerns the way the input bits slide to constitute a new vector to be encoded. This mechanism is related to the convolutional encoder behaviour and will be named convolutional graph.

The high-order expansion graph constitutes the main original part and it can be obtained as follows. We consider at first an indicator function of high dimensional q-ary expansion:

$$g(\boldsymbol{x}_k,\boldsymbol{d}_k,...,\boldsymbol{d}_{k-Q}) = \begin{cases} 1, \text{ if } \boldsymbol{x}_k = \sum_{i=0}^{Q} 2^{-(i+1)}.\boldsymbol{A}^{Q-i}.\boldsymbol{d}_{k+i-Q} + \frac{q}{2}.\boldsymbol{p} \bmod q \\ 0, \text{ otherwise} \end{cases} \quad (21)$$

We can use then additional variables $\boldsymbol{\mu}_{i,j}$ defined as:

$$\boldsymbol{x}_k = \sum_{i=0}^{Q} \boldsymbol{\mu}_{i,Q-i} + 2^{-(Q+1)}.\boldsymbol{p} \bmod q$$

Of course, we have the relationship: $\boldsymbol{\mu}_{i,j+1} = \boldsymbol{A}.\boldsymbol{\mu}_{i,j} \bmod q$ with: $\boldsymbol{\mu}_{i,0} = 2^{-(i+1)}\boldsymbol{d}_{k+i-Q}$. With these variables, function g becomes a function only of variables: $\boldsymbol{\mu}_{i,j}$. To keep on factorizing g we introduce functions $\boldsymbol{g}_{i,j+1}$ defined as :

$$g_{i,j+1}(\boldsymbol{\mu}_{i,j+1},\boldsymbol{\mu}_{i,j}) = \begin{cases} 1, \text{ if } \boldsymbol{\mu}_{i,j+1} = \boldsymbol{A}.\boldsymbol{\mu}_{i,j} \bmod q \\ 0, \text{ otherwise} \end{cases} \quad (22)$$

and g_0 :

$$g_0(\boldsymbol{x}_k,\boldsymbol{\mu}_{0,Q},\boldsymbol{\mu}_{1,Q-1},...) = \begin{cases} 1, \text{ if } \boldsymbol{x}_k = \sum_{i=0}^{Q} \boldsymbol{\mu}_{i,Q-i} + 2^{-(Q+1)}.\boldsymbol{p} \bmod q \\ 0, \text{ otherwise} \end{cases}$$

The corresponding factorization of g is given by:

$$g(.) = g_0.\prod_{i=0}^{Q}\prod_{j=0}^{Q-i} g_{ij}(.) \quad (23)$$

The factorization is drawn below on **Figure 7**.

It is possible to further factorize the class of functions: $g_{i,j+1}$. The variables at the left side of Equation (22) will be named the checks and the variables on the right side will be considered as the noisy symbols. We define similarly as in the case of LDPC codes: $\mathcal{N}(l) = \{m:a_{lm} \neq 0\}$ the set of noisy symbols that participate in the check l. In the same way, we define: $\mathcal{M}(m) = \{l:a_{lm} \neq 0\}$ the set of checks that depend on the noisy symbol m. In this case (22) can be written as:

$$\boldsymbol{\mu}_{i,j+1}^{(l)} = \sum_{m\in\mathcal{N}(l)} a_{lm}.\boldsymbol{\mu}_{i,j}^{(m)} \bmod q \quad m,l \in [1,n]\times[1,n] \quad (24)$$

Let:

$$g_{i,j+1}^{(l)} = \begin{cases} 1, \text{ if } \boldsymbol{\mu}_{i,j+1}^{(l)} = \sum_{m\in\mathcal{N}(l)} a_{lm}.\boldsymbol{\mu}_{i,j}^{(m)} \bmod q \\ 0, \text{ otherwise} \end{cases} \quad (25)$$

The symbols on **Figure 7** correspond either to variable nodes (circle on the figure) or check nodes (square on the figure). The symbolise decoding of the complete chaotic trajectory is given by:

$$\begin{aligned} &\arg_{d_{k+i-Q}^{(.)}\in\{0,1\}} \max \sum_{\approx d_{k+i-Q}^{(.)}} p(\boldsymbol{x}_0)\prod_{j=1}^{M+Q} p\left(\boldsymbol{y}_j \middle| \boldsymbol{x}_j\right) \\ &\times g\left(\boldsymbol{x}_j,\boldsymbol{d}_j,...,\boldsymbol{d}_{j-Q}\right) \\ &\times p\left(\boldsymbol{d}_j,...,\boldsymbol{d}_{j-Q}\right)\times p\left(\boldsymbol{x}_{j+1}\middle|\boldsymbol{x}_j,\boldsymbol{d}_{j+1}\right). \end{aligned} \quad (26)$$

The quantity $\approx \boldsymbol{d}_{k+1-Q}$ means summation over all components except: $\boldsymbol{d}_{k+1-Q}$. Furthermore, the graph of matrix $\boldsymbol{A}$ is classically those of a LDPC code over $GF(q)$ and is drawn on **Figure 8**.

The shift register and the binary q-ary conversion set operation, which represent transition state from time j to time $j+1$ can be given by the indicator function: $g_c = p(\boldsymbol{x}_{j+1}|\boldsymbol{x}_j,\boldsymbol{d}_{j+1})$. The state at time $j+1$ depends on the symbol sequence: $\boldsymbol{d}_{j+1},\ldots,\boldsymbol{d}_{j+1-Q}$, and it can be computed using likelihoods of symbols $\boldsymbol{d}_j,\ldots,\boldsymbol{d}_{j+1-Q}$ and additional likely-

Copyright © 2010 SciRes.

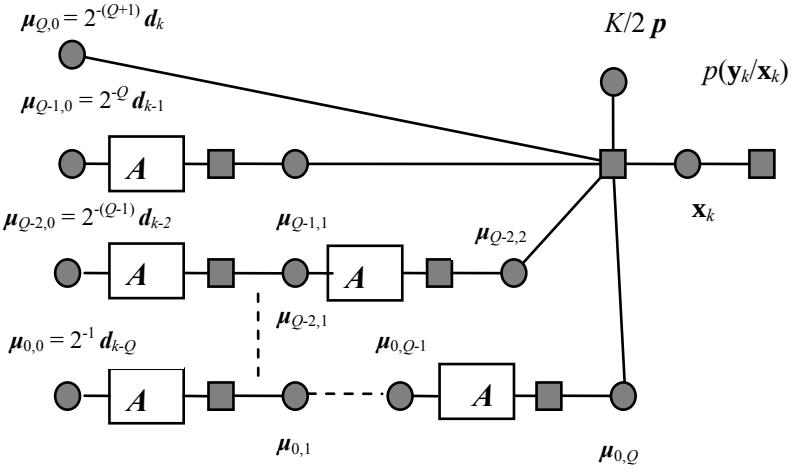

Figure 7. high-order expansion factor graph.

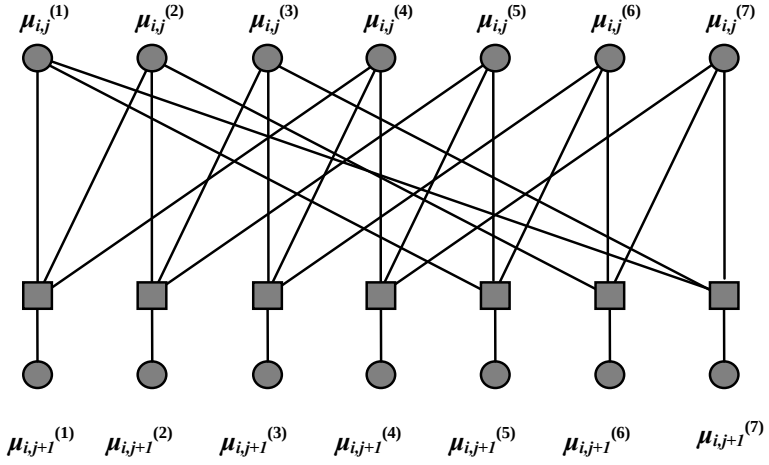

Figure 8. Factor graph for matrix *A*.

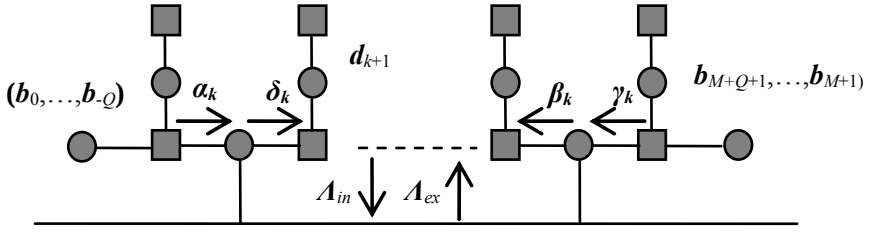

Figure 9. Factor graph of the complete chaotic code.

about symbol: $\boldsymbol{d}_{j+1}$. Using together factorization g_c and factorization of the high-order expansion of **Figure 7**, the decoding problem of (26) can be presented with the factor graph of **Figure 9**. This graph takes into account the shift register process which includes new incoming bits into the encoding process and consists of two recursions: forward and backward recursions as in the well known BCJR algorithm.

The parameters α_k, β_k, γ_k and δ_k are defined in the same way as in [27] except that we work at symbol level for the computation of α_k, β_k, γ_k and δ_k.

Note that since the main difference with the scheme proposed by Kozic, *et al*. in [27] consists in the use of a non-binary encoding scheme, we have to transform a priori probabilities on bits to a priori probabilities in symbols. This is done using the formula:

$$P[\boldsymbol{d}_{k+i-Q} = (b_{k+i-Q}^{(1)}, b_{k+i-Q}^{(2)}, ..., b_{k+i-Q}^{m})^T] = \prod_{j=1}^{m} \frac{e^{b_{k+i-Q}^{(j)} \cdot \tilde{\Lambda}_e(b_{k+i-Q}^{(j)})}}{1 + e^{b_{k+i-Q}^{(j)} \cdot \tilde{\Lambda}_e(b_{k+i-Q}^{(j)})}} \quad (27)$$

Copyright © 2010 SciRes.

where $\tilde{\Lambda}_e(b_{k+i-Q}^{(j)})$ designs the log-likelihood ratio corresponding to bit: $b_{k+i-Q}^{(j)}$. For the complementary problem, *i.e.* when we have to express the log-likelihood ratio of bit $b_{k+i-Q}^{(j)}$ from the log-likelihood ratios of corresponding symbols, we have:

$$\Lambda_e(b_{k+i-Q}^{(j-1).m+k}) = \log \frac{\sum_{d_{k+i-Q}^{(j)}:b_{k+i-Q}^{(j-1).m+k}=1} e^{\Lambda_e(d_{k+i-Q}^{(j)})}}{\sum_{d_{k+i-Q}^{(j)}:b_{k+i-Q}^{(j-1).m+k}=0} e^{\Lambda_e(d_{k+i-Q}^{(j)})}} \quad (28)$$

where, obviously, $\Lambda_e(d_{k+i-Q}^{(j)})$ corresponds to the log-likelihood ratio of symbol:

$$d_{k+i-Q}^{(j)} = [b_{k+i-Q}^{(j-1).m+1}, b_{k+i-Q}^{(j-1).m+2}, ..., b_{k+i-Q}^{(j-1).m+m}] .$$

3.3. Iterative Decoding

The main steps of the iterative decoding are the same as those of [27] except for the use of a non-binary generator matrix ***A***. The decoding of LDPC codes over $GF(q)$ has been an extensive research topic recently. Among all the decoding algorithms, we choose the Extended Min-Sum (EMS) Algorithm in the log-domain proposed by Declercq and Fossorier [28] since it exhibits a good trade-off between performance and complexity. To explain the main principles we use the following notations. A parity node in a LDPC code over $GF(q)$ with $q = 2^m$ represents the following parity equation:

$$\sum_{k=1}^{d_c} h_k(x).i_k(x) = 0 \mod m(x) \quad (29)$$

where $m(x)$ in the modulo operator is a degree m -1 primitive polynomial of $GF(q)$. Equation (29) expresses that the variable nodes needed to perform the BP algorithm on a parity node are the codeword symbols multiplied by non-zeros values of the parity matrix ***H***. The corresponding transformation of the graph is performed by adding variable nodes corresponding to the multiplication of the codeword symbols $i_k(x)$ by their associated nonzero ***H*** values and is illustrated on **Figure 10**.

The function node that connects the two variable nodes $i_k(x)$ and $h_k(x)$. $i_k(x)$ performs a permutation of the message values. The permutation that is used to update the message corresponds to the multiplication of the tensor indices by $h_k(x)$.from node $i_k(x)$ to node $h_k(x)$. $i_k(x)$ and to the division of the indices by $h_k(x)$ the other way. With this transformation of the factor graph, the parity node update is indeed a convolution of all incoming messages as in the binary case.

To express the EMS algorithm, we use the following notations for the messages in the graph. Let $\{V_{pv}\}$ v = 1,…,d_v be the set of messages entering a variable node of degree d_v, and $\{U_{vp}\}$v = 1,…,d_v be the output messages for this variable node. The index 'p.v' indicates that the message comes from a permutation node to a variable node, and 'v.p' is for the other direction. We define similarly the messages $\{U_{pc}\}$ c = 1,…,d_c (resp. $\{V_{pc}\}$ c = 1,…,d_c) at the input (resp. output) of a degree d_c check node. The EMS algorithm works in the log-domain and uses reduced configuration sets to simplify the computational task. We define then:

$$\bar{U}[i_1...i_m] = \log\left(\frac{U[i_1,...,i_m]}{U[0,...,0]}\right) \quad \forall (i_1,...,i_m) \in \{0,1\}^m \quad (30)$$

As the log-density-ratio (LDR) representations of the messages. In the considered q-ary case, the message is composed of q -1 nonzero LDR values. The purpose of the EMS algorithm is to simplify the parity check node update by selecting only the most probable configuration sets of q-ary symbols which get involved in the parity check equations. To do that, we start by selecting in each incoming message $\bar{U}_{pc}$ the n_q largest values (we will take n_q fixed in our simulation results for simplicity reasons) that we denote: $\bar{u}_{pc}^{(k_c)}$, k_c = 1,…,n_q. We use the following notation for the associated field element: $\alpha_c^{(k_c)}(x)$, so that we have:

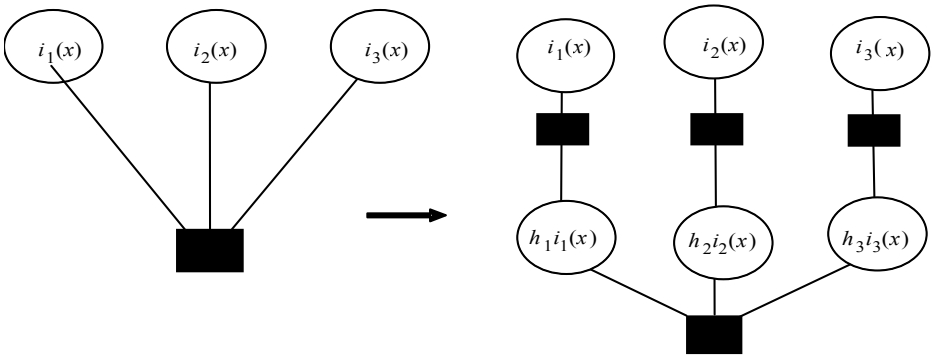

Figure 10. Transformation of the factor graph for the nonzero values in the *H*.

Copyright © 2010 SciRes.

$$\bar{u}_{pc}^{(k_c)} = \log\left(\frac{\text{Prob}(h_c(x).i_c(x)=\alpha_c^{(k_c)}(x))}{\text{Prob}(h_c(x).i_c(x)=0)}\right) = \bar{U}_{pc}[\alpha_{c_1}^{(k_c)}...\alpha_{c_m}^{(k_c)}] \quad (31)$$

With these largest values, we build the following set of configurations:

$$\text{Conf}(n_q) = \left\{\boldsymbol{\alpha}_k = [\alpha_1^{(k_1)}(x),...,\alpha_{d_c-1}^{(k_{d_c-1})}(x)]^T : \forall \boldsymbol{k} = [k_1,...,k_{d_c-1}] \in \{1,...,n_q\}^{d_c-1}\right\} \quad (32)$$

any vector of d_c-1 field elements in this set is called a configuration. The set Conf(n_q) corresponds to the set of configurations built from the n_q largest probabilities in each incoming message. Its cardinality is:

$$\text{Conf}(n_q) = n_q^{d_c-1}.$$

we need to assign a reliability to each configuration; we take as in [28]:

$$L(\boldsymbol{\alpha}_k) = \sum_{c=1...d_c-1} \bar{u}_c^{(k_c)}.$$

The initialization of the decoder is achieved with the channel log-likelihoods defined as: $L[i_1,\ldots,i_m]$.

The EMS proceeds in three steps as given below:

***Sum-step*:** variable node update for a degree d_v node:

$$\bar{U}_{tp} = \bar{L} + \sum_{v=1,v\neq t}^{d_v} V_{pv} \quad t = 1,...,d_v \quad (33)$$

$$\bar{U}_{tp}[i_1,...,i_m] = \bar{L}[i_1,...,i_m] + \text{ or: } \sum_{v=1,v\neq t}^{d_v} V_{pv}[i_1,...,i_m] \quad (i_1,...,i_m)\in\{0,1\}^m$$

***Permutation-step*:** from variable to check nodes:

$$\bar{U}_{pc}[i_1,...,i_m] = \bar{U}_{vp}[j_1,...,j_m] \quad (i_1,...,i_m)\in\{0,1\}^m \quad (34)$$
$$\text{with } i(x) = h(x).j(x)$$

The permutation step from check to variable nodes is performed using: $P_{h(x)}^{-1}$.

***Message update*:** for a degree d_c check node:

From the $\boldsymbol{d_c}$**-1** incoming messages $\bar{U}_{pc}$, build the sets:

$$S_{i_{d_c}(x)} = \text{Conf}_{i_{d_c}(x)}(q,1) \cup \text{Conf}_{i_{d_c}(x)}(n_p,n_c),$$

Then:

$$V_{d_c p}[i_{d_{c_1}},...,i_{d_{c_p}}] = \max_{\boldsymbol{\alpha}_k \in S_{i_{d_c}(x)}}\{L(\boldsymbol{\alpha}_k)\} \quad (i_{d_{c_1}},...,i_{d_{c_p}})\in\{0,1\}^m \quad (35)$$

With:

$$\text{Conf}_{i_{d_c}(x)}(n_p,n_c) = \{\boldsymbol{\alpha}_k \in \text{Conf}(n_p,n_c) : h_{d_c}(x).i_{d_c}(x) + \sum_{c=1}^{d_c-1}\alpha_c^{(k_c)}(x) = 0\}$$

Post-processing:

$$\bar{V}_{cp}[i_1,...,i_m] = \bar{V}_{cp}[i_1,...,i_m] - \bar{V}_{cp}[0,...,0] \quad (i_1,...,i_m)\in\{0,1\}^m, c = 1,...,d_c \quad (36)$$

3.4. Simulation Results

We give here some simulation results to show the performance of the proposed scheme. Since the target comparison is the work of Kozic & al [27], we use their results as benchmark for our proposed system. In his work, Kozic plots the obtained BER results for n = 512 and 1024 as the size of the vector input bits together with Q = 2 or 3 and a random sparse matrix with weight ρ = 3 or 6 on each column. We take each time the best performances he obtained.

Using the same size of input blocks, we have to choose the desired spectral efficiency. Due to the heavy computational task, we only take here: q = 4 and q = 8; *i.e.*; we work with *GF*(4) and *GF*(8) with spectral efficiencies respectively equal to 2 and 3 bits/s/Hz. The obtained results are drawn on **Figure 11** for block size 512 and on **Figure 12** with block size 1024.

One notices that the performances of our *GF*(q) LDPC codes of size 512 are quite similar to those of Vucetic & al for size 1024 and, using block size of length 1024, our designs outperform clearly those of Vucetic & al. The SNR gain for block size 1024 is approximately equal to 0.5 dB for Q = 2 and for *GF*(8) and becomes 0.75 dB for Q = 2 and for *GF*(4). The improvement is slightly better in the case Q = 3 since we obtain gains of 1.0 dB for *GF*(8) and 1.5 dB for *GF*(4). This result is not really surprising since many authors have shown that LDPC codes over *GF*(q) exhibit better performances than their counterparts on *GF*(2). One can notice that the slopes *i.e.*; the diversity gain are the same each time in the waterfall region. A more detailed study should be done to determine the starting point SNR of the waterfall region with the EXIT-CHART curves.

4. Conclusions

In this paper we have proposed new insights of the work of Kozic *et al.* in the field of channel coding using chaos-based encoding process. First, using non-linear MOD-MAP mapping with matrices of small dimension, we are able, thanks to an original EM based guessing algorithm, to optimize the distance spectrum of the corresponding Chaos Coded Modulation (CCM) schemes and

Copyright © 2010 SciRes.

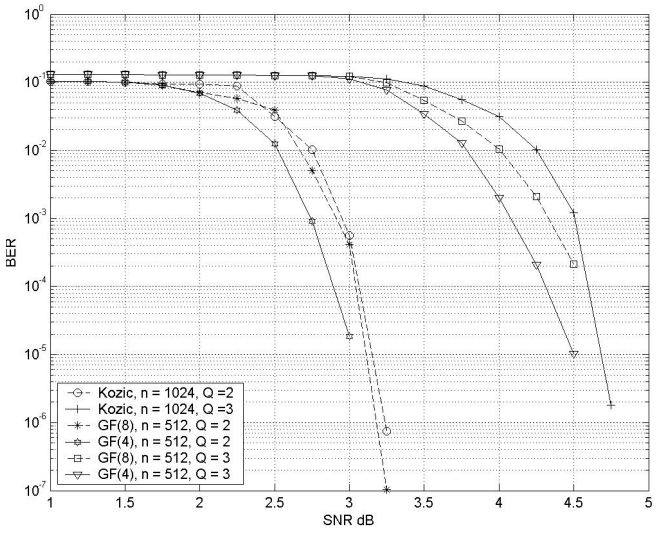

Figure 11. BER performances for chaos based LDPC codes over *GF*(*q*); block-length size equal to: 512.

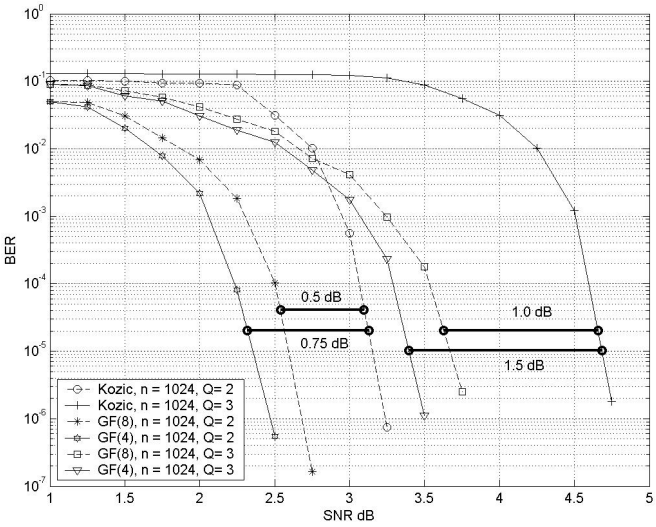

Figure 12. BER performances for chaos based LDPC codes over *GF*(*q*); block-length size equal to: 1024.

hence we can optimize the BER performances of such schemes. In the case where we use high dimensional sparse matrices for the MOD-MAP mapping, we can use a decoding process similar to those of LDPC codes. When we compare our obtained results with those of the former literature we noticed that, working on *GF*(*q*) enables to obtain significant gains of approximately 1. dB. This encouraging result entails the necessity to further optimize the design to reduce the hardware complexity. In fact, despite the use of the Extended Min-Sum algorithm, the obtained coding structure remains of prohibitive complexity.

5. References

[1] D. R. Frey, "Chaotic Digital Encoding: An Approach to Secure Communication," *IEEE Transactions on Circuits and Systems* II, Vol. 40, No. 10, 1993, pp. 660-666.

[2] A. Layec, "Développement de modèles de CAO pour la simulation système des systèmes de communication. Application aux communications chaotiques," Ph.D. Thesis, Xlim University of Limoges, 2006.

[3] F. J. Escribano, L. Lopez, M. A. F. Sanjuan, "Evaluation of Channel Coding and Decoding Algorithms Using Discrete Chaotic Maps," Chaos, American Institute of Physics, No. 16, 2006, pp. 1054-1500.

[4] I. P. Marino, L. Lopez, M. A. F. Sanjuan, "Channel Coding in Communications Using Chaos," *Physics Letters Elsevier Science*, Vol. 295, No. 4, 2002, pp. 185-191.

[5] E. Bollt, Y. C. Lai, C. Grebogi, "Channel Channel Capacity and Noise Resistance in Communicating with

Copyright © 2010 SciRes.

Chaos," *Physical Review Letters American Physical Society*, Vol. 79, No. 19, pp. 3787-3790.

[6] T. Schimming and M. Hasler, "Coded Modulation Based On Controlled 1-D and 2-D Piecewise Linear Chaotic Maps," *IEEE International Symposium on Circuits and Systems* (*ISCAS*), pp. 762-765.

[7] B. Chen and G. W. Wornel, "Analog Error Correcting Codes Based on Chaotical Dynamical Systems," *IEEE Transactions on Communications*, Vol. 46, No. 7, pp. 881-890.

[8] T. Erseghe and N. Bramante, "Pseudo Chaotic Encoding Applied to Ultra-Wide-Band Impulse Radio," *IEEE Vehicular Technology Conference*, Vancouver, September 2002, pp. 1711-1715.

[9] J. Lee, C. Lee and D. B. Williams, "Secure Communications Using Chaos," *IEEE Globecom*'95, Singapore, November 1995, pp. 1183-1187.

[10] J. Lee, S. Choi and D. Hong, "Secure Communications Using a Chaos System in a Mobile Channel," *IEEE Globecom*'98, Sydney, November 1998. pp. 2520-2525.

[11] C. Lee and D. B. Williams, "A Noise Reduction Method for Chaotic Signals," 44*th IEEE Acoustic, Sensor and Signal Processing Conference* (*ICASSP*), Detroit, May 1995, pp. 1348-1351.

[12] A. M. Guidi, "Turbo and LDPC Coding for the AWGN and Space-Time Channel," Ph.D. Thesis, University of South Australia, South Australia, June 2006.

[13] S. A. Barbulescu, A. Guidi and S. S. Pietrobon, "Chaotic Turbo Codes," *IEEE Conference International Symposium on Information Theory* (*ISIT*), June 2000, p. 123.

[14] X. L. Zhou, J. B. Liu, W. T. Song and H. W. Luo, "Chaotic Turbo Codes in Secure Communications," *Conference EUROCON*'2001*, International Conference on Trends in Communications*, July 2001, pp. 199-201.

[15] A. Abel and W. Schwarz, "Chaos Communications-Principles, Schemes, and System Analysis," *Proceedings of the IEEE*, Vol. 90, No. 5, May 2002, pp. 691-710.

[16] W. M. Tam, F. C. M. Lau and C. K. Tse, "Digital Communications with Chaos," Elsevier, Oxford, 2007.

[17] S. Kozic, K. Oshima and T. Schimming, "How to Repair CSK Using Small Perturbation Control-Case Study and Performance Analysis," *Proceedings of ECCTD*, Krakow, August 2003.

[18] Y. S. Lau, Z. M. Hussain, "A New Approach in Chaos Shift Keying for Secure Communication," *Proceedings of the third International Conference on Information Technology and Applications* (*ICITA*'05), Sydney, pp. 630-633.

[19] H. Dedieu, M. P. Kennedy and M. Hasler, "Chaos Shift Keying: Modulation and Demodulation of a Chaotic Carrier Using Self-Synchronizing Chua's Circuits," *IEEE Transactions on Circuits and Systems* II: *Analog and Digital Signal Processing*, Vol. 40, No. 10, 1993, pp. 634-642.

[20] J. Schweitzer, "The Performance of Chaos Shift Keying: Synchronization Versus Symbolic Backtracking," *Proceedings of the IEEE International Symposium on Circuits and Systems* (*ISCAS*), Monterey, 1998, pp. 469-472.

[21] F. J. Escribano, L. Lopez and M. A. F. Sanjuan, "Parallel Concatenated Chaos Coded Modulations," *IEEE Conference* 15*th International Conference on Software*, *Telecommunications and Computer Networks*, Softcom, 2007.

[22] F. J. Escribano, L. Lopez and M. A. F. Sanjuan, "Iteratively Decoding Chaos Encoded Binary Signals," *Proceedings of the Eighth International Symposium on Signal Processing and its Applications*, 2005, Sydney, August 2005, pp. 275-278.

[23] S. Kozic, T. Schimming and M. Hasler, "Controlled One- and Multidimensional Modulations Using Chaotic Maps," *IEEE Transactions on Circuits and Systems* I: *Regular Papers*, Vol. 53, No. 9, September 2006, pp. 2048-2059.

[24] F. J. Escribano, L. Lopez and M. A. F. Sanjuan, "Chaos-Coded Modulations Over Rician and Rayleigh Flat Fading Channels", *IEEE Transactions on Circuits and Systems* II, Vol. 55, No. 6, June 2008, pp. 581-585**.**

Copyright © 2010 SciRes.

Int. J. Communications, Network and System Sciences, **2010, 3, 507-510**
doi:10.4236/ijcns.2010.36068 Published Online June 2010 (http://www.SciRP.org/journal/ijcns/).

Scientific Research

Efficiency Improvement of Space Time Block Codes

Zahoor Ahmed Baloch[1], Mohammad Usman Baloch[2], Noor Hussain[3]
[1]*Université de Limoges-Ecole Nationale Supérieure d'Ingénieurs de Limoges* (*ENSIL*), *Rue Atlantis-Parc ESTER-BP Limoges cedex, France*
[2]*Balochistan University of Engineering & technology, Khuzadar, Pakistan*
[3]*Universiti Teknologi Petronas, Bandar Seri Iskandar, Malaysia*
E-mail: *zahoor.ahmed@ensil.unilim.fr, musman@buetk.edu.pk, nhussain@petronas.com.my*
Received March 24, 2010; *revised April* 29, 2010; *accepted May* 30, 2010

Abstract

Unlike most of the existing methods in Space Time coding (STC) system which focus on design of STC gaining full rate and/or maximum diversity, we propose an approach to improve spectral efficiency of the code. The proposed scheme carries more information symbols in each transmission block as compared to its counterpart code, and yet retains the property of simple decoding. Simulation results show that transmit diversity is retained with improvement of code efficiency. We mainly focus on Four transmit antenna scheme but it can be generalized for any number of transmit antennas.

Keywords: Space Time Block Code, Spectral Efficiency

1. Introduction

Since 1998 when Alamouti in [1] presented the idea of Space Time Coding, significant progress has been made in code design for achieving better diversity and code rate over multiple wireless communication channels. Space Time Coding (STC) system is one of the compromising scheme to meet the fast growing challenges for reliable and high data rate communication over multiple input multiple out (MIMO) channels. In [2,3] V.Tarokh et el discusses in detail the design of different classes of ST codes for achieving maximum diversity and full rate. However to counter the problem of unfeasibility/impracticability of having multiple receiver antennas at end users has put the researchers on work for alternates. In [2] it was shown that code rate cannot be greater than one. In fact even the maximum diversity and full rate codes do not exploit high efficiency. For example, if we look at (1), which is a Space Time Block Code (STBC) transmission matrix for four transmit antennas.

$$\begin{bmatrix} x_1 & x_2 & x_3 & x_4 \\ -x_2 & x_1 & -x_4 & x_3 \\ -x_3 & x_4 & x_1 & -x_2 \\ -x_4 & -x_3 & x_2 & x_1 \end{bmatrix} \quad (1)$$

where only the four symbols of first row of the matrix (*i.e.* x_1, x_2, x_3, x_4) have been taken from a particular constellation (QPSK) while the other symbols are redundant and totally depend on four useful symbols. In other words out of sixteen symbols, only four symbols are carrying useful information.

In [4], Foschini proposed BLAST coding technique, which offers higher spectral efficiency by exploiting the spatial multiplexing to transmit independent data streams over Multiple-Input Multiple-output channels. Such type of scheme outperforms to its counterpart STBC having multiple antennas at both transmitter and receiver, but contrary in [5] it was shown that the decoding of such a scheme does not work well if the numbers of receiver antennas are less than that of number of transmit antennas.

In [6] a scheme for increasing the spectral efficiency of Alamouti code has been presented. But such a scheme does not contribute significant improvement in code efficiency for more than two transmit antennas.

In this paper we propose a technique to improve the spectral efficiency of STBC for four transmit antennas retaining maximum diversity, full rate and simple maximum likelihood (ML) decoding characteristics of original code. Although the main focus of this paper is to design efficient code for four transmit antennas scenario, but same idea can be extended in a straightforward manner for STBC having more than four antennas.

The rest of the paper is organized as follow: Section 2 presents the system model. In Section 3, different techniques for increasing the code efficiency are discussed. Simulation results are given in Section 4 and finally conclusion in Section 5.

Copyright © 2010 SciRes.

2. System Model

We consider a wireless communication system having four transmit antennas and one receiver antenna. We assume that transmission at the base band employs a real constellation $\mathcal{A}$ with 2^b elements. The input binary stream is first split into two sub-stream by a serial to parallel converter. Each binary sub stream then passes through a QPSK constellation denoted by $\mathcal{A}$ to map binary bits into symbols, *i.e.* setting $x_i = s_i$ for $i = 1,2,3,4$, We arrive at a matrix $\mathrm{C} = \mathrm{O}(s_1, s_2, s_3, s_4)$ with entries $\pm s_1, \pm s_2, \pm s_3, \pm s_4$. At each time slot $t = 1,2,3,4$ signals $C_{t,i}$ are transmitted simultaneously from four transmit antennas. Clearly the rate of transmission is *b* bit/s/Hz.

The fading coefficients from first to last transmit antennas to receiver antenna at time *t* are denoted by $h_1(t)$, $h_2(t)$, $h_3(t)$ and $h_4(t)$ respectively. Assuming that the fading coefficients are constant across four consecutive symbols transmission periods, and are expressed as

$$\begin{aligned} h_1(t) &= h_1(t+T) = h_1 = |h_1| e^{jQ_1} \\ h_2(t) &= h_2(t+T) = h_2 = |h_2| e^{jQ_2} \\ h_3(t) &= h_3(t+T) = h_3 = |h_3| e^{jQ_3} \\ h_4(t) &= h_4(t+T) = h_4 = |h_4| e^{jQ_4} \end{aligned} \tag{2}$$

where $|h_i|$ and θ_i, for $i = 1,2,3,4$ are the amplitude gain and phase shift for the path from transmit antenna *i* to the receive antenna, and *T* is the symbol duration.

At the receive antenna, the received signals over four consecutive symbol periods, denoted by r_1, r_2, r_3 and r_4 for $t = 1,..,4$ respectively, can be expressed as

$$\begin{aligned} r_1 &= h_1 x_1 + h_2 x_2 + h_3 x_3 + h_4 x_4 + n_1 \\ r_2 &= -h_1 x_2 + h_2 x_1 - h_3 x_4 + h_4 x_3 + n_2 \\ r_3 &= -h_1 x_3 + h_2 x_4 + h_3 x_1 - h_4 x_2 + n_3 \\ r_4 &= -h_1 x_4 - h_2 x_3 + h_3 x_2 + h_4 x_1 + n_4 \end{aligned} \tag{3}$$

where n_1, n_2, n_3 and n_4 respectively from time 1 to 4 are independent complex variable with zero mean power spectral density *No*/2 per dimension, representing additive white Gaussian noise. We may re-write Equation (3) into matrix form as:

$$\begin{aligned} \begin{bmatrix} r_1 & r_2 & r_3 & r_4 \end{bmatrix} = \begin{bmatrix} h_1 & h_2 & h_3 & h_4 \end{bmatrix} \begin{bmatrix} x_1 & x_2 & x_3 & x_4 \\ -x_2 & x_1 & -x_4 & x_3 \\ -x_3 & x_4 & x_1 & -x_2 \\ -x_4 & -x_3 & x_2 & x_1 \end{bmatrix} \\ + \begin{bmatrix} n_1 & n_2 & n_3 & n_4 \end{bmatrix} \end{aligned} \tag{4}$$

or more precisely

$$r_t = \sum_{i=1}^{4} \alpha_i c_t^i + n_t \tag{5}$$

where α_i denotes channel coefficients. Assuming perfect channel state information is available at receiver, the receiver computes the decision metric

$$\sum_{t=1}^{4} \left| r_t - \sum_{t=1}^{4} a_i c_t^i \right|^2 \tag{6}$$

The maximum likelihood decoding for s_i can be achieved by decoupling the signals transmitted from different antennas, [4,6].

$$\hat{s}_i = \arg \min_{s \in \mathcal{A}} \left\{ \left| r_i - s \right|^2 \right\} \tag{7}$$

For $i = 1,..,4$ and decide in favour of s_i among all the constellation symbols

3. Efficiency Improvement Code

Assume that all the symbols in (1) are drawn from a QPSK constellation with gray constellation as shown in **Figure 1**. Although the code given in (1) is full rate code but its efficiency is too low. To find out the code efficiency over a QPSK constellation, we represent (1) by its corresponding bit representation. There might be 256 different patterns, and each pattern comprises of 32 bits. To lay down all 256 different patterns is a fatigable and un-necessary work. To save space we lay down just one such pattern below in (8), by assuming

$s_1 = e^{j\pi 0}$, $s_2 = e^{\frac{j\pi}{2}}$, $s_3 = e^{j\pi}$ and $s_4 = e^{\frac{j3\pi}{2}}$

$$\begin{bmatrix} 00 & 01 & 11 & 10 \\ 10 & 00 & 01 & 11 \\ 00 & 10 & 00 & 10 \\ 01 & 00 & 10 & 00 \end{bmatrix} \tag{8}$$

Now if we look at (8), the useful or informative bits are only 8 bits enumerated in first row of (8) while all other 24 (in 2nd, 3rd and 4th rows of (8)) bits are redundant and totally depends on 8 useful bits. We define the code efficiency η as the ratio of the number of useful bits and the total number of bits in each pattern of code matrix. In this particular case, the code efficiency is η = 8/32 = 0.25.

All full rate Space Time Block Codes having 4 or more than 4 transmit antennas do not gain code efficiency more than 0.25, even the case is worse for non-full rate codes.

Here we discuss some technique to improve the spectral efficiency of the code for four transmit antennas.

One way is to split the original data bit stream into group of 4 × 8 like that in (8), *i.e.* the redundant bits have dual function, at the same time they represent as redundant bits and information bits. In this case we can have

Copyright © 2010 SciRes.

full efficient code η = 1. But as our original data is random, so the probability of getting such a code pattern is $2^8/2^{32} = 0.6^{-6}\%$ which is too small and practically near to zero probability.

Another way to improve the code efficiency η is the technique very similar to that used in [6] for two transmit antenna Alamouti code. The original data stream is divided into group of nine bits. The first eight bits are arranged as useful bits in matrix form as in (8) and the ninth bit is used to decide which constellation to choose between the two constellation schemes shown in **Figure 1** and **Figure 2**, for transmission of eight useful bits. For example if ninth bit 1, we choose the constellation A, shown in **Figure 1**, otherwise constellation B shown in **Figure 2**. It turns out that the transmission matrix has the same format as that in (8) but each transmission block now contains nine information bits instead of eight bits. The code efficiency increases to 9/32 = 0.28125.

As in this technique the code efficiency increases by a single bit we call this technique, bit efficient E_b code.

Another way to increase the code efficiency is to first divide the source binary data in to group of ten bits and then convert them into two binary sub-stream by a serial to parallel converter. For simplicity we show these five, 2-bits parallel bit stream by following symbols.

$$\left[x_1\ x_2\ x_3\ x_4\ x_5\right] \tag{9}$$

Before passing the symbol through constellation we tally the fifth symbol with other four symbols in (9) by its corresponding bit representation and find out the symbol which is same as fifth symbol. In case if there are more than one matching symbols, then we take the first one in that vector and in case if there is no any matching symbol then we ignore the fifth symbol for that specific transmission.

We use two type of constellation (as shown in **Figure 1** and **Figure 2**). In transmitting the useful symbols $\left[x_1\ x_2\ x_3\ x_4\right]$, the symbol which is same as x_5 is transmitted from constellation A whereas the rest of the symbols are transmitted from constellation B.

As our source data stream is random, so it difficult to calculate the matching probability between fifth and other symbols. However for large data size we expect

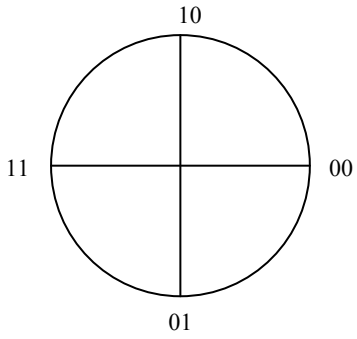

Figure 1. QPSK Constellation 'A' with gray coding.

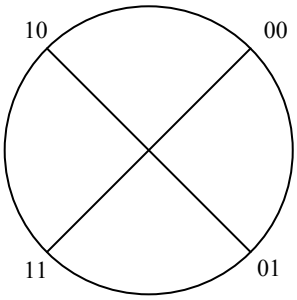

Figure 2. QPSK Constellation 'B' with gray coding.

maximum probability. If first four symbol in (9), in its corresponding bit representation, are different to each other, then the probability that the fifth symbol will match with one of the other four symbols is 100%, if any three symbols are different then the probability that the fifth symbol will match with one of the other four symbols is 75%, so probability is 50% if two symbols are different and it is 25% if one symbol is different.

We assume that in each block of transmission we find a matching symbol. In this case the code efficiency is 10/32 = 0.3125. As code efficiency is increased by a symbol, we call this technique as symbol efficient E_s code

Let $x_5 \in \left\{x_1\ x_2\ x_3\ x_4\ x_5\right\}$ denote the fifth symbol and $\left\{x_1\ x_2\ x_3\ x_4\ x_5\right\} \in A, B$

Then the transmission matrix (1) can be represented as

$$\begin{bmatrix} x_1 e^{j\frac{\pi}{2}s_5} & x_2 e^{j\frac{\pi}{2}s_5} & x_3 e^{j\frac{\pi}{2}s_5} & x_4 e^{j\frac{\pi}{2}s_5} \\ -x_2 e^{j\frac{\pi}{2}s_5} & x_1 e^{j\frac{\pi}{2}s_5} & -x_4 e^{j\frac{\pi}{2}s_5} & x_3 e^{j\frac{\pi}{2}s_5} \\ -x_3 e^{j\frac{\pi}{2}s_5} & x_4 e^{j\frac{\pi}{2}s_5} & x_1 e^{j\frac{\pi}{2}s_5} & -x_2 e^{j\frac{\pi}{2}s_5} \\ -x_4 e^{j\frac{\pi}{2}s_5} & -x_3 e^{j\frac{\pi}{2}s_5} & x_2 e^{j\frac{\pi}{2}s_5} & x_1 e^{j\frac{\pi}{2}s_5} \end{bmatrix} \tag{10}$$

S_5 is decided by the location of $r_i = 1,..,4$ which is closer to the decision boundary. Maximum likelihood decoding of $S_i = 1,..,4$ can be decoupled

$$\hat{s}_i = \arg\min_{s\in\mathcal{A}} \left\{ \left| r_i - s_i e^{j\frac{\pi}{2}s_5} \right|^2 \right\} \tag{11}$$

4. Simulation Results

At transmitter two types of QPSK constellation are used. The minimum Euclidean distance between two QPSK constellations is the same as that of 8PSK constellation. Therefore in worse case the BER performance of the symbol efficient STBC code will be slightly worse due to additional error of symbol S_5, as compare to 8PSK modulation. On the contrary, if the recovery of S_5 is per-

Copyright © 2010 SciRes.

fect *i.e.* the number of errors related to S_5 is zero, then the selection of the QPSK constellation at the receiver is always correct, and the minimum Euclidean distance turns out to be the same as that of a QSPK constellation. Thus in the best case, the BER performance of symbol efficient STBC will be slightly better as compare to ordinary STBC code.

Our simulation results in **Figure 3** prove our claim of better spectral efficiency of symbol efficient E_s STBC code as compare to conventional STBC.

Table 1 shows some specific results of a neat comparison between STBC, Bit efficient STBC, symbol efficient STBC and 8PSK.

Table 1. Performances of QPSK modulation under different scenarios.

Scheme	Efficiency	R bit/s/Hz	BER
4-QPSK	0.25	2	Low
4-PSK E_b	0.282	2.25	↓
4-PSK E_s	0.32	0.5	
8PSK	0.25	3	High

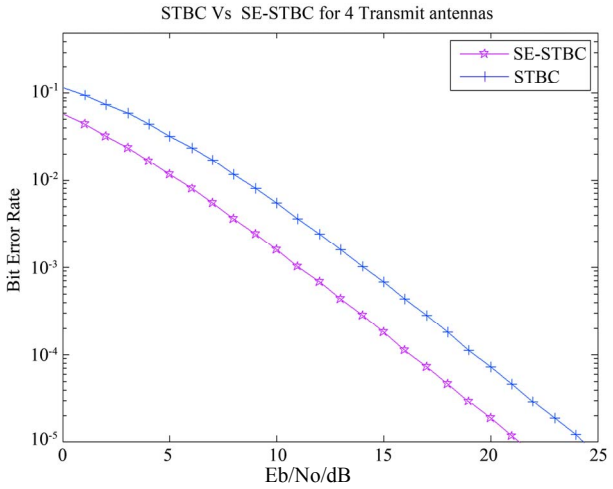

Figure 3. BER performance of STBC and spectral efficiency STBC with 4 -Transmit antennas.

5. Conclusions

Unlike most of the recent work, which are concentrated on design to achieve full rate and full diversity codes. We tried to invite researchers' concentration to explore new techniques to augment the spectral efficiency of STB Codes. We presented a technique which enables us to send more symbols per transmission as compared to ordinary STB Codes. This approach also achieves full transmit diversity and allows maximum likelihood decoding for signals. The additional plus point of this technique is its flexibility to any number of transmit antennas.

6. References

[1] S. M. Alamouti, "A Simple Transmit Diversity Technique for Wireless Communication," *IEEE Journal on Selected Areas in Communications*, Vol. 16, No. 8, 1998, pp. 1451-1458.

[2] V. Tarokh, H. Jafarkhani and A. R Calderbank, "Space Time Block Codes from Orthogonal Designs," *IEEE Transactions on Information Theory*, Vol. 45, No. 5, 1999, pp. 1456-1467.

[3] V. Tarokh, H. Jafarkhani and A. R. Calderbank, "Space Time Block Coding for Wireless Communication: Performance Result," *Journal on Selected Areas in Communications*, Vol. 17, No. 3, 1999, pp. 451-462.

[4] G. J. Foschini, "Layered Space-Time Architecture for Wireless Communication in a Fading Environment When Using Multi-Element Antennas," *Bell Labs Technical Journal*, Vol. 1, No. 2, 1996, pp. 41-59.

[5] G. D. Golden, G. J Foschini, R. A. Valenzuela and P. W. Wolniansky, "Detection Algorithm and Initial Laboratory Results Using V-BLAST Space Time Communication Architecture," *Electronics Letters*, Vol. 35, No. 1, 1999, pp. 14-16.

[6] Q. Ling and T. T. Li, "Efficiency Improvement for Alamouti Codes," *IEEE 40th annual conference on Information Sciences and systems*, Princeton, 22-24 March 2006, pp. 569-572.

Copyright © 2010 SciRes.

Int. J. Communications, Network and System Sciences, **2010, 3, 511-522**
doi:10.4236/ijcns.2010.36069 Published Online June 2010 (http://www.SciRP.org/journal/ijcns/).

Scientific Research

An Empirical Examination of Routing Protocols in Mobile Ad Hoc Networks

Kuncha Sahadevaiah[1], Oruganti Bala Venkata Ramanaiah[2]
[1]*Department of Computer Science & Engineering, University College of Engineering, Jawaharlal Nehru Technological University, Kakinada, India*
[2]*Department of Computer Science & Engineering, University College of Engineering, Jawaharlal Nehru Technological University, Hyderabad, India*
E-mail: {*ksd1868, obvramanaiah*} *@gmail.com*
Received March 26, 2010; *revised April* 28, 2010; *accepted May* 29, 2010

Abstract

A Mobile Ad hoc NETwork (MANET) is a self-organizing, temporary, infrastructure-free, multi-hop, dynamic topology wireless network that contains collection of cooperative autonomous freely roaming mobile nodes. The nodes communicate with each other by wireless radio links with no human intervention. Each mobile node functions as a specialized router to forward information to other mobile nodes. In order to provide efficient end-to-end communication with the network of nodes, a routing protocol is used to discover the optimal routes between the nodes. The routing protocols meant for wired networks can not be used for MANETs because of the mobility of nodes. Routing in ad hoc networks is nontrivial due to highly dynamic nature of the nodes. Various routing protocols have been proposed and widely evaluated for efficient routing of packets. This research paper presents an overview on classification of wide range of routing protocols for mobile ad hoc wireless networks proposed in the literature and shows the performance evaluation of the routing protocols: DSDV, AODV, FSR, LAR, OLSR, STAR and ZRP using the network simulator *QualNet* 4.0 to determine which protocols may perform best in large networks. To judge the merit of a routing protocol, one needs performance metrics (throughput, end-to-end delay, jitter, packet delivery ratio, routing overhead) with which to measure its suitability and performance. Our simulation experiments show that the LAR protocol achieves relatively good performance compared to other routing protocols.

Keywords: Mobile Ad Hoc Networks, Routing Protocols, LAR, QualNet 4.0, Performance Metrics, Simulations, Performance Evaluation

1. Introduction

The advent of ubiquitous computing and the proliferation of portable computing devices have raised the importance of mobile and wireless networking. Wireless networking is an emerging technology that allows users to access information and services electronically, regardless of their geographic position. *Ad hoc* is a Latin word, which means "*for this purpose only*". The term "ad hoc" tends to imply "can take different forms" and "can be mobile, stand alone, or networked" [1]. Ad hoc networks have the ability to form "on the fly" and dynamically handle the joining or leaving of nodes in the network. Mobile nodes are autonomous units that are capable of roaming independently. Typical mobile ad hoc wireless nodes are Laptops, Personal Digital Assistants, Pocket PCs, Cellular Phones, Internet Mobile Phones, Palmtops or any other mobile wireless devices. All of these have the capability and need to exchange information over a wireless medium in a network. Mobile ad hoc wireless devices are typically lightweight and battery operated.

A mobile ad hoc network (MANET) is an adaptive, self-configurable, self-organizing, infrastructure-less multi-hop wireless network with unpredictable dynamic topologies [2]. By adaptive, self-configurable and self-organizing, means an ad hoc network can be formed, merged together or partitioned into separated networks on the fly depending on the networking needs. *i.e.* a formed network can be deformed on the fly without the need for any system administration. By infrastructure-less, means an ad hoc network can be promptly deployed without relying on any existing infrastructure such as base stations for wireless cellular networks. By multi-hop wireless, means, in an ad hoc network the routes between end users may consists of multi-hop wireless links.

Copyright © 2010 SciRes.

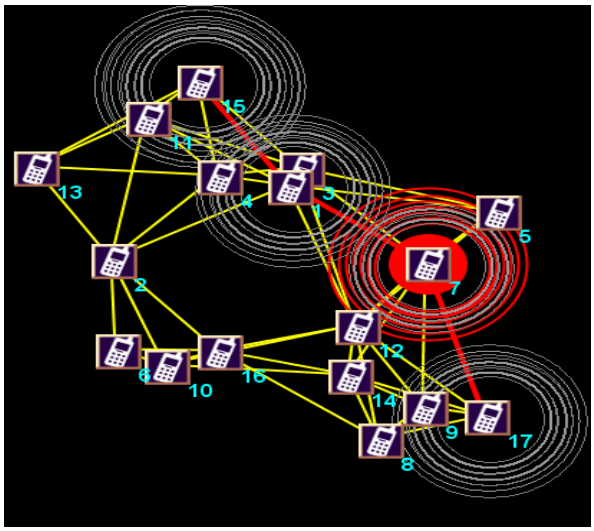

Figure 1. Communication scenario in MANET.

In addition, each node in a mobile ad hoc network is capable of moving independently and forwarding packets to other nodes.

The important characteristics of ad hoc wireless networks [2] are: dynamic topologies, low bandwidth, limited battery power, decentralized control, weak physical protection, etc. *Dynamic Topologies*: The nodes in ad hoc wireless networks are free to move independently in any direction. The network topology changes randomly at unpredictable times and primarily consists of bidirectional links. *Low Bandwidth*: These networks have lower capacity and shorter transmission range than fixed infrastructure networks. The throughput of wireless communication is lesser than wired communication because of the effect of the multiple access, fading, noise, and interference conditions. *Limited Battery Power*: The nodes or hosts operate on small batteries and other exhaustible means of energy. So, energy conservation is the most important design optimization criteria. *Decentralized Control*: Due to unreliable links, the working of ad hoc wireless network depends upon cooperation of participating nodes. Thus, implementation of any protocol that involves a centralized authority or administrator becomes difficult. *Weak Physical Protection*: Nodes in ad hoc wireless networks are usually compact, soft, and hand-held in nature. Today, portable devices like mobile phones or personal digital assistants (PDAs) are getting smaller and smaller. They could get damaged or lost or stolen easily and misused by an adversary.

The domain of applications for ad hoc wireless networks is diverse, ranging from small, static networks that are constrained by power sources, to large-scale, mobile, highly dynamic networks [2,4]. Such networks are frequently viewed as a key communications technology enabler for network-centric warfare and military tactical operations-for fast establishment of military communications and troop deployments in hostile and/or unknown environments, disaster relief operations-for communication in environments where the existing infrastructure is destroyed, search and rescue operations and emergency situations-for communication in areas with no wireless infrastructure support, law enforcement-for secure and fast communication during law enforcement operations, commercial use-for enabling communications in exhibitions, conferences & large gatherings, intelligent transportation systems and fault-tolerant mobile sensor grids. Most of these applications demand a secure and reliable communication.

2. Routing in Mobile Ad Hoc Networks

Mobile hoc network (MANET) is built on the fly where a number of mobile nodes work in cooperation without the engagement of any centralized access point or any fixed infrastructure. The nodes in the network are free to move independently in any direction. Node mobility causes route changes. The nodes themselves are responsible for dynamically discovering other nodes to communicate. When a node wants to communicate with a node outside its transmission range, a multi-hop routing strategy is used which involves some intermediate nodes. The network's wireless topology changes frequently and randomly at unpredictable times. Every node in ad hoc wireless network acts as a router that discovers and maintains routes in the network. Hence, the primary challenge is to establish a correct and efficient route between a pair of nodes and to ensure the correct and timely delivery of packets. Route construction should be done with a minimum of overhead and bandwidth consumption. Various protocols-proactive, reactive and hybrid-have been proposed and widely evaluated for efficient routing of packets in the literature [3].

Routing protocols [5] often are very vulnerable to node misbehavior. A node dropping all the packets is considered as malicious node or selfish nodes. A malicious node misbehaves because it intends to damage network functioning. A selfish node does so because it wants to save battery life for its own communication by simply not participating in the routing protocol or by not executing the packet forwarding. A malicious node could falsely advertise very attractive routes and thereby convince other nodes to route their messages via that malicious node.

3. Routing Protocols in Mobile Ad Hoc Networks

The main objective of ad hoc routing protocols is how to deliver data packets among nodes efficiently without predetermined topology or centralized control. Expected properties of MANET routing protocols are [6]: a routing

Copyright © 2010 SciRes.

protocol for MANET should be distributed in manner in order to increase its reliability, the routing protocol should assume routes as unidirectional links, the routing protocol should be power-efficient, the routing protocol should consider its security, and a routing protocol should be aware of Quality of Service (QoS). Based on the method of delivery of data packets from the source to destination, classification of the MANET routing protocols could be done as unicast, multicast or geocast routing protocols [6].

Unicast Routing Protocols: The routing protocols that consider sending information packets to a single destination from a single source.

Multicast Routing Protocols: Multicast is the delivery of information to a group of destinations simultaneously. Multicast routing protocols for MANET use both multicast and unicast for data transmission. Multicast routing protocols for MANET can be classified again into two categories: tree-based and mesh-based multicast routing protocols. *Mesh-based routing protocols* use several routes to reach a destination while the *tree-based protocols* maintain only one path. Tree-based protocols ensure less end-to-end delay in comparison with the mesh-based protocols.

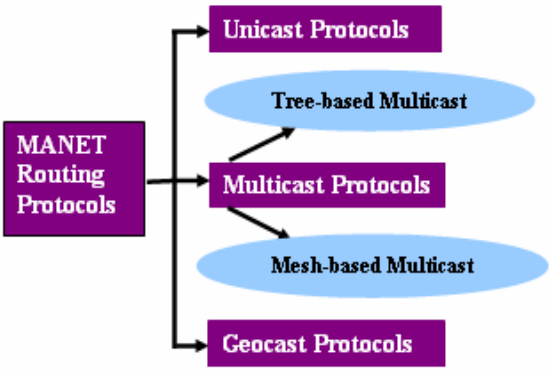

Figure 2. Classification of routing protocols.

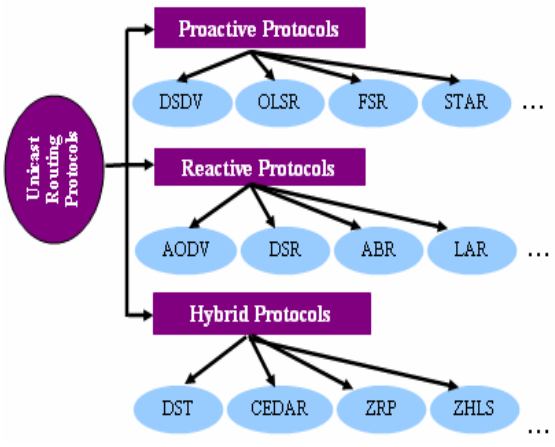

Figure 3. Classification of unicast routing protocols.

Geocast Routing Protocols: The routing protocols aim to send messages to some or all of the wireless nodes within a particular geographic region. Often the nodes know their exact physical positions in a network, and these protocols use that information for transmitting packets from the source to the destination(s).

Ad hoc wireless network unicast routing protocols can be further classified into three major categories based on the routing information update mechanism: proactive or table driven, reactive or on-demand, and hybrid routing protocols.

3.1. Proactive Routing Protocols

In *proactive routing protocols*, also known as table-driven routing protocols, each node maintains one or more tables that contain consistent and up-to-date routing information to every other node in the network. The routing information is usually kept in a number of different tables. Proactive protocols continuously learn the global topology of the network by exchanging topological information among the network nodes. When the network topology changes, the nodes propagate update messages and the topology change information is distributed across the network. If the network topology changes too frequently, the cost of maintaining the network might be very high. Each node continuously evaluates routes to all reachable nodes. The overhead to maintain up-to-date network topology information is high.

Some of these protocols are: Destination Sequenced Distance Vector routing protocol (*DSDV*), Optimized Link State Routing protocol (*OLSR*), Fisheye State Routing protocol (*FSR*), Source Tree Adaptive Routing protocol (*STAR*), Wireless Routing Protocol (*WRP*), Global State Routing (*GSR*), Cluster-head Gateway Switch Routing protocol (*CGSR*), Hierarchical State Routing protocol (*HSR*).

3.1.1. Destination Sequenced Distance Vector Routing Protocol (DSDV)

The Destination Sequenced Distance Vector (DSDV) [9] is a proactive unicast routing protocol that solves the major problem associated with distance vector routing of wired networks, *i.e.* count-to-infinity, by using destination sequence numbers. It uses the classical Bellman-Ford routing algorithm with some improvements on routing performance that guarantees loop free routes. Each node maintains a routing table that stores all possible available routes for each destination, the hop counts as routing metrics to reach the destination and the unique sequence numbers to keep up-to-date information about its neighbors. A sequence number created by the destination is used to distinguish stale routes from new one and avoids formation of route loops. The route with higher sequence number is newer. If two routes have the same sequence number then the route with the best metric (*i.e.* shortest route)

Copyright © 2010 SciRes.

is used.

Every node periodically exchange routing table updates to its immediate neighbors. The route updates can be either time-driven or event-driven. Two types of route update packets: full dump and incremental packets are used. The *full dump* packet carries all the available routing information, *i.e.,* the entire routing table to the neighbors and the *incremental* packet carries only the information changed since the last full dump. For updating the routing information in a node, the update packet with the highest sequence number is used. The incremental update messages are sent more frequently than the full dump packets. The protocol will not scale in large network since a large portion of the network bandwidth is used in the updating procedures.

3.1.2. Optimized Link State Routing Protocol (OLSR)

The Optimized Link State Routing (OLSR) [11] is a proactive unicast optimized version of a pure link state routing protocol that employs an efficient link state packet forwarding mechanism called multipoint relaying. This protocol performs hop-by-hop routing; that is, each node in the network uses its most recent information to route a packet. The routing optimization is done mainly in two ways. *Firstly*, OLSR reduces the size of the control packets for a particular node during each route update by declaring only a subset of links with the node's neighbors who are its multipoint relay selectors, instead of all links in the network. Any node which is not in the set can read and process each packet but do not retransmit. *Secondly*, it minimizes flooding of the control traffic by using only the selected nodes, called multipoint relays to disseminate information in the network. To select the multipoint relaying, each node periodically broadcasts a list of its one hop neighbors using hello messages. From the list of nodes in the hello messages, each node selects a subset of one hop neighbors, which covers all of its two hop neighbors. It provides optimal routes to every destination in terms of number of hops, which are immediately available when needed. As only multipoint relays of a node can retransmit its broadcast messages, this protocol significantly reduces the number of retransmissions in a flooding or broadcast procedure.

Therefore, the protocol works based on the mechanisms of: neighbors-sensing based on periodic exchange of *hello* messages, efficient flooding of control traffic using the concept of multipoint relays, and computation of an optimal route using the shortest-path algorithm. This protocol does not notify the source immediately after detecting a broken link and source node comes to know that route is broken when the intermediate node broadcasts its next packet. The proposed protocol is best suitable for large and dense ad hoc networks.

3.1.3. Fisheye State Routing Protocol (FSR)

The Fisheye State Routing (FSR) [12] is a proactive unicast routing protocol based on link state routing algorithm with effectively reduced overhead to maintain network topology information. The novelty of FSR is that it uses a special structure of the network called the "fisheye". FSR maintains the accurate distance and path quality information about the immediate neighboring nodes and progressively reduces detail as the distance increases. In link state routing algorithm, used for wired networks, link state updates are generated and flooded through the network whenever a node detects a topology change. However, in FSR nodes exchange link state information periodically only with the neighboring nodes to maintain up-to-date full topology information of the network. To reduce the size of link state update messages, FSR uses different update periods for different entries in the routing table. Link state updates corresponding to the nodes within a smaller scope are propagated with higher frequency.

The FSR protocol is an improvement of Global State Routing (GSR). The large size of update messages in GSR wastes a considerable amount of network bandwidth. In FSR, each update message does not contain information about all nodes. Instead, it reduces the size of the update messages by exchanging information about closer nodes more frequently than it does about farther nodes, which lie outside the fisheye scope. The scope is defined in terms of the nodes that can be reached in a certain number of hops. So, each node gets accurate information about neighbors and accuracy of information decreases as the distance from node increases.

The advantage of FSR is that even though a node does not have accurate information about a destination, as the packet moves closer to the destination, more correct information about the route to the destination becomes available. FSR exhibits a better scalability concerning the network size compared to others as the overhead is controlled in this scheme.

3.1.4. Source Tree Adaptive Routing Protocol (STAR)

The Source Tree Adaptive Routing [13] protocol is based on the link state algorithm. Each node maintains a source routing tree, which is a set of links containing the preferred paths to every destinations and broadcasts its source-tree information to its neighbors and builds a partial graph of the topology. When a node has data packets to send to a destination for which no path exists in its source-tree, it originates an update message to all its neighbors indicating the absence of a path .This update message triggers another update message from a neighbor which has a path. After getting this, the node updates its source-tree and then finds path to all nodes in the network. In addition to path breaks, the intermediate nodes are responsible for handling the routing loops.

STAR will scale well in large networks since it has significantly reduced the amount of routing overhead disseminated into the network by using a least overhead

Copyright © 2010 SciRes.

routing approach (LORA) to exchange routing information. However, this protocol may have significant memory and processing overheads in large and highly mobile networks, because each node is required to maintain a partial topology graph of the network (it is determined from the source tree reported by its neighbors), which changes frequently as the neighbors keep reporting different source trees.

3.2. Reactive Routing Protocols

In *reactive routing protocols*, also known as on-demand routing protocols, a node creates a route in an on-demand fashion, *i.e.* it computes a route only when needed. When a source wants to send packets to a destination, it invokes the route discovery mechanisms to find the path to the destination. Route discovery usually occurs by flooding a route request packet throughout the network. Route reply is sent back if the destination itself or node with route to the destination is reached. The discovery procedure terminates either when a route has been found or no route available after examination for all route permutations. Reactive routing does not maintain global topological information and, therefore, substantially reduces energy consumption. Some of these protocols are: Ad hoc On-Demand Distance Vector routing protocol (*AODV*), Dynamic Source Routing protocol (*DSR*), Associativity Based Routing protocol (*ABR*), Location Aided Routing protocol (*LAR*), Light-weight Mobile Routing protocol (*LMR*), Temporally Ordered Routing Algorithm (*TORA*), Ant-colony-based Routing Algorithm (*ARA*), Cluster-based Routing Protocol (*CBRP*).

3.2.1. Ad Hoc On-Demand Distance Vector Routing Protocol (AODV)

The Ad hoc On-Demand Distance Vector (AODV) [14] routing protocol is a reactive unicast routing protocol. The protocol constructs efficient route on demand with minimal control overhead and minimal route acquisition latency. AODV is essentially a combination of both DSR and DSDV algorithms and it borrows the basic on demand mechanism of route discovery and route maintenance from DSR, plus the use of hop-by-hop routing sequence numbers from DSDV. The destination sequence number can be used to ensure loop-free and to identify which route with the greatest sequence number is newer one.

AODV has bidirectional route from source to destination. To find a path from source to destination, the source broadcasts a route request packet. The neighbors in turn broadcast the packet to their neighbors till it reaches an intermediate node that has recent route information about the destination or till it reaches the destination. A node discards a route request packet that it has already seen. The route request packet uses sequence numbers to ensure that the routes are loop free. When a node forwards a route request packet to its neighbors, it also records in its tables the node from which the first copy of the request came. This information is used to construct the reverse path for the route reply packet. AODV uses only symmetric links because the route reply packet follows the reverse path of route request packet. As the route reply packet traverses back to the source, the nodes along the path enter the forward route into their tables. For route maintenance, when a source node moves, it can reinitiate route discovery to the destination. If one of the intermediate nodes moves, then the moved nodes neighbor realizes the link failure and sends a link failure notification to its upstream neighbors and so on till it reaches the source upon which the source can reinitiate route discovery if needed.

The difference between DSR and AODV is that in DSR, each packet carries full routing information, whereas in AODV, the packets carry the destination address. This means that AODV has potentially less routing overheads than DSR. The other difference is that the route replies in DSR carry the address of every node along the route, whereas in AODV, the route replies only carry the destination IP address and the sequence number.

The advantage of AODV is that it is adaptable to highly dynamic networks. However, node may experience large delays during route construction, and link failure may initiate another route discovery, which introduces extra delays and consumes more bandwidth as the size of the network increases.

3.2.2. Location Aided Routing Protocol (LAR)

The Location Aided Routing (LAR) [15] protocol is a reactive unicast routing scheme. In this, a source node estimates the current location range of the destination based on information of the last reported location and the mobility pattern of the destination. In this, an expected zone is defined as a region that is expected to hold the current location of the destination node. During route discovery procedure, the route request flooding is limited to a request zone, which contains the expected zone and location of the sender node. LAR decreases overhead of the route discovery by using the location information. It limits the search to a smaller request zone, causing significant reduction of the number of routing messages.

This protocol assumes that each node knows its location through a GPS. Two different LAR schemes were proposed in [15], the first scheme calculates a request zone which defines a boundary where the route request packets can travel to reach the required destination. The second scheme stores the coordinates of the destination in the route request packets. These packets can only travel in the direction where the relative distance to the destination becomes smaller as they travel from one hop to another. Both methods limit the control overhead transmitted through the network and hence conserve bandwidth. They will also determine the shortest path to

Copyright © 2010 SciRes.

the destination, since the route request packets travel away from the source and towards the destination.

The disadvantage of LAR protocol is that each node is required to carry a GPS. Another disadvantage is, especially for the first method, that protocols may behave similar to flooding protocols (e.g., DSR and AODV) in highly mobile networks.

3.3. Hybrid Routing Protocols

In *hybrid routing protocols*, some of the characteristics of proactive protocols and some of the characteristics of reactive protocols are combined into one to get better solution for mobile ad hoc networks. These protocols exploit the hierarchical network architecture and allow the nodes with close proximity to work together to form some sort of backbone, thus increasing scalability and reducing route discovery. Nodes within a particular geographical region are said to be within the routing zone of the given node. For routing within this zone, a table-driven approach is used. For nodes that are located beyond this zone, an on demand approach is used.

Some of the hybrid routing protocols are: Distributed Spanning Tree based Routing Protocol (DST), Core-Extraction Distributed Ad Hoc Routing protocol (CEDAR), Zone Routing Protocol (ZRP), Zone-based Hierarchical Link State Routing Protocol (ZHLS), Distributed Dynamic Routing protocol (DDR), Scalable Location Update Routing Protocol (SLURP), Hybrid Ad hoc Routing Protocol (HARP).

3.3.1. Zone Routing Protocol (ZRP)

The Zone Routing Protocol (ZRP) [16] is a hybrid routing protocol, where the network is divided into routing zones according to the distances between nodes and the routing zone defines a range (in hops) that each node is required to maintain network connectivity proactively. In this, proactive routing approach-Intra Zone Routing Protocol (IARP) is used inside routing zones and reactive routing approach-Inter Zone Routing Protocol (IERP) is used between routing zones. Therefore, for nodes within the routing zone, routes are immediately available. For nodes that lie outside the routing zone, routes are determined on-demand (*i.e.* reactively), and it can use any on-demand routing protocol to determine a route to the required destination. Route creation is done using a query-reply mechanism. During the forwarding of the query packet, a node identifies whether it is coming from its neighbor or not. If yes, then it marks all of its known neighboring nodes in its same zone as covered. A covered node is a node which belongs to the routing zone of a node that has received a route query. The query is thus relayed till it reaches the destination. The destination in turn sends back a reply message via the reverse path and creates the route.

ZRP is suitable for the networks with large span and diverse mobility patterns. The advantage of this protocol is that it has significantly reduced the amount of communication overhead when compared to pure proactive protocols. It also has reduced the delays associated with pure reactive protocols such as DSR, by allowing routes to be discovered faster. This is because, to determine a route to a node outside the routing zone, the routing only has to travel to a node which lies on the boundaries (edge of the routing zone) of the required destination. Since the boundary node would proactively maintain routes to the destination (*i.e.* the boundary nodes can complete the route from the source to the destination by sending a reply back to the source with the required routing address).

The disadvantage of ZRP is that for large values of routing zone, the protocol can behave like a pure proactive protocol, while for small values it behaves like a reactive protocol.

4. Overall Comparison of All Unicast Routing Protocols

Advantages and disadvantages of proactive, reactive and hybrid approaches are shown in **Table 1** and overall comparison of all unicast routing protocols are shown in **Table 2**.

Table 1. Advantages and disadvantages of proactive, reactive and hybrid routing protocols.

	Advantages	Disadvantages
Proactive	-Up-to-date routing information -Quick establishment of routes -Small delay -A route to every other node in the network is always available	-Slow convergence -Tendency of creating loops -Large amount of resources are needed -Routing information is not fully used
Reactive	-Reduction of routing load -Saving of resources -Loop-free	-Not always up-to-date routes -Large delay -Control traffic and overhead cost
Hybrid	-Scalability -Limited search cost -Up-to-date routing information within zones	-Arbitrary proactive scheme within zones -Inter-zone routing latencies -More resources for large size zones

Copyright © 2010 SciRes.

Table 2. Overall comparison of all unicast routing categories [20].

Routing Property	Proactive	Reactive	Hybrid
Routing Structure	Both flat and hierarchical	Mostly flat, except CBRP	Mostly hierarchical
Route Availability	Always available, if the nodes are reachable	Determined when needed	Depends on the location of the destination
Traffic Control Volume	Usually high	Low	Mostly lower than proactive and reactive
Mobility Handling Effects	Usually updates occur based on mobility at fixed intervals	ABR introduced LBQ, AODV uses local route discovery	Usually more than one path may be available
Storage Requirements	High	Usually lower than Proactive protocols	Usually depends on the size of each cluster
Delay Level	Small routes are predetermined	Higher than proactive	For local destinations small, since Inter-zone may be as large as reactive protocols
Scalability Level to Perform Efficient Routing	Usually up to 100 nodes	Source routing protocols up to few 100 nodes Point-to-point may scale higher	Designed for up to 1000 or more nodes

5. Performance Evaluation and Analysis

5.1. Simulation Model

The simulations were performed using the network simulator *QualNet* 4.0 which is a discrete event simulator developed by Scalable Networks. It is extremely scalable accommodating high fidelity models of networks. QualNet makes good use of computational resources and models large-scale networks with heavy traffic and mobility in reasonable simulation times.

The study has been done to compare the efficiency of the various categories of routing protocols: DSDV, AODV, FSR, LAR, OLSR, STAR, and ZRP. The overall goal of our simulation study is to analyze the behavior and performance of the protocols under a range of various scenarios. Simulations have been run using a mobile ad hoc networks composed of 10, 15, 25, 50 and 75 nodes moving over a rectangular 1500 m × 1500 m space and operating over 30 seconds of simulation time. All nodes move according to the random way point mobility model. The traffic sources in our simulation are constant bit rate (CBR) traffic. Each traffic source originates 512 bytes data packets. The simulation parameters are shown in **Table 3**.

Table 3. Simulation parameters.

Parameter	Value
Number of nodes	10, 15, 25, 50, 75
Number of traffic sources	3
Simulation Time	30 Seconds
Traffic Type	CBR
Packet Size	512 bytes
Topology Size	1500m × 1500m
Mobility Pattern	Random way point

5.2. Simulation Metrics

The metrics that are used to evaluate the performance of the routing protocols are: throughput, average end-to-end delay, average jitter, total packets received, packet delivery ratio and routing overhead.

Throughput is the average rate of successful message/ packets delivery over a communication channel. *i.e.* Throughput is the measure of how fast we can actually send the packets through network. The throughput is usually measured in bits per second (bit/s or bps), and sometimes in data packets per second or data packets per time slot.

Average end-to-end delay is the delay experienced by a packet from the time it was sent by a source till the time it was received successfully at the destination. *i.e.*, the *end-to-end delay* is the time a data packet is received by the destination minus the time the data packet is generated by the source. Average end-to-end delay includes all possible delays caused by buffering during route discovery latency, queuing at the interface queue, retransmission delays at the MAC, and propagation and transfer times of data packets.

Average jitter measures the packet delay variation. It is calculated as the average of the difference of the inter arrival time between subsequently received packets.

Total packets received is the number of packets received by the TCP sink at the final destination and the number of packets generated by the traffic sources.

Packet delivery ratio is the ratio of the number of data packets successfully delivered to the destinations to those generated by the constant bit rate (CBR) sources. *Routing overhead* is the number of control packets produced per mobile node. Control packets include route requests, replies and error messages. The routing load specifies the load over communications links for traffic flow.

Copyright © 2010 SciRes.

5.3. Simulation Scenarios

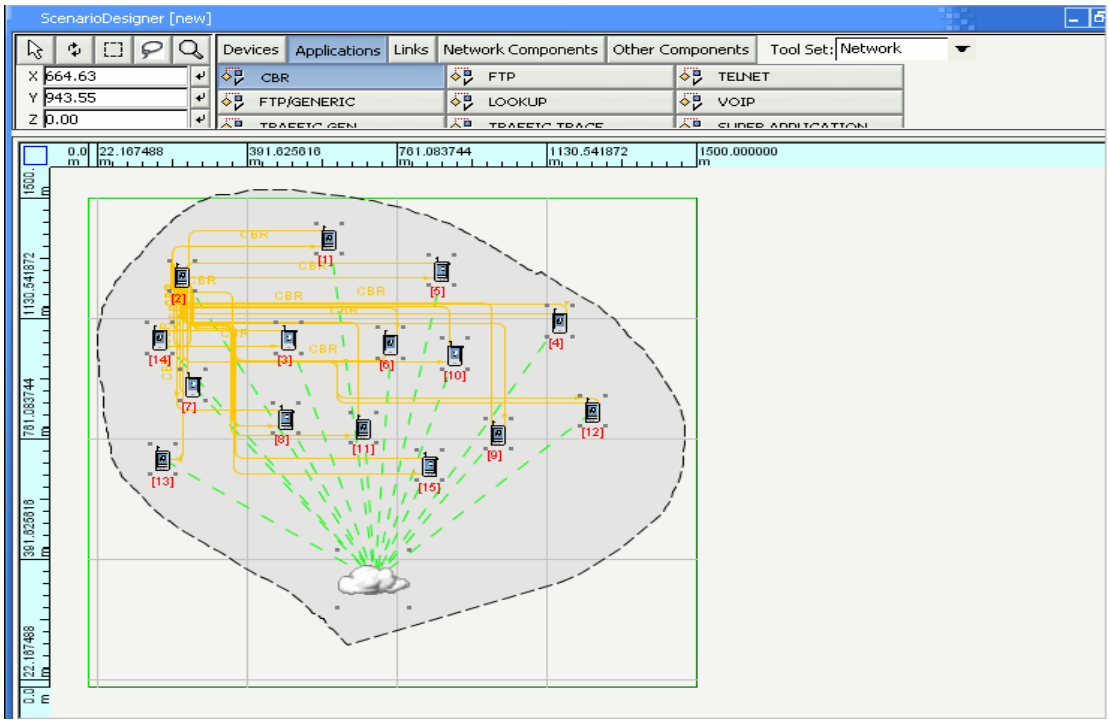

Figure 4. Designer window scenario for 15 nodes.

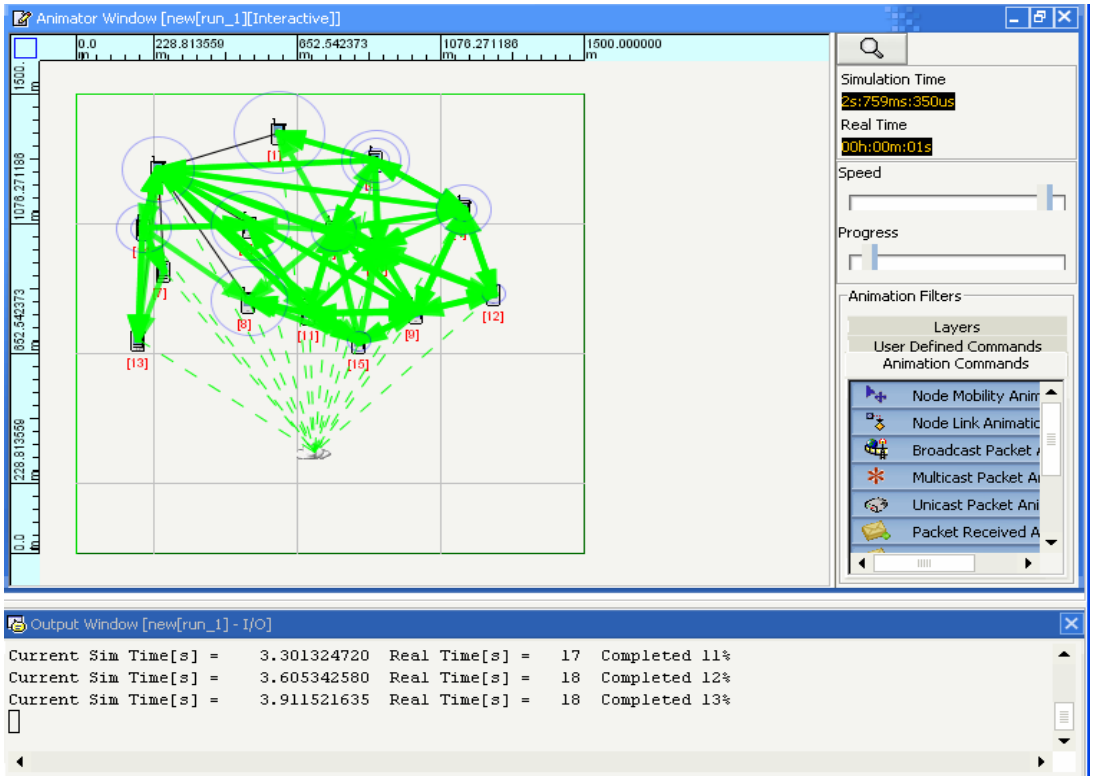

Figure 5. Animator window scenario for 15 nodes.

Copyright © 2010 SciRes.

Table 4. Metric values for 15 nodes.

Protocols/ Parameters	DSDV	AODV	FSR	LAR	OLSR	STAR	ZRP
Throughput(10^4)	5.85	5.85	4.0	6.1	5.7	3.65	4.85
End-To-End Delay	-	-	1.17	3.25	0.08	0.4	1.56
Average Jitter	-	-	3.48	2.5	0.5	0.4	4.68
Total Packets Received (10^2)	3.35	3.35	1.9	3.22	2.97	1.83	2.56

Table 5. Metric values for 25 nodes.

Protocols/ Parameters	DSDV	AODV	FSR	LAR	OLSR	STAR	ZRP
Throughput(10^5)	0.99	1.01	0.63	0.98	0.94	0.51	0.48
End-To-End Delay	-	-	2.8	11.6	0.1	0.6	3.8
Average Jitter	0.1	-	1.2	11.7	0.6	0.6	3.5
Total Packets Received (10^2)	5.6	5.7	2.8	5.4	4.8	2.7	2.4

Table 6. Metric values for 50 nodes.

Protocols/ Parameters	DSDV	AODV	FSR	LAR	OLSR	STAR	ZRP
Throughput(10^5)	2	0.07	1.24	1.17	0.98	1.96	0.75
End-To-End Delay	-	-	7.5	46	0.75	31	40.8
Average Jitter	-	-	20.75	21.3	0.5	36.75	32.5
Total Packets Received(10^3)	1.16	1.16	0.53	1.13	0.08	0.61	0.41

Table 7. Metric values for 75 nodes.

Protocols/ Parameters	DSDV	AODV	FSR	LAR	OLSR	STAR	ZRP
Throughput(10^5)	3.14	3.14	1.87	1.76	3.04	1.28	0.38
End-To-End Delay	-	-	13	78	1	67	42
Average Jitter	-	-	16	96	5	50	25
Total Packets Received (10^3)	1.76	1.76	0.78	0.84	1.54	0.8	0.25

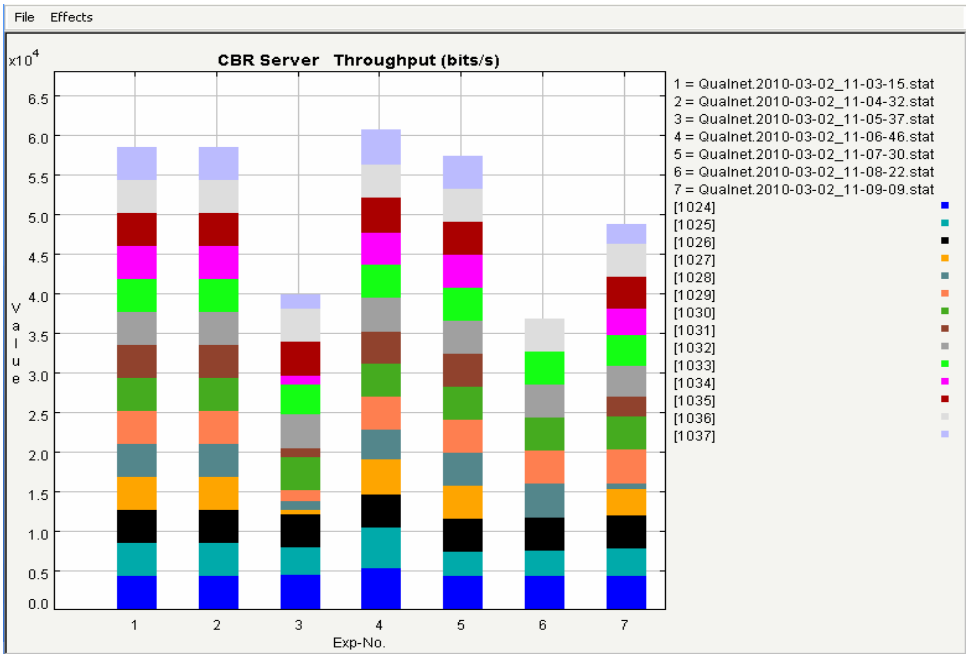

Figure 6. Multi experimental comparison chart (15 nodes) for the metric: throughput.

Copyright © 2010 SciRes.

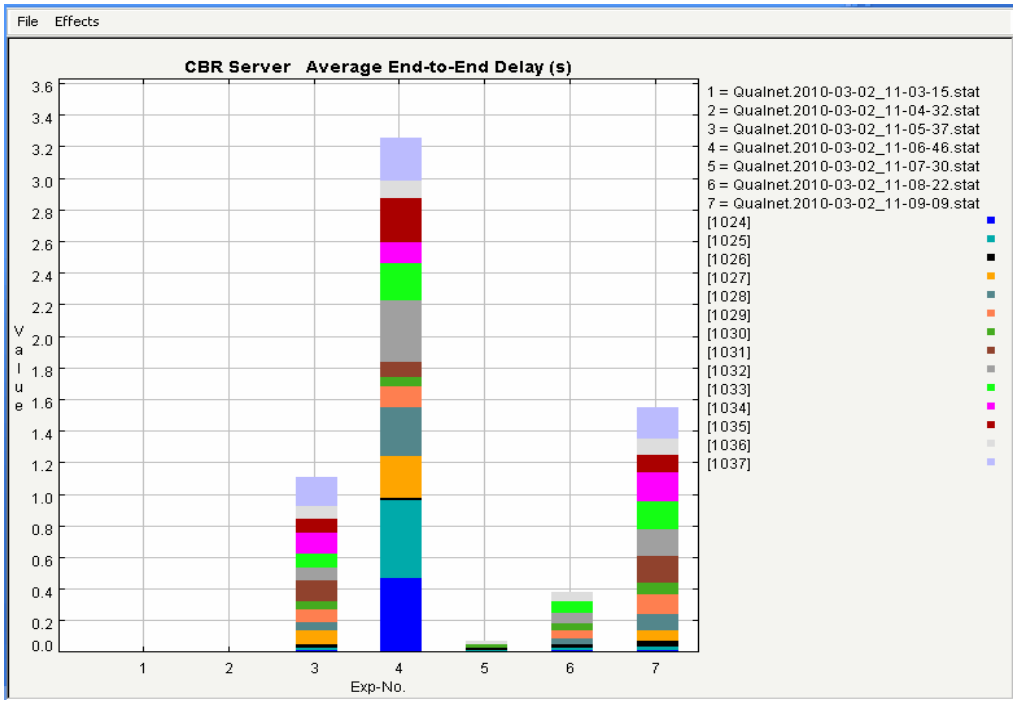

Figure 7. Multi experimental comparison chart (15 nodes) for the metric: Average end-to-end delay.

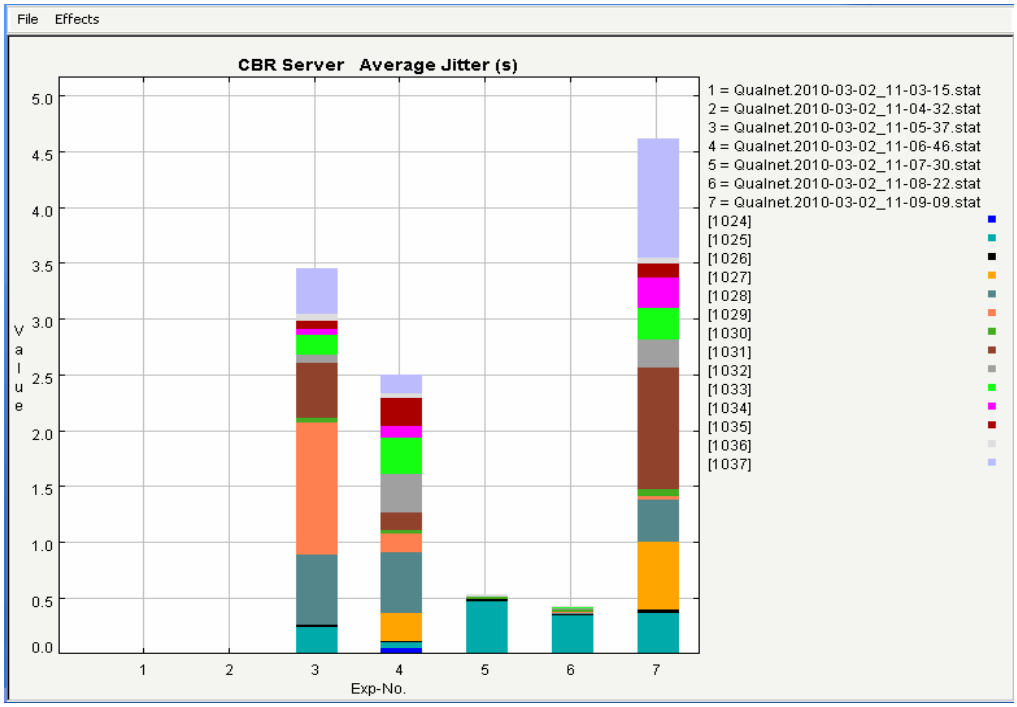

Figure 8. Multi experimental comparison chart (15 nodes) for the metric: Average jitter.

Copyright © 2010 SciRes.

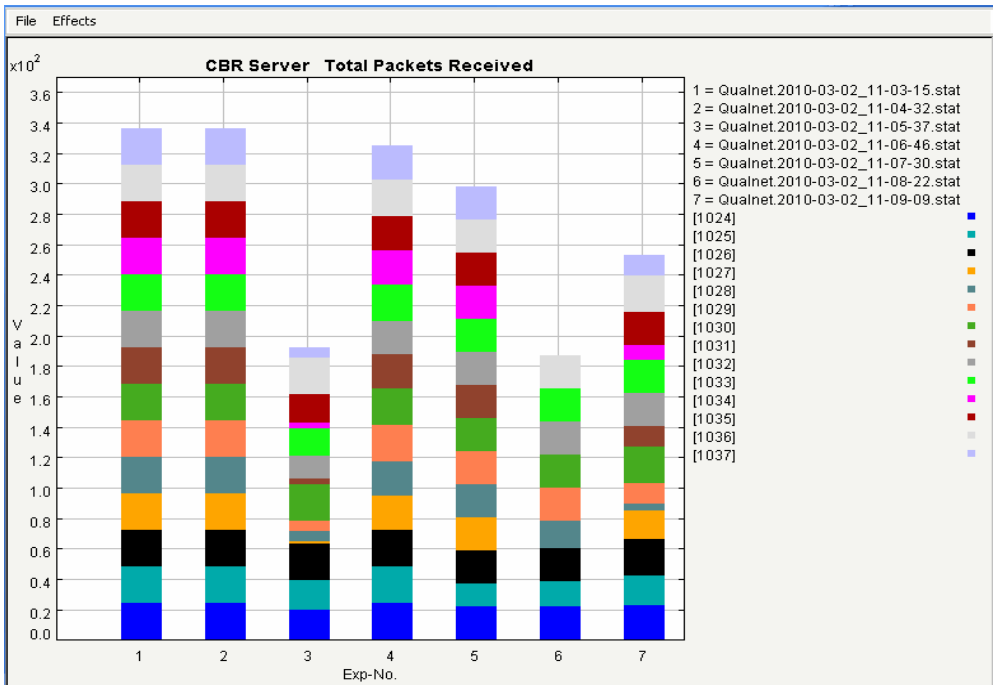

Figure 9. Multi experimental comparison chart (15 nodes) for the metric: Total packets received.

5.4. Simulation Results and Analysis

The simulation study has been done using the network simulator *QualNet* 4.0 for performance comparison of the protocols: DSDV, AODV, FSR, LAR, OLSR, STAR and ZRP. The all seven routing protocols result in improvements of the performance metrics that include throughput, jitter, end-to-end delay and total packets received.

It was observed from the simulation that DSDV and AODV gives nearly same and maximum throughput in small sized networks. Throughput of FSR, LAR, OLSR, and STAR is increasing as the network size is increasing, but OLSR performs well in large sized networks. Throughput of ZRP is well and it is nearer for small and large networks, but for large sized networks it is decreasing. For end-to-end delay and average jitter, the performance of DSDV and AODV is better than FSR, LAR, OLSR, STAR and ZRP in case of small sized networks. In medium and large sized networks, the end-to-end delay and average jitter of AODV and DSDV protocols are same.

The improvements shown in LAR are gradually increasing than others. Hence, it can be concluded that LAR is the best among the studied routing protocols.

6. Conclusions

In this article, the classifications of routing protocols for ad hoc wireless networks were discussed. In proactive protocols, each node maintains network connectivity and up-to-date routing information to all the nodes in the network. In reactive protocols, a node finds the route to a destination when it desires to send packets to the destination. In hybrid routing protocols, some of the characteristics of proactive and some of the characteristics of reactive are combined, by maintaining intra-zone information proactively and inter-zone information reactively, into one to get better solution for mobile ad hoc networks.

Generally speaking, reactive protocols require fewer amounts of memory, processing power, and energy than that of the proactive protocols. The mobility and traffic pattern of the network must play the key role for choosing an appropriate routing strategy for a particular network. It is quite natural that one particular solution cannot be applied for all sorts of situations and, even if applied, might not be optimal in all cases. Often it is more appropriate to apply a hybrid protocol rather than a strictly proactive or reactive protocol as hybrid protocols often possess the advantages of both types of protocols.

DSDV and GSR uses destination sequence numbers to keep routes up-to-date and loop-free. HSR and ZHLS are hierarchical routing protocols. FSR reduces the size of tables to be exchanged by maintaining less accurate information about nodes farther away. CGSR and CBRP are cluster-based routing protocol where nodes are grouped into clusters. AODV is an on-demand version of DSDV routing protocol. ABR uses the degree of associativity to select routes and a localized broadcast query is initiated when a link goes down. WRP maintains the best-path information to a destination, avoids routing loops during route discovery process, and converges quickly after a link failure. In LAR, the route request packets propagate in the request zone only. DSR is a source routing proto-

Copyright © 2010 SciRes.

col where the route is in each packet. DSR had higher routing overhead as compared to AODV. ZHLS and SLURP are highly adaptable to changing topology, since only the node ID and zone ID of the destination is required for routing to occur. They do not use a cluster-head to coordinate data transmission, which means that a single point of failure and performance bottlenecks can be avoided. The ZRP routing protocol is designed to increase the scalability of mobile ad hoc networks. The advantage of this protocol is that it maintains strong network connectivity (proactively) within the routing zones while determining remote route (outside the routing zone) quicker than flooding.

The simulation study has been done using the network simulator *QualNet* 4.0 for performance comparison of the protocols: DSDV, AODV, FSR, LAR, OLSR, STAR and ZRP. The improvements shown in LAR are gradually increasing than others. Hence, it can be concluded that LAR is the best among the studied routing protocols.

7. References

[1] C. K. Tok, "Ad Hoc Mobile Wireless Networks: Protocols and Systems," Pearson Education, Boston, 2002, pp. 28-30.

[2] X. Cheng, X. Huang and D. Z. Du, "Ad Hoc Wireless Networking," Kluwer Academic Publishers, Boston, 2006, pp. 319-364.

[3] C. S. R. Murthy and B. S Manoj, "Ad Hoc Wireless Networks: Architectures and Protocols," Pearson Education, Boston, 2006.

[4] P. Mohaptra and S. V. Krishnamurthy, "Ad Hoc Networks: Technologies and Protocols," Springer International Edition, New Delhi, 2005.

[5] F. Anjum and P. Mouchtaris, "Security for Wireless Ad hoc Networks," John Wiley & Sons, Chichester, 2007.

[6] S. Misra, I. Woungang and S. C. Misra, "Guide to Wireless Ad Hoc Networks," Springer, Berlin, 2009, pp. 59-96.

[7] S. Basagni, M. Conti, S. Giordono and I. Stojmenovic, "Mobile Ad Hoc Networks," John Wiley & Sons, Chichester, 2003.

[8] C. E. Perkins, "Ad Hoc Networks," Addition Wesley, 2001.

[9] C. E. Perkins and P. Bhagwat, "Highly Dynamic Destination Sequenced Distance Vector Routing (DSDV) for Mobile Computers," *ACM Computer Communication Review, Special Interest Group on Data Communication* (*ACM SIGCOMM*'94), Vol. 24, No. 4, 1994, pp. 234-244.

[10] E. M. Royer and C. K. Toh, "A Review of Current Routing Protocols for Ad Hoc Mobile Wireless Networks," *IEEE Personal Communications*, Vol. 6, No. 2, 1999, pp. 46-55.

[11] P. Jacquet, P. Muhlethaler, T. Clausen, A. Laouiti, A. Qayyum and L. Viennot, "Optimized Link State Routing Protocol for Ad Hoc Networks," *IEEE International Multi Topic Conference* (*IEEE INMIC*), Islamabad, 2001, pp. 62-68.

[12] M. Gerla, X. Hong and G. Pei, "Fisheye State Routing (FSR) Protocol for Ad Hoc Networks," 2002. http://tools.ietf.org/html/draft-ietf-manet-fsr-03

[13] J. J. Garcia-Luna-Aceves and M. Spohn, "Source-Tree Routing in Wireless Networks," *Proceedings of the Seventh Annual International Conference on Network Protocols*, Toronto, October 1999, p. 273.

[14] C. E. Perkins, E. M. Belding-Royer and S. R. Das, "Ad hoc On-Demand Distance Vector (AODV) Routing," 2002. http://tools.ietf.org/html/draft-ietf-manet-aodv-11

[15] Y. B. Ko and N. H. Vaidya, "Location-Aided Routing (LAR) in Mobile Ad Hoc Networks," *Wireless Networks*, Kluwer Academic Publishers, Vol. 6, No. 4, 2000, pp. 307-321.

[16] Z. J. Hass, M. R. Pearlman and P. Samar, "Zone Routing Protocol for Ad Hoc Networks," 2002. http://www.ietf.org/proceedings/55/I-D/draft-ietf-manet-zone-zrp-04.txt

[17] M. Abolhasan, T. Wysocki and E. Dutkiewicz, "A Review of Routing Protocols for Mobile Ad Hoc Networks," *Ad Hoc Networks*, Vol. 2, No. 2, 2004, pp. 1-22.

[18] A. C. Sun, "Design and Implementation of Fisheye Routing Protocol for Mobile Ad Hoc Networks," Massachusetts Institute of Technology, 2000.

[19] M. Mauve, J. Widmer and H. Hartenstein, "A Survey on Position Based Routing in Mobile Ad hoc Networks," *IEEE Network*, Vol. 15, No. 6, 2001, pp. 30-39.

[20] M. Abolhasan, T. Wysocki and E. Dutkiewicz, "A Review of Routing Protocols for Mobile Ad Hoc Networks," *Ad Hoc Networks*, Vol. 2, No. 1, 2004, pp. 1-22.

Copyright © 2010 SciRes.

Int. J. Communications, Network and System Sciences, **2010, 3, 523-529**
doi:10.4236/ijcns.2010.36070 Published Online June 2010 (http://www.SciRP.org/journal/ijcns/).

Scientific Research

Nonlinear Blind Equalizers: NCMA and NMCMA

Donglin Wang, Sandeep Chandana
Department of Electrical and Computer Engineering, University of Calgary, Calgary, Canada
E-mail: {*dowang, schandan*} *@ucalgary.ca*
Received March 5, 2010; *revised April* 19, 2010; *accepted May* 20, 2010

Abstract

This paper proposes two nonlinear blind equalizers: the nonlinear constant modulus algorithm (NCMA) and the nonlinear modified constant modulus algorithm (NCMA) by applying a nonlinear transfer function (NTF) into constant modulus algorithm (CMA) and modified constant modulus algorithm (MCMA), respectively. The effect of the NTF on CMA and MCMA is theoretically analyzed, which implies that the NTF can make their decision regions much sharper so that the proposed two nonlinear blind equalizers are more robust against the convergency error compared to their linear counterparts. The embedded single layer in NCMA and NMCMA simultaneously guarantees a comparably speedy convergency. On 16-quadrature amplitude modulation (QAM) symbols, computer simulations show that NCMA achieves an 8dB lower convergency mean square error (MSE) than CMA, and NMCMA achieves a 15dB lower convergency MSE than MCMA.

Keywords: Nonlinear Blind Equalizer, Nonlinear Transfer Function (NTF), CMA, Nonlinear CMA (NCMA), Nonlinear MCMA (NMCMA)

1. Introduction

Constant modulus algorithm (CMA) [1-6] is widely used for blind equalization [2,5,6,7-10] for constant modulus transmissions in communication systems in order to overcome the propagation channel corruption, mitigate the inter-symbol interference (ISI) and recover the transmitted symbols, which usually has a satisfied performance in common situations. However, under a complicated multipath channel, the transmitted symbols suffer from severe distortion and CMA will perform poor for multi-modulus symbols, *i.e.* for high-order quadrature amplitude modulation (QAM) symbols, mainly due to the inability of CMA on phase error correction [11].

To suppress the convergence error and improve the equalization performance for multi-modulus symbols, [11-14] proposed a classical modified constant modulus algorithm (MCMA), in which the real component and the imaginary component of the equalizer output are respectively considered to compress the phase error, leading to a better performance. However, its performance is not good enough in some severe cases, since its decision region is comparably smooth, which does not tolerate the convergency error very much.

The method for further improvement is to bring in nonlinearity instead of linearity, which can be realized by utilizing multilayer architecture, nonlinear transfer function (NTF) [15] or neural network [16-18]. However, as a tradeoff, the complicated multiple architecture results in a slower convergency. As we all know, the speedy convergency is significant for adaptive blind equalization. Consequently, in this paper, we preferentially consider introducing a NTF into blind equalization to improve the performance. A NTF, $f(x) = x + \alpha \sin(\pi x)$, is proposed in [18] for blind equalizer according to its provided properties. However, there is a remaining unsolved question: in essence, why can this NTF be helpful for equalization performance? Or equivalently, what is the theoretical effect of NTF on equalization performance? This paper will answer this question via theoretical analysis. The following theoretical derivation provides that the NTF can make the decision region much sharper so that the proposed nonlinear blind equalizers are more robust against the convergency error. Based on this discovery, by applying the nonlinear transfer function (NTF) to CMA and MCMA, the nonlinear CMA (NCMA) and nonlinear modified CMA (NMCMA) are thus proposed, and their adaptive learning rules are also theoretically derived in this paper.

The remainder of this paper is organized as follows. Section II theoretically analyzes the effect of the NTF on blind equalizers. Based on the analysis given in Section 2, the nonlinear blind equalizer, NCMA, is proposed in Section III. Moreover, another blind equalizer, NMCMA, is proposed in Section 4. Simulation results of the proposed

Copyright © 2010 SciRes.

nonlinear blind equalizers on 16-QAM symbols are reported in Section 5, which are compared to their linear counterparts, followed by conclusion in Section 6.

Notation: $E[\bullet]$ represents expectation of a random variable. $|\bullet|$ denotes the modulus of a complex number or the absolute value of a real number. The superscripts $(\bullet)^*$ and $(\bullet)'$ denote the conjugate and derivative, respectively. Both $\mathrm{Re}\{\bullet\}$ and $(\bullet)_R$ denote the real component while both $\mathrm{Im}\{\bullet\}$ and $(\bullet)_I$ denote the imaginary component.

2. Effect of NTF

2.1. CMA

The cost function of CMA can be expressed as [1]

$$J_{CMA}(n) = \frac{1}{4}E\left[\left(|y(n)|^2 - R_2\right)^2\right] \quad (1)$$

where n denotes the time index; $y(n)$ represents the equalized symbol; assuming that $s(n)$ is the complex-valued transmitted symbol, the constant modulus, R_2, is given by $R_2 = \dfrac{E\left[|s(n)|^4\right]}{E\left[|s(n)|^2\right]}$. The 3D performance function of CMA, J_{CMA}, is shown versus $y(n)$ in [1].

2.2. Performance Function without NTF

Considering the case without a NTF in CMA [1],

$$y(n) = X^T(n)W = \sum_{m=0}^{M-1} x(n-m)w_m \quad (2)$$

where, $X(n) = \left[x(n), x(n-1), \cdots, x(n-M+1)\right]^T$ is the corrupted signal at the receiver, which is also the input signal of the equalizer, and $W = \left[w_0, w_1, \cdots, w_{M-1}\right]^T$ is the adaptive weight vector. Assuming keeping all weights unchanged except w_p, $0 \le p \le M-1$, (2) can be expressed as

$$\begin{aligned} y(n) &= \sum_{m=0, m\neq p}^{M-1} x(n-m)w_m + x(n-p)w_p \\ &= C + x(n-p)w_p \end{aligned} \quad (3)$$

where $C = \sum_{m=0, m\neq p}^{M-1} x(n-m)w_m$ is a constant in this case. Using (3) together with (1), the 2D performance function, J_{CMA}, is shown versus $\mathrm{Re}\{w_p\}$ in **Figure 1**, similar as

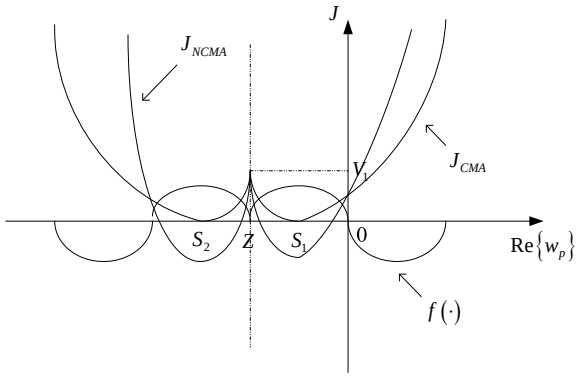

Figure 1. Comparison of performance functions, J, versus $\mathrm{Re}\{w_p\}$, where $f(\bullet)$ represents the NTF, S_1 and S_2 correspond to two stable minimum values and V_1 corresponds to an unstable local maximum.

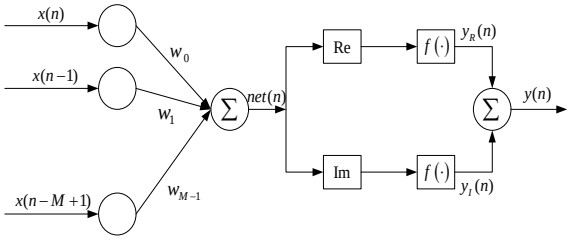

Figure 2. Architecture representation for the proposed nonlinear blind equalizers: NCMA and NMCMA, where it is noticed that the real component and the imaginary component of the received symbols are separately considered.

J_{CMA} versus $y(n)$ in [1]. In **Figure 2**, two stable points, S_1 and S_2, are given by $S_1 = \mathrm{Re}\left\{\dfrac{-\sqrt{R_2}e^{j\theta} - C}{x(n-p)}\right\}$ and $S_2 = \mathrm{Re}\left\{\dfrac{\sqrt{R_2}e^{j\theta} - C}{x(n-p)}\right\}$, respectively, θ denotes an arbitrary phase; $Z = \mathrm{Re}\left\{\dfrac{-C}{x(n-p)}\right\}$; and the value at Z is given by $V_1 = \dfrac{R_2^2}{4}$.

2.3. Performance Function with NTF

Let us consider the blind equalizer with a NTF, *i.e.* NCMA. Define its corresponding cost function by $J_{NCMA}(n) \triangleq J_{CMA}(n)$, *i.e.*

$$J_{NCMA}(n) = J_{CMA}(n) = \frac{1}{4}E\left[\left(|y(n)|^2 - R_2\right)^2\right]$$

Without loss of generality, a NTF with the expression of $f(x) = x + \alpha\sin(2\pi fx)$, where α is a nonlinear

Copyright © 2010 SciRes.

coefficient and f denotes the frequency of the sine function, is considered in this paper for performance analysis. With this NTF, based on the proposed architecture as shown in **Figure 2**, we have

$$\begin{aligned} y(n) &= f\left(\mathrm{Re}\left\{X^T(n)W\right\}\right) + jf\left(\mathrm{Im}\left\{X^T(n)W\right\}\right) \\ &= C + x(n-p)w_p \\ &+ \alpha\sin\left(2\pi f\ \mathrm{Re}\left\{C + x(n-p)w_p\right\}\right) \\ &+ j\alpha\sin\left(2\pi f\ \mathrm{Im}\left\{C + x(n-p)w_p\right\}\right) \end{aligned} \tag{4}$$

Since the performance function is symmetrical around the $J-axis$, *i.e.* the cost function is independent with the phase of $y(n)$ or w_p, without loss of generality, let us consider the simplest case, *i.e.* w_p is real. In this case, (4) can be approximated as

$$\begin{aligned} \frac{y(n)-C}{x(n-p)} &= w_p + \frac{\alpha - C}{x(n-p)}\sin\left(2\pi f\ \mathrm{Re}\left\{C + x(n-p)w_p\right\}\right) \\ &+ j\frac{\alpha - C}{x(n-p)}\sin\left(2\pi f\ \mathrm{Im}\left\{C + x(n-p)w_p\right\}\right) \\ &\overset{(a)}{\approx} w_p + \frac{\alpha - C}{x(n-p)}\sin\left(2\pi f\ \mathrm{Re}\left\{C + x(n-p)w_p\right\}\right) \\ &\overset{(b)}{\approx} w_p + \frac{\alpha - C}{x(n-p)}\sin\left(2\pi f\left|x(n-p)\right|w_p\right) \end{aligned} \tag{5}$$

where, the approximation (a) is based on the fact that the closer the directions of two vectors with fixed modules, the bigger their summation, and the approximation (b) is true because C in (5) is a constant, same as that in (3) and the value of the sine function in (5) is determined by the item containing w_p. Furthermore, we have

$$y(n) \approx \left[C + x(n-p)w_p\right] + \alpha\sin\left(2\pi f\left|x(n-p)\right|w_p\right) \tag{6}$$

Based on (6) together with (1), the 2D performance function, J_{NCMA}, is shown versus $\mathrm{Re}\left\{w_p\right\}$ in **Figure 1**, compared to that without NTF. One can see that using this NTF, its performance function becomes sharper than its previous linear counterpart. Once the convergency point is not exactly the minimum value but one of its surrounding points, namely, there is an estimation bias, *i.e.* δW, its estimation error gets smaller after implanting this NTF. In other words, NCMA is more robust against the convergency error than CMA. It is noticed that, the NTF will provide a good equalization performance under the constraint that $2\pi f\left|x(n-p)\right| \le \frac{\pi}{2}$, *i.e.* $0 < f \le \frac{1}{4\sqrt{R_2}}$. Particularly, when $f = \frac{1}{4\sqrt{R_2}}$, the NTF exhibits the optimal equalization performance.

2.4. Discussion and Extension

As shown in **Figure 1**, where the cost function, J, is plotted versus the adaptive weights, $\mathrm{Re}\left\{w_p\right\}$, J_{NCMA} looks similar with J_{CMA} except that it has a sharper decision region than J_{CMA}. The resulting sharper decision region will lead to a better equalization performance in the end. On the other hand, denote by J_{MCMA} and J_{NMCMA} the cost functions for MCMA and NMCMA, respectively. Since MCMA is similar to CMA except that in NMCA, the real part and the imaginary part are separately considered, after adding a NTF into the linear equalizer, the relationship between J_{NMCMA} and J_{MCMA} is the same with that between J_{MCMA} and J_{CMA}. Therefore, one can know that J_{NMCMA} also looks similar with J_{MCMA} except that it has a sharper decision region than J_{MCMA}.

3. Proposed NCMA

In **Figure 2**, $x(n), x(n-1), \cdots, x(n-M+1)$, as mentioned, are the corrupted symbols at the receiver, $w_0, w_1, \cdots, w_{M-1}$, as mentioned, are the equalizer taps with the length of M, and the variable *net* is an intermediate variable for convenience. For a time index of n, the input and its corresponding output can be formulated as

$$net(n) = X^T(n)W \tag{7}$$

and

$$y(n) = y_R(n) + jy_I(n), \tag{8}$$

where

$$y_R(n) = f\left(net_R(n)\right) \tag{9}$$

and

$$y_I(n) = f\left(net_I(n)\right). \tag{10}$$

Furthermore, the real component and the imaginary component of $net(n)$ can be obtained as

$$net_R(n) = \sum_{m=0}^{M-1}\left[x_R(n-m)w_{m,R} - x_I(n-m)w_{m,I}\right] \tag{11}$$

and

$$net_I(n) = \sum_{m=0}^{M-1}\left[x_R(n-m)w_{m,I} - x_I(n-m)w_{m,R}\right]. \tag{12}$$

Based on (1), using the statistic gradient descent (SGD) in terms of w_p, we have

Copyright © 2010 SciRes.

$$\frac{\partial J_{NCMA}(n)}{\partial w_p} = \left(|y(n)|^2 - R_2\right)|y(n)| \times \left(\frac{\partial |y(n)|}{\partial w_{p,R}} + j\frac{\partial |y(n)|}{\partial w_{p,I}}\right), \tag{13}$$

where

$$\frac{\partial |y(n)|}{\partial w_{p,R}} = f\left(net_R(n)\right) f'\left(net_R(n)\right) x_R(n-p) + f\left(net_I(n)\right) f'\left(net_I(n)\right) x_I(n-p) \tag{14}$$

and

$$\frac{\partial |y(n)|}{\partial w_{p,I}} = f\left(net_R(n)\right) f'\left(net_R(n)\right) x_I(n-p) + f\left(net_I(n)\right) f'\left(net_I(n)\right) x_R(n-p). \tag{15}$$

Assuming μ is the learning rate, the weights update from the *nth* step to the $(n+1)th$ step can be expressed as

$$W(n+1) = W(n) - \mu e(n) X^*(n)$$
$$e(n) = \left(|y(n)|^2 - R_2\right)|y(n)| f\left(net_R(n)\right) f'\left(net_R(n)\right) + j\left(|y(n)|^2 - R_2\right)|y(n)| f\left(net_I(n)\right) f'\left(net_I(n)\right) \tag{16}$$

4. Proposed NMCMA

The cost function of NMCMA is the same as MCMA shown in [11] and [12]. In order to derive the NMCMA using SGD, the expectation operation is removed and the resulting cost function, J_{NMCMA}, is given by

$$J_{NMCMA}(n) = J_R(n) + J_I(n) \tag{17}$$

where

$$J_R(n) = \frac{1}{4}\left[\left(|y_R(n)|^2 - R_{2,R}\right)^2\right] \tag{18}$$

and

$$J_I(n) = \frac{1}{4}\left[\left(|y_I(n)|^2 - R_{2,I}\right)^2\right]. \tag{19}$$

Similar to the derivation in NCMA, considering w_p, we have

$$\frac{\partial J_{NMCMA}(n)}{\partial w_p} = \left(|y_R(n)|^2 - R_{2,R}\right)|y_R(n)|\frac{\partial y_R(n)}{\partial w_p} + \left(|y_I(n)|^2 - R_{2,I}\right)|y_I(n)|\frac{\partial y_I(n)}{\partial w_p}, \tag{20}$$

Where

$$\frac{\partial y_R(n)}{\partial w_p} = \frac{\partial y_R(n)}{\partial w_{p,R}} + j\frac{\partial y_R(n)}{\partial w_{p,I}} = f'\left(net_R(n)\right) x_R(n-p) - jf'\left(net_R(n)\right) x_I(n-p) \tag{21}$$

and

$$\frac{\partial y_I(n)}{\partial w_p} = \frac{\partial y_I(n)}{\partial w_{p,R}} + j\frac{\partial y_I(n)}{\partial w_{p,I}} = f'\left(net_I(n)\right) x_I(n-p) - jf'\left(net_I(n)\right) x_R(n-p). \tag{22}$$

Organizing (19)-(21), and assuming μ as the learning rate, the weights update from the *n*th step to the $(n+1)th$ step can be expressed as

$$W(n+1) = W(n) - \mu e(n) X^*(n), \tag{23}$$

where

$$e(n) = e_R(n) + je_I(n), \tag{24}$$

where

$$e_R(n) = \left(|y_R(n)|^2 - R_{2,R}\right)|y_R(n)| f'\left(net_R(n)\right) \tag{25}$$

and

$$e_I(n) = \left(|y_I(n)|^2 - R_{2,I}\right)|y_I(n)| f'\left(net_I(n)\right). \tag{26}$$

5. Computer Simulations

The proposed NCMA and NMCMA are demonstrated by using the 16-QAM symbols through a multipath channel. Their performances are compared to those of the pre-existing CMA and MCMA. A typical complex-valued 10-path communication propagation channel, labeled $H(z)$ [18], is used in this simulation, which is given by

$$H(z) = (0.0410 + j0.0109) + (0.0495 + j0.0123)z^{-1} + (0.0672 + j0.0170)z^{-2} + (0.0919 + j0.0235)z^{-3} + (0.7920 + j0.1281)z^{-4} + (0.3960 + j0.0871)z^{-5} + (0.2715 + j0.0498)z^{-6} + (0.2291 + j0.0414)z^{-7} + (0.1287 + j0.0154)z^{-8} + (0.1032 + j0.0119)z^{-9}. \tag{27}$$

We set signal-to-noise ratio (SNR) to 30dB for all cases. For 16-QAM symbols, the constant modulus, R_2, is equal to 13.2. The real component, $R_{2,R}$, and the imaginary component, $R_{2,I}$, are both equal to 8.2. The length of NCMA, M, is set as 15, the same as CMA. The length of NMCMA, M, is set as 21, the same as MCMA. The adaptation step-size is set as 0.00001 for all. All initialized weights are set randomly with small values of approximately 10^{-5} except for the center weights,

Copyright © 2010 SciRes.

which are set as 1.0 + *j*0. The NTF $f(x) = x + \alpha \sin(2\pi fx)$ is used, where the nonlinear coefficient α is set as 0.3 and the frequency of the sine function, f, is chosen as $\frac{1}{4\sqrt{R_2}}$ for NCMA, and $\frac{1}{4\sqrt{R_{2,R}}}$ or $\frac{1}{4\sqrt{R_{2,I}}}$ for NMCMA.

After 12000 training symbols, the following 2000 received symbols are tested for evaluating the equalization performance. The symbols' constellation after CMA equalizer is illustrated in **Figure 3**, whose estimation error is comparatively large. For comparison, the symbol's constellation after NCMA equalizer is shown in **Figure 4**, where the equalized symbols more concentrate on their supposed position and their bias are much smaller. To be clear, the MSEs of CMA and MCMA are plotted in **Figure 5**. One can see that, NCMA, with the MSE of approximate –13 dB, performs better than CMA, with the MSE of approximately –7 dB.

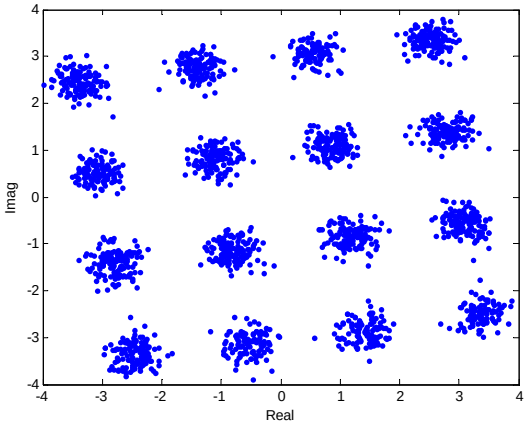

Figure 3. Constellation of 16-QAM symbols after CMA equalizer.

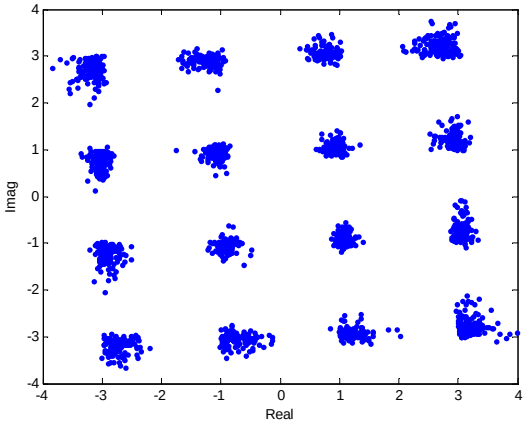

Figure 4. Constellation of 16-QAM symbols after the proposed NCMA equalizer.

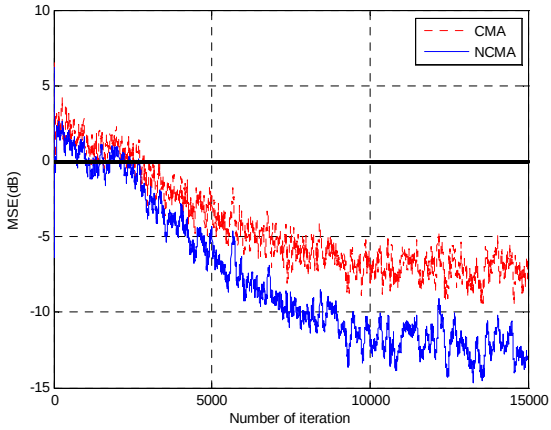

Figure 5. Performance comparison of CMA and the proposed NCMA in terms of MSE.

Similarly, the symbols' constellation after MCMA equalizer is illustrated in **Figure 6**, whose estimation error is comparatively large. For comparison, the symbol's constellation after NMCMA equalizer is shown in **Figure 7**, where the equalized symbols much more concentrate on their supposed position and their bias are much smaller. To be clear, the MSEs of MCMA and NMCMA are plotted in **Figure 8**. One can see that, NMCMA, with the MSE of approximately –30 dB, performs better than MCMA, with the MSE of approximately –15 dB.

5. Conclusions

Two Nonlinear blind equalizers: NCMA and NMCMA, were proposed in this paper by applying the NTF into the existing CMA and MCMA, respectively. The NTF effect

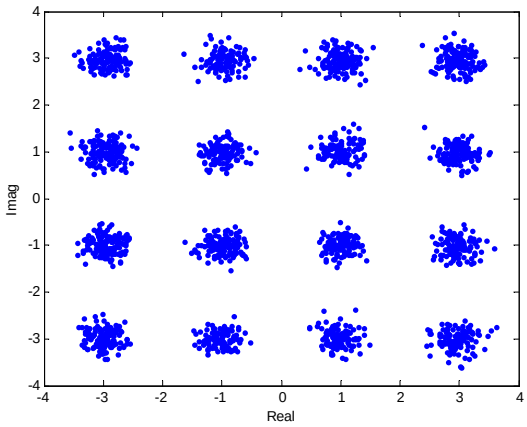

Figure 6. Constellation of 16-QAM symbols after MCMA equalizer.

Copyright © 2010 SciRes.

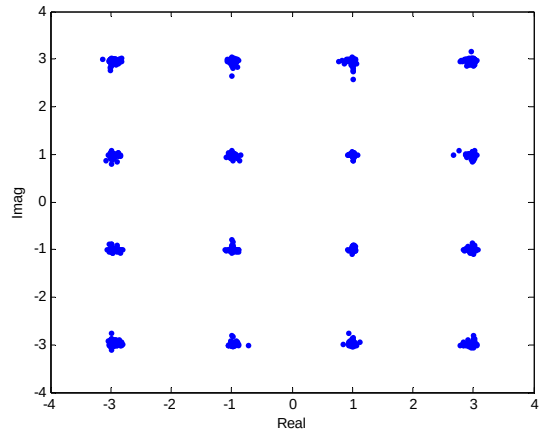

Figure 7. Constellation of 16-QAM symbols after the proposed NMCMA equalizer.

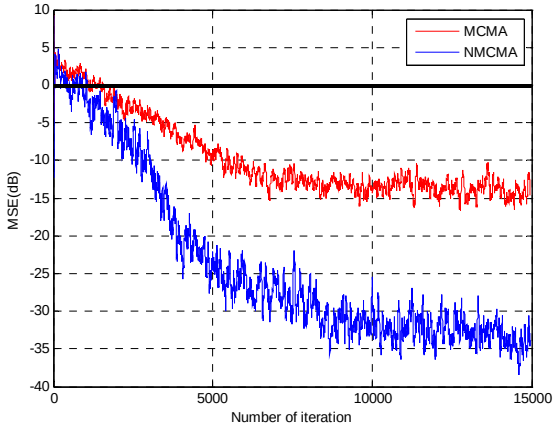

Figure 8. Performance comparison of MCMA and the proposed NMCMA in terms of MSE.

on linear blind equalizers was theoretically analyzed. It is shown that the NTF can make their decision regions sharper so that the proposed NCMA and NMCMA are more robust against the convergency error than CMA and MCMA, respectively. Computer simulations demonstrate that, for 16-QAM symbols, NCMA can reach up to approximately –13 dB MSE compared with –7 dB by CMA, and NMCMA can reach up to approximately –30 dB MSE compared with –15 dB by MCMA.

6. Acknowledgements

The author would like to thank all the anonymous reviewers of the paper. The critical comments by all the reviewers have helped us to improve the quality of our paper.

7. References

[1] J. R. Treichler and B. G. Agee, "A New Approach to Multipath Correction of Constant Modulus Signals," *IEEE Transactions on Acoustics, Speech, and Signal Processing*, Vol. 27, No. 10, October 1979, pp. 512-530.

[2] X. H. Dai, "CMA-Based Nonlinear Blind Equalizer Modeled by a Two-Layer Feed forward Neural Network," *IEE Proceedings-Communications*, Vol. 148, No. 4, April 2001, pp. 243-248.

[3] S. A. Athuraliya and L. M. Garth, "Quantized CMA Equalization for Shaped Signal Constellations," *IEEE Signal Processing Letters*, Vol. 11, No. 2, February 2004, pp. 67-70.

[4] B. Baykal and A. G. Constantinides, "Matched Filtering for CMA-Based Blind Channel Estimation," *IEEE Electronics Letters*, Vol. 39, No. 17, August 2003, pp. 1285-1287.

[5] D. L. Wang, H. Leung, K.-C. Kwak and H. Yoon, "Enhanced Speech Recognition with Blind Equalization for Robot 'WEVER-R2'," *Proceedings of IEEE International Symposium on Robot and Human Interactive Communication*, Jeju Island, August 2007, pp. 684-488.

[6] G. Gelli and F. Verde, "Two-Stage Interference-Resistant Adaptive Periodically Time-Varying CMA Blind Equalization," *IEEE Transactions on Signal Processing*, Vol. 50, No. 3, March 2002, pp. 662-672.

[7] K. Wesolowski, "Analysis and Properties of The Modified Constant Modulus Algorithm for Blind Equalization," *European Transactions on Telecommunications*, Vol. 3, No. 3, September 2008, pp. 225-230.

[8] M. Chen, Q. J. Tu and Z. Ding, "A Quadratic Programming Approach to Blind Equalization and Signal Separation," *IEEE Transactions on Signal Processing*, Vol. 57, No. 6, June 2009, pp. 2232-2244.

[9] Kyuho Hwang and Sooyong Choi, "Blind Equalization Method Based on Sparse Bayesian Learning," *IEEE Signal Processing Letters*, Vol. 16, No. 4, April 2009, pp. 315-318.

[10] I. Santamaria, C. Pantaleon, L. Vielva and J. Ibanez, "Blind Equalization of Constant Modulus Signals Using Support Vector Machines," *IEEE Transactions on Signal Processing*, Vol. 52, No. 6, June 2004, pp. 1773-1782.

[11] K. Nam Oh and Y. O. Chin, "Modified Constant Modulus Algorithm: Blind Equalization and Carrier Phase Recovery Algorithm," *Proceedings of IEEE International Conference on Communications*, Seattle, June 1995, pp. 498-502.

[12] M. Amin, H. Lin, C. R Reed. Jr. and R. Malkemes, "A Modified Constant Modulus Algorithm for Adaptive Channel Equalization for QAM Signals," *Proceedings of IEEE Signal Processing Workshop*, Cannes, August 2001, pp. 563-566.

[13] I. Chahed, J. Belzile and A. B. Kouki, "Blind Decision Feedback Equalizer Based on High Order MCMA," *Proceedings of IEEE CCECE*, Niagara Falls, Ontario, May 2004, pp. 2111-2114.

Copyright © 2010 SciRes.

[14] Z. X. Jiang, M. Zhang, Z. C. Li and S. L. Lu, "A Newly High-Speed MCMA Algorithm for QAM System," *Proceedings of WiCOM*, Dalian, September 2008, pp. 1-4.

[15] D. L. Wang, "A Nonlinear Modified Constant Modulus Algorithm for Blind Equalization," *Proceedings of IEEE CCECE*, Calgary, May 2010, pp. 1-4.

[16] D. L. Wang and D. G. Wang, "Generalized Derivation of Neural Network Constant Modulus Algorithm for Blind Equalization," *Proceedings of WiCOM*, Beijing, September 2009, pp. 1-4.

[17] D. L. Wang, H. Leung, A. P. Kurian, K.-C. Kwak and H. Yoon, "A Deconvolutive Neural Network for Speech Classification with Applications to Home Service Robot," *IEEE Transactions on Instrumentation and Measurement*, Vol. 59, No. 9, September 2010, pp. 1297-1303.

[18] C. You and D. Hong, "Nonlinear Blind Equalization Schemes Using Complex-Valued Multilayer Feedforward Neural Networks," *IEEE Transactions on Neural Networks*, Vol. 9, No. 11, November 1998, pp. 1442 -1455.

Copyright © 2010 SciRes.

Int. J. Communications, Network and System Sciences, **2010, 3, 530-539**
doi:10.4236/ijcns.2010.36071 Published Online June 2010 (http://www.SciRP.org/journal/ijcns/).

Scientific Research

A Multi-Objective QoS Optimization with Fuzzy Based Parameter Setting for Real-Time Multicasting

Satyananda Champati Rai[1], Bijan Bihari Misra[1], Ajit Kumar Nayak[1], Rajib Mall[2], Sateesh Kumar Pradhan[3]

[1]*Department of Computer Science and Engineering, Silicon Institute of Technology, Bhubaneswar, India*
[2]*Department of Computer Science and Engineering, Indian Institute of Technology, Kharagpur, India*
[3]*Department of Computer Science and Application, Utkal University, Bhubaneswar, India*
E-mail: {*satya,bijan,ajit*}*@silicon.ac.in, rajib@cse.iitkgp.ernet.in, sateesh*1960*@gmail.com*
Received April 6, 2010; *revised May* 8, 2010; *accepted June* 10, 2010

Abstract

We propose a multi-objective Pareto-optimal technique using Genetic Algorithm (GA) for group communication, which determines a min-cost multicast tree satisfying end-to-end delay, jitter, packet loss rate and blocking probability constraints. The model incorporates a fuzzy-based selection technique for initialization of Quality of Service (QoS) parameter values at each instance of multicasting. The simulation results show that the proposed algorithm satisfies on-demand QoS requirements (like high availability, good load balancing and fault-tolerance) made by the hosts in varying topology and bursty data traffic in multimedia communication networks.

Keywords: QoS, Fuzzy, Multicast, Real-Time, Multi-Objective

1. Introduction

Multicast services have been used for real-time multimedia applications to transport audio-video frames, among a group of users. During real-time communication the related audio-video frames are required to be delivered at the end nodes in a synchronous manner [1]. Further, the frequent change of service types, session timings with QoS requirements by the group members increases the communication complexity of the network [2,3]. In a wireless medium the situation further deteriorates than fixed network due to unpredictable mobility of the host nodes as well as their variations in resource requirements. It is also important to keep the network live with all possible satisfactions to the users during that period. Such a scenario requires multi-objective optimizations with constraints satisfactions [4,5]. The situation becomes critical when the destination nodes require multi-rate multicast sessions [6]. Hence development of multi-objective optimization algorithm for multi-rate traffic during multicasting is a challenge for efficient allocation of resources in a dynamically changing network [7,8]. However, a Pareto optimal algorithm can provide better results by fulfilling users' requirement, irrespective of irrelevant transformation of parameters [4].

To fulfill the on-demand request of the users we use Pareto optimal GA, which guarantees for achieving better QoS from a large search space. When the size of the network is large the situation demands optimization of QoS parameters such as: delay, jitter, path length (hops), packet loss rate and variation of load among the nodes involved, with high fault-tolerance from the network within acceptable cost. Most of the research works focus on multicasting to a group for near optimal, fast solution with multi-tree backups using GA [9-11].

However, real-time multimedia applications require multi-rate data flow to the served nodes in an on-demand basis with optimized resource allocation and cost incurred. For addressing multi-objective optimization issues GAs are suitable [9].

In this paper, we propose a multi-objective evolutionary algorithm supporting multi-rate data flow across the network using GA. The algorithm approximates Pareto front by generating a set of non-dominated solutions. Multiple services can be formulated as a multi-objective model [12]. Our model assumes that complete knowledge about the network is available to all the nodes present inside the region.

The paper is organized as follows. In Section 2, we define the multi-objective optimization (MOO) and

Copyright © 2010 SciRes.

Pareto-optimality concepts. Our proposed model, its environment setup procedure and implementation with GA are presented in Section 3. The performance evaluation and analysis of the model are elaborated in Section 4. Section 5 concludes the paper and discusses potential future work.

2. Multi-Objective Quality of Service

Multi-objective optimization is used to solve optimization problems that have two or more number of conflicting objectives, where there may not exist an unique optimal solution. Discovering and fixing optimal solutions in such scenarios is an open problem [6,11]. In general, almost all real-world problems are of multiple objectives, where each objective needs to be satisfied. For such type of problems a single best solution does not exist with simultaneous satisfaction of all objectives. In fact, we may have a set of optimal solutions in the entire search space, when all objectives are considered. These solutions are known as *Pareto-optimal solutions*. None of the solutions in this set is absolutely better then any other. So, any one of the solution can be an acceptable solution. In this context, mathematically we can define our problem more precisely, and introduce some related definitions in order to explain our GA based proposed model. It is noted that all of the objectives are in a minimized form in the following discussion.

Multi-Objective Optimization (MOO): Let $Z_1(X)$, $Z_2(X)$, …, $Z_n(X)$ are n number of objectives to be optimized with $g_i(X) \le 0$, $i = 1, 2,\ldots, k_1$ as inequality constraints and $h_i(X) = 0$, $i = 1, 2, \ldots, k_2$, as equality constraints for the m-dimensional vector $X = (x_1, x_2, \ldots, x_m)$ then MOO [13] can be defined as follows:

$$\begin{aligned} &\textit{Minimize}\ \ Z(X) = (Z_1(X),\ Z_2(X),\ \cdots,\ Z_n(X)) \\ &\textit{subject to}\ \ g_i(X) \le 0,\ i = 1,\ 2,\ \cdots, k_1 \\ &h_i(X) = 0,\ i = 1,\ 2,\ \ldots,\ k_2 \\ &\textit{where}\ \ X = (x_1,\ x_2, \cdots,\ x_m) \in \Omega \\ &\Omega \subseteq \Omega_1 \times \Omega_2 \times \cdots \times \Omega_m\ \ \textit{and}\ \ x_i \in \Omega_i, \\ &\forall\ \ i = 1,\ 2, \cdots,\ m \end{aligned} \tag{1}$$

Pareto Dominance: If $U = (u_1, u_2, \cdots, u_m)$ and $V = (v_1, v_2, \cdots, v_m)$ are two characteristic functions then U dominates V(u $\prec$ v) if and only if the condition is satisfied for $\forall i \in \{1, 2, \cdots, m\} : u_i \le v_i$ and $i \in \{1, 2, \cdots, m\} : u_i \prec v_i$.

***Pareto Optimality*:** A solution $X \in \Omega$ is said to be Pareto Optimal if and only if $\neg\exists\, \overline{X} \in \Omega : Z(\overline{X}) \prec Z(X)$

Pareto Optimality Set: A Pareto Optimality set P is defined as $P = \{X \in \Omega \mid \neg\exists\, \overline{X} \in \Omega : Z(\overline{X}) \prec Z(X)\}$ where $\overline{X} = (\overline{x}_1, \overline{x}_2, \cdots, \overline{x}_m)$ is any other element of.

***Pareto Front*:** It is defined as $PF = \{Z(X) \mid X \in P\}$.

3. Proposed Model

In this section we introduce the multi-objective model with its attributes, and their mapping to GA with Pareto-optimal verification.

3.1. Network Model

The network consists of n number of similar mobile hosts moving within a three-dimensional space. The nodes can communicate among themselves either directly or indirectly via intermediate nodes. All nodes are capable of transreceiving as well as forwarding the request of their neighbors to its near by nodes with broadcasting. For any instant of time the nodes along with their links can be represented as G = (V, E), where V and, E represent the set of nodes and edges in the network respectively. A multicast tree $T = (V_T, E_T)$ in the graph G is rooted at source node **s** with destination nodes $\{d_1, d_2, \ldots, d_t\}$ $(t \le n)$ act as group members for the source node. A tree is having $k\,(k \le t)$ number of branches and each branch is of r number of edges. The QoS parameters considered for multi-objective optimization during multicasting from a single source to its group members are as follows:

Bandwidth (BW): The bandwidth of a tree is the average bandwidth of all its branches; whereas bandwidth of any branch of a tree is the minimum of all its edge bandwidths (BW_l) from source to the corresponding destination node. Both *branch bandwidth* (BW_b) and *tree bandwidth* (BW_T) are represented in Equations (2) and (3) as follows:

$$BW_b = \min\{BW_l, l = 1, 2, \cdots, r\} \tag{2}$$

$$BW_T = mean\{BW_b, b = 1, 2, \ldots, k\} \tag{3}$$

Delay (DL): Delay between two corresponding node (branch delay: DL_b) is the sum of the delay at the intermediate nodes (node delay: DL_v) as well as the propagation delay through the links (link delay: DL_e) from source to destination. For a multicast tree the tree delay (DL_T) is the maximum delay among all branch delays (DL_b). The two different delays can be shown as:

$$DL_b = \sum_{e \in E_T} DL_e + \sum_{v \in V_T} DL_v \tag{4}$$

$$DL_T = \max\{DL_b, b = 1, 2, \ldots, k\} \tag{5}$$

Jitter (JT): It is defined as the average delay variation between any source and destination nodes during transmission of data packets. It is due to processing delay variation at the intermediate nodes as well as the propa-

Copyright © 2010 SciRes.

gation delay variation during communication through the links. In a multicast tree the jitter for any branch (JT_b) is the sum of the jitter at the intermediate vertices (JT_v) and in each edge (JT_e); whereas the jitter for a multicast tree is the maximum among all branches and are given in the following equations.

$$JT_b = \sum_{e \in E_T} JT_e + \sum_{v \in V_T} JT_v \quad (6)$$

$$JT_T = \max\{JT_b, b = 1, 2, ..., k\} \quad (7)$$

Packet Loss Rate (PLR): It is defined as a ratio of the number of lost packets to the total number of transmitted packets. PLR for a tree branch (PLR_b) is the cumulative (PLR_e) along each edge of the path from root to the leaf node; where as the PLR for a multicast tree (PLR_T) is the average loss rate of all branches present in the tree. Both can be represented mathematically as:

$$PLR_b = 1 - \prod_{e \in E_T} (1 - PLR_e) \quad (8)$$

$$PLR_T = mean\{PLR_b, b = 1, 2, ..., k\} \quad (9)$$

Blocking Probability (BP): The ratio between number of blocked calls to the number of offered calls in a tree is considered as the blocking probability for that tree. In other words it is the ratio of unreached nodes to the total number of destination nodes available in a multicast tree. Mathematically it is represented as:

$$BP_T = \frac{number\ of\ destinations\ not\ reached}{total\ number\ of\ destinations} \quad (10)$$

3.2. Formulation of Problem

The Bandwidth (BW), end-to-end delay (DL), jitter (JT), packet loss rate (PLR) and blocking probability (BP) are the five QoS parameters as defined in Subsection 3.1 are considered for our model. All the five objectives are to be satisfied simultaneously within their desired acceptable range for multi-objective optimization. Except BW all other objectives will be minimized, where as the former is to be maximized for optimal utilization. As defined in Equation (1) our MOO problem can be formulated as:

$$\begin{aligned} &Optimize\ Z = Z(BW, DL, JT, PLR, BP) \\ &subject\ to\ DL \le \varepsilon_1, JT \le \varepsilon_2, PLR \le \varepsilon_3, BP \le \varepsilon_4 \\ &and\ BW \ge \Theta, \\ &where\ \varepsilon_i \ge 0, \forall\, i = 1, 2, 3, 4 \\ &and\ \Theta\ is\ some\ positive\ threshold\ value \end{aligned} \quad (11)$$

3.3. Simulation Model Using GA

In our proposed model, we choose a heuristic based Genetic Algorithm with binary crossover and Roulette Wheel Selection approach. The fitness/objective function is the multi-objective function defined in Equation (11). The different phases of GA for natural evolution through encoding, selection, crossover and mutation operations are discussed as below.

Encoding: We use tree encoding for each chromosome to represent a multicast tree due to the 5 properties such as 1) all feasible trees can be represented; 2) the probability of representing all feasible tree is same; 3) only trees are represented; 4) low time complexity for encoding and decoding, and 5) no global effect on the tree, due to small change in representation, as proposed in [14].

The Genetic Operators:

1) *Selection*: We have used an elitist model for selection of the individuals for the next generation of population. 30 percent of the best fit individuals are selected at the first step for the next generation. Rest 70 percent of the population are selected using Roulette Wheel selection method.

2) *Crossover*: Standard uniform crossover technique is used for the crossover of two parents selected randomly from the matting pool.

3) *Mutation*: We observe that using the standard mutation technique we do not obtain the requisite level of performance. When the mutation probability is bit low it does not yield any result. In our model we have kept the mutation probability very high, *i.e.*, 0.2 and slowly decrease it with the progress of the generations using the following method.

$$P_m = \max P_m - \frac{(\max P_m - \min P_m) \times curGen}{\max Gen} \quad (12)$$

where, P_m: current mutation probability, $\max P_m$: Maximum mutation probability, $\min P_m$: Minimum mutation probability, $curGen$: current generation, and $\max Gen$: maximum generation

Fitness Test: The fitness of a tree is evaluated in two steps. In the first step, we evaluate Delay, Jitter, PLR and BP using Equations (5), (7), (9) and (10) respectively. Instead of bandwidth we evaluate deficiency from maximum bandwidth (BW^s). So, BW_b and BW_T represented in Equations (2) and (3) are modified as follows.

$$BW_b^s = \max\{BW_l^s, l = 1, 2, ..., r\} \quad (13)$$

$$BW_T^s = mean\{BW_b^s, b \in E_T\} \quad (14)$$

At the time of evaluation, if we find an invalid node, which is not an intermediate node in the respective path, then a penalty value is added to the delay. If the BW, JT, PLR and BP values lie outside the desired range, for each case we add a small penalty to the delay. The values of DL, BW^s and JT are rationalized within the range of 0 and 1. Then in the second step the fitness value is evalu-

Copyright © 2010 SciRes.

ated as follows

$$f = w_1 DL + w_2 BW^s + w_3 JT + w_4 PLR + w_5 BP \quad (15)$$

where w_1, w_2, w_3, w_4, and w_5 are user defined constants in the range [0, 1]. The fit value *i.e.* $fit = 1/(1+f)$ in the range [0, 1] is maximized by using GA.

3.4. Simulation Procedure

1) *Scenario Generation*: For our simulation purpose, we have considered a three dimensional (3D) space to simulate real life wireless scenarios. The 3D coordinates of a node are randomly generated. The Euclidean distance between each pair of nodes is measured. If the distance between any two nodes is found to be less then 250 meters then a link is established between these two nodes and accordingly the adjacency matrix is formed. The scenario represented in **Figure 1** is one of our network topology formed during simulation.

Once the network is formed, the source and destinations are generated randomly and GA is applied to find out the optimal multicast tree over a set of evolutions. Also we define different cut-off ranges for various network parameters to fulfill the demands of multimedia applications. These cut-off values were considered in the algorithm while a tree is selected for optimality.

2) *Simulation Parameters*: The Network and GA parameter values considered for our simulation are given in the **Table 1** and **Table 2** respectively. During initial stage of our simulation, we have given a constant low value to the mutation probability, which did not yield good result. For the subsequent simulations, we take a high value such as 0.2 for the mutation probability to ensure a diversified search and slowly reduces as the network converges to an optimal solution to narrow down the search in the close proximity.

Table 1. Network Parameters.

Network Parameters	Min	Max
Bandwidth	0	25
Delay	200	1000
Jitter	0	650
Packet Loss Rate	0	1

Table 2. GA Parameters.

GA Parameter	Value
Population Size	100
Crossover Probability	0.6
Mutation Probability	0.2

In our model we have considered the nodes are of homogeneous with respect to their transmission range, processing capability and buffer length [15,16]. The wireless bandwidth is equally shared among the mobile entities. At any instance of the simulation the available bandwidth is optimized in consideration with the QoS required by the end nodes. To emulate the scenario the available bandwidth for each node can be obtained randomly. However, random initialization of other QoS parameters like de-

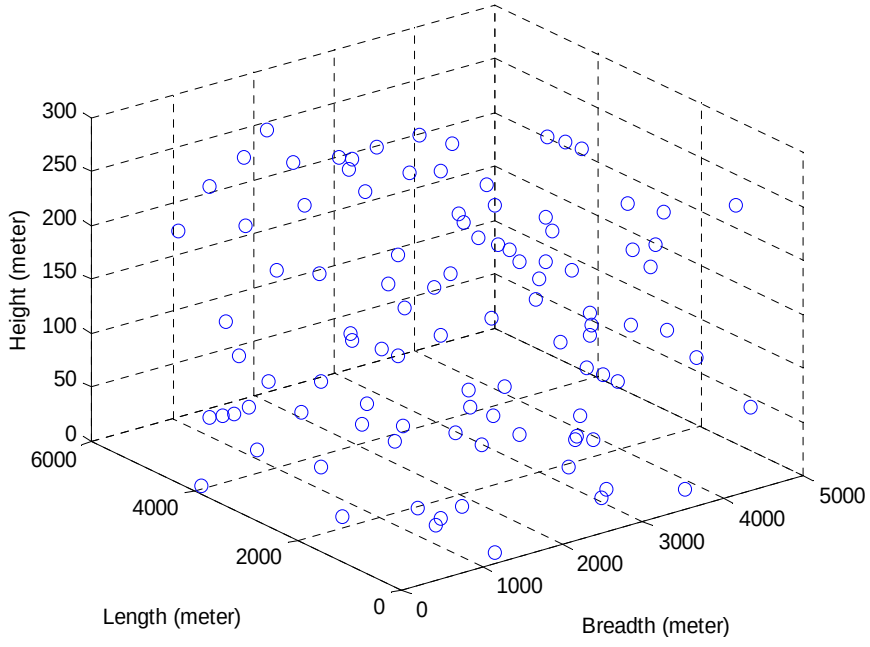

Figure 1. 3-D Network topology generation with 100 nodes (volume: 6000 × 5000 × 300 cubic meters).

Copyright © 2010 SciRes.

lay(DL), jitter (JT) and packet loss rate (PLR) and blocking probability (BP) may results unpredictable network performance. Although there is no established relationship among the parameters [7,17], we propose a sigmoidal fuzzy-logic based parameter initialization with error model for our GA approach in (17).

$$sig(x;a,c)=\frac{1}{1+\exp(-a(x-c))} \quad (16)$$

$$fs = sig \pm 0.2 \times rand \times sig \quad (17)$$

We establish the relationship between available bandwidth and other parameters with the following formulae as given in Equations (18) to (21).

$$D_i = nD + (XD - nD) \times fs((xW - x_i); a_D, c_D) \quad (18)$$

$$J_i = nJ + (xJ - nJ) \times fs((xW - x_i); a_J, c_J) \quad (19)$$

$$L_i = nL + (xL - nL) \times fs((xW - x_i); a_L, c_L) \quad (20)$$

$$P_i = nP + (xP - nP) \times fs((xW - x_i); a_P, c_P) \quad (21)$$

where the triplets (xD, nD, D_i), (xJ, nJ, J_i), (xL, nL, L_i) and (xP, nP, P_i) represent maximum, minimum and current values of DL, JT, PLR, and BP of the ith node respectively. xW and x_i represent maximum and allocated BW for the ith node respectively. The parameters (a_D, c_D), (a_J, c_J), (a_L, c_L), and (a_P, c_P) used in evaluation of sigmoidal function are suitably selected constants which are obtained after a maximum number of testing.

4. Simulation Results and Performance Analysis

In this simulation our objective is to test if the proposed model is producing an optimal solution with multi-objective constraints. During simulation, the total number of nodes were varied from 10 to 100 by keeping density of the nodes in the space same by changing the space volume according to total number of nodes such that the maximum number of neighbors present for a node is limited to 6. The multicast group size was kept as one fourth of the total nodes. The maximum numbers of generations for evolution were fixed at 250. As the objectives are conflicting in nature, to obtain the Pareto-optimal solution we have considered different sets of randomly selected weights in Equation (15) for each simulation. However, one may consider meta-heuristic approach for dynamic selection of those weights. The range of network parameters and GA parameters considered for evaluating QoS parameters are represented in **Table 1** and **Table 2** respectively. The simulation results of QoS parameters are shown in **Table 3**.

Table 3. Average results of QoS parameters with different group size.

Tot	Gr	HC	DL	PLR	JT	BW	BP	PP
10	3	2.16	442.43	0.012	40.14	21.99	0	3.01E+07
20	5	2.76	413.36	0.013	46.39	22.52	0	2.88E+10
30	8	8.13	1545.4	0.033	53.9	20.44	0	6.13E+11
40	10	5.34	726.61	0.02	57.86	21.05	0	5.61E+12
50	13	7.9	3123.7	0.032	58.39	21.59	0	3.81E+13
60	15	9.48	3581.3	0.035	60.01	21.31	0	1.81E+14
70	18	5.93	1835.1	0.025	51.86	21.23	0	2.26E+14
80	20	6.81	1902.3	0.026	52.59	21.57	0	3.66E+14
90	23	7.6	2240.4	0.02	48.59	20.02	0	7.28E+14
100	25	8.44	2190.1	0.023	42.66	20.42	0	6.08E+14

4.1. A Study of QoS Parameters

Hop Count (HC) represents the maximum number of hops required to reach any destination in the multicast tree.

Delay (DL): is the maximum delay along any branch of the tree. A penalty is added if no link found between two nodes.

Packet Loss Rate (PLR): is the average packet loss along the tree branches. The cut-off for PLR is set at 10%. If a branch having more than 10% packet loss then it is assigned a penalty, such that the model tries to search a path less then10% PLR.

Jitter (JT): is the maximum delay variation along any branch of the tree. The cut-off is set at 20% otherwise a penalty is added.

Bandwidth (BW): of the multicast tree is the average bandwidth requirement of all the tree branches. The cut-off BW is taken as 2 Mbps.

Blocking Probability (BP): is the ratio of not getting a node to the total number of destination nodes in the multicast tree.

Possible Paths (PP): in the tree are the average possible paths available for any destinations in the tree. The PP field gives an estimation of the search space and also proves the efficiency of our algorithm to find an optimal tree from such a huge search space. Also the BP field proves the definiteness of this algorithm to find a path from source node to destination node (if exists).

The 'Tot' represents the total number of nodes considered for the simulation and 'Gr' represents the multicast group size. In order to maintain node density, we have increased the volume of the search space proportionately as the total number of nodes. The QoS parameter values were obtained by changing the total number of nodes and the respective multicast group size.

The QoS parameter values presented in the table are the average values of 25 simulations. The multicast targets are randomly chosen for each simulation and QoS

Copyright © 2010 SciRes.

parameters are also reinitialized for each simulation. We have not considered HC as a parameter for optimization; as a result we obtained different results for different target size depending upon the availability connectivity. As we have considered a minimum delay of 200 ms per node, the delay affects with increase in the number of hops. However, this algorithm has ensured to find a path where the delay gets minimized.

The robustness of our GA based approach is the inherent capability of obtaining optimal solution after searching from a large search space, which is shown in **Figure 2**.

Further the increase in group size of a multicast environment results in marginal elevation in the node density. The node density of a multicast tree is considered as the ratio between numbers of nodes in the tree to the size of the group. *i.e.* represented as

$$node\ density = \frac{number\ of\ nodes\ in\ the\ tree}{size\ of\ the\ group} \qquad (22)$$

While measuring intermediate node density, the network conditions is assumed to be constant, *i.e.* the adjacency matrix representing the links among the nodes is not altered.

The results of QoS parameter values obtained from simulation show that our proposed model can adapt and scale well to large group members and capable of obtaining near optimal solution from a large search space.

4.2. A Simulation Study

The overall results from our simulation studies have been presented in **Table 3**. We now present the details of a single simulation study to show the working of the algorithm and the performance results that were obtained. In this simulation, we have considered 10 nodes as a network from the environment consisting of 100 nodes. In the selected group, the node with index number 14 was taken as the source node and nodes with indices 5, 11, 15, 17, 20 were considered as the target nodes.

Table 4 presents the status of a typical simulation. The

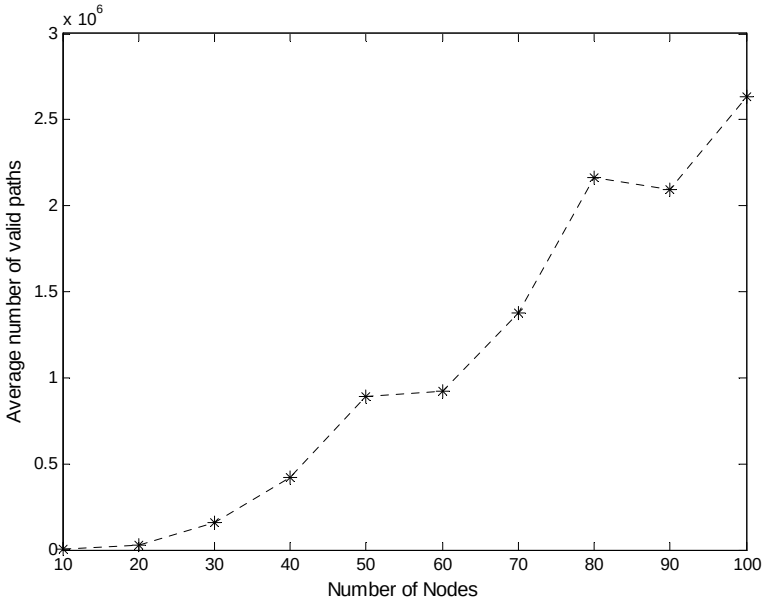

Figure 2. A subset of total search space representing average number of valid paths with 5 intermediate nodes.

Table 4. Multicast Tree with QoS Parameter Values.

	Result obtained after generation					
	25	50	75	100	125	150
Multicast Tree	14→11 14→15 14→5 14→17 14→6→20	14→11 14→15 14→5 14→12→17 14→6→20	14→11 14→15 14→5 14→12→17 14→6→20	14→11 14→15 14→5 14→12→17 14→6→20	14→11 14→15 14→5 14→12→17 14→6→20	14→11 14→15 14→5 14→12→17 14→6→20
HC	1.2	1.4	1.4	1.4	1.4	1.4
DL	240.52	280.35	280.35	280.35	280.35	280.25
PLR	0.097278	0.09291	0.09291	0.09291	0.09291	0.09016
JIT	48.462	46.835	46.835	46.835	46.835	43.37
BW	21.521	21.672	21.672	21.672	21.672	22.006
BP	0.0	0.0	0.0	0.0	0.0	0.0

Copyright © 2010 SciRes.

results obtained after every 25 simulations were recorded, the multicast tree obtained and the QoS parameter values at that instance have been represented in this table. From the table it can be observed that the multicast tree produced by this method does not change after 50 iterations and stabilizes. Please note that the values given in **Table 4** for HC, DL, PLR, JIT, BW, and BP are the mean values of the different multicast trees represented in the population for the respective generation. These values converge after 150 generations.

4.3. Performance Analysis

For the purpose of comparison, we have simulated the approach presented in [18] and the performance results have been represented as Model 1 results. The simulation results of the current study have been presented as Model 2 results. In a typical simulation we have taken the total number of nodes in the network as 20, one source and 5 destinations, with a population size 10, the GA was allowed to run for 250 generations. The QoS metric values of the population are recorded after every 25 generations.

The results of Model 1 are presented in **Figures 3**, **5**, **7**, **9**, **11** and that of Model 2 in **Figures 4**, **6**, **8**, **10** and **12**.

The objective of this experimentation (given in Equation 11) is to maximize the bandwidth (BW) and to minimize all other parameters. From **Figures 3 and 4**, we can see that optimal bandwidth allocation in the current study is 22.01 Kbps as against 5.98 Kbps in Model 1, giving performance improvement of 267.99%.

One of the objectives is to minimize the delay while optimizing all other parameters. The Pareto fronts for delay in Model 1 and Model 2 have been presented in **Figures 5** and **6** respectively. The optimal delay was rounded to be 794.47 ms in Model 1 as against 280.25 ms in Model 2, which shows a performance improvement of 64.72 % in delay parameter.

The Pareto fronts for HC have been presented in **Figures 7** and **8** respectively for Model 1 and Model 2. The Pareto fronts for jitter have been presented in **Figures 9** and **10** respectively. The optimal level of jitter was 149.87 ms for Model 1 and 43.37 ms for Model 2, giving an improvement in performance of 71.06 %. The Pareto fronts for PLR have been presented as **Figures 11** and **12**.

The optimal level of PLR for Model 1 is 0.4368 and for Model 2 is 0.09016, giving an improvement of performance of 79.36%.

The performance of this work is compared with the performance of the models suggested by other researchers. On comparing our results with that of Roy *et al.* [19], we find that our approach outperforms the approach presented in [19]. However, Roy *et al*. has considered only three parameters such as bandwidth requirement, bandwidth utilization and end-to-end delay. The bandwidth requirement and bandwidth utilization possibly relates to one parameter, resulting multi-objective for two parameters only as against 5 distinct parameters considered in our study.

The non-dominated solution of bandwidth utilization and end-to-end delay converges almost in the same number of generations as pointed by Roy *et al*. [20]. The call blocking (BP) percentage was found to be 10% with 10 requests per second in [20]. However in our study, we have obtained 0.0 BP with network size in the range of [10, 100] where the respective maximal group size is one fourth of the network size.

In the following, we compare our work with some of the other related work. Gomathy *et al.* [11] have evaluated the packet delivery ratio and end-to-end delay of ODMRP, CAMP, and NTPMR multicast routing protocols after incorporation of a fuzzy based priority scheduler. Pinto *et al*. [21] has considered maximum end-to-end delay, average delay, maximum link utilization and cost of multicast tree as the four multi objective parameters for

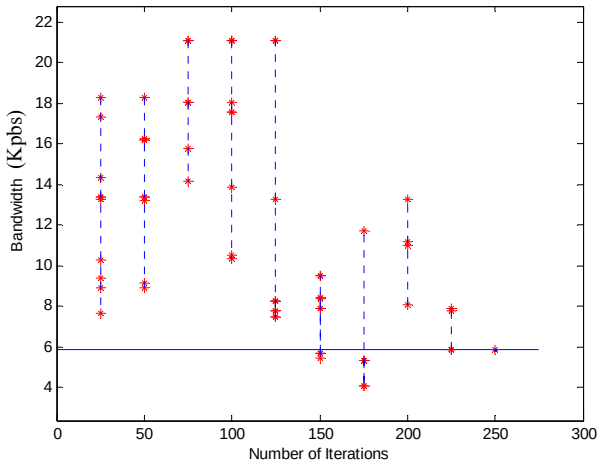

Figure 3. Pareto front of bandwidth allocation in Model 1.

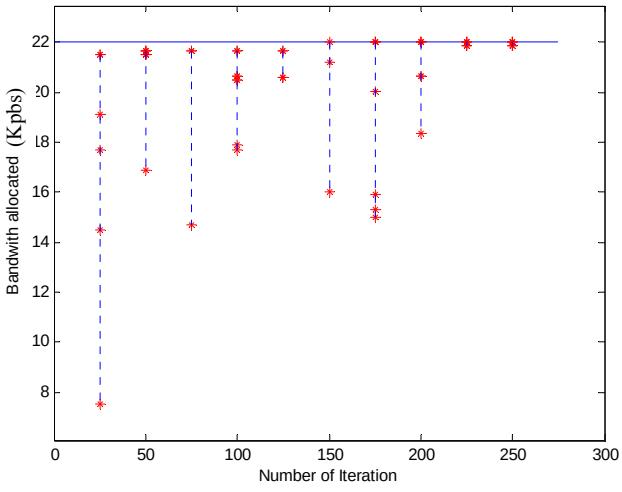

Figure 4. Pareto front of bandwidth allocation in Model 2.

Copyright © 2010 SciRes.

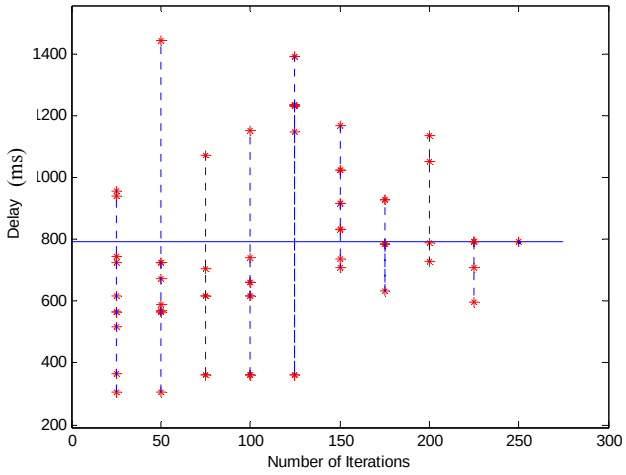

Figure 5. Pareto front of delay in Model 1.

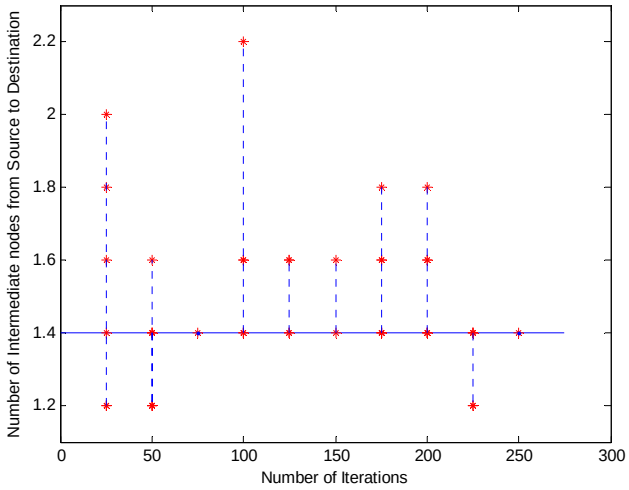

Figure 8. Pareto front of HC in Model 2.

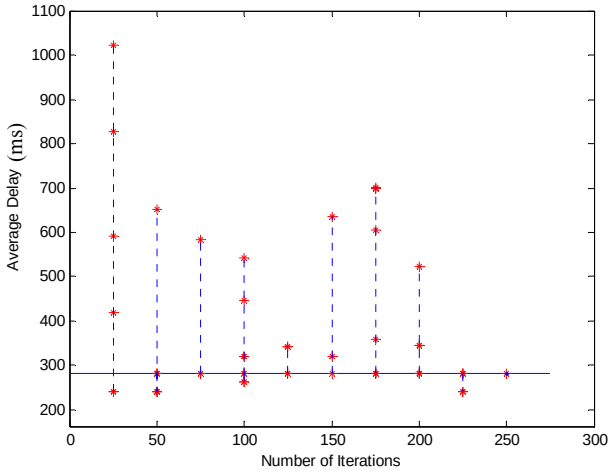

Figure 6. Pareto front of delay in Model 2.

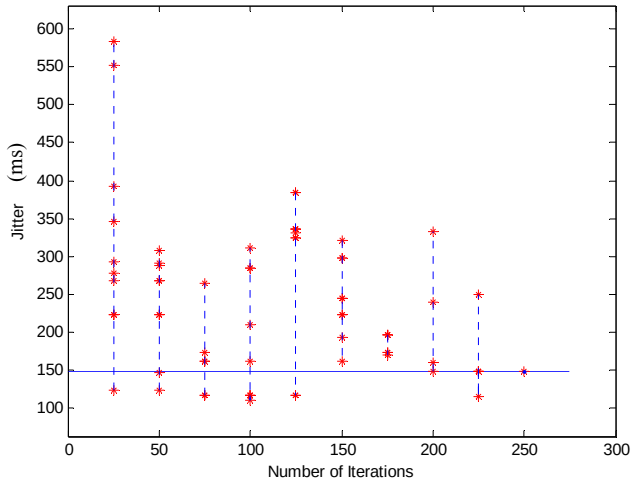

Figure 9. Pareto front of jitter in Model 1.

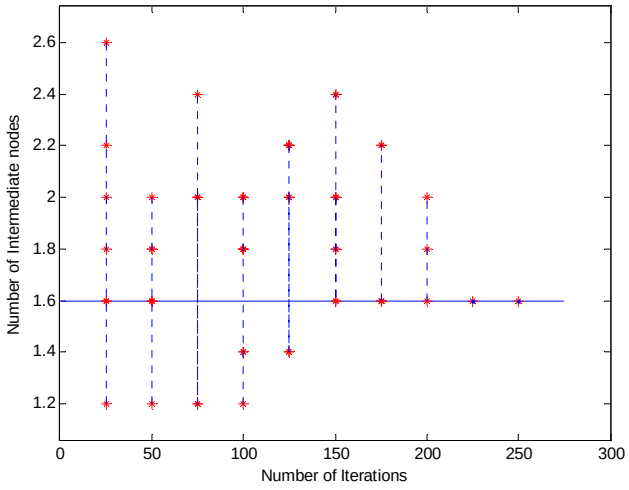

Figure 7. Pareto front of HC in Model 1.

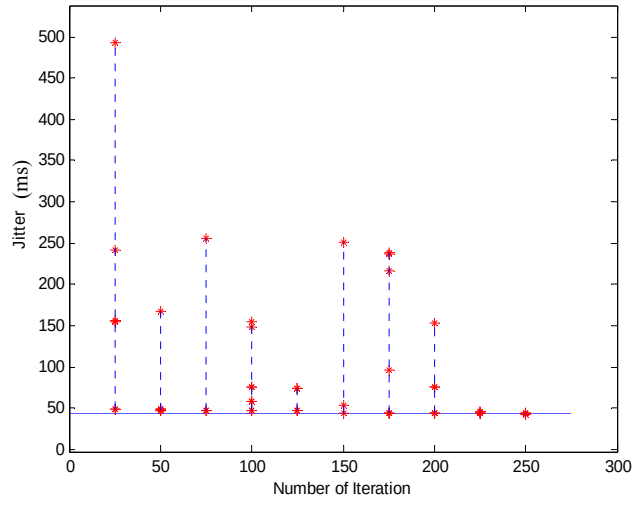

Figure 10. Pareto front of jitter in Model 2.

Copyright © 2010 SciRes.

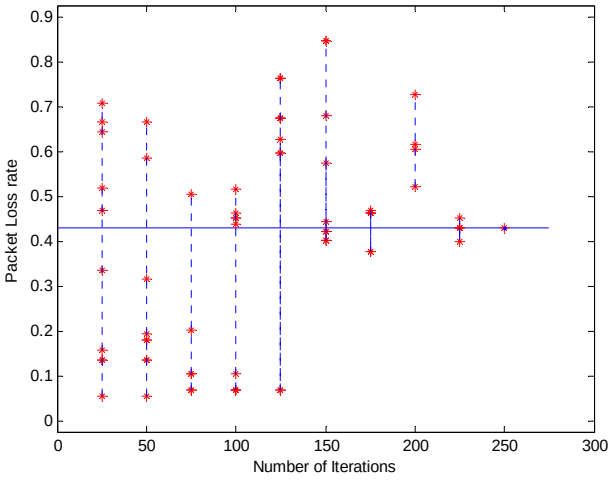

Figure 11. Pareto front of PLR in Model 1.

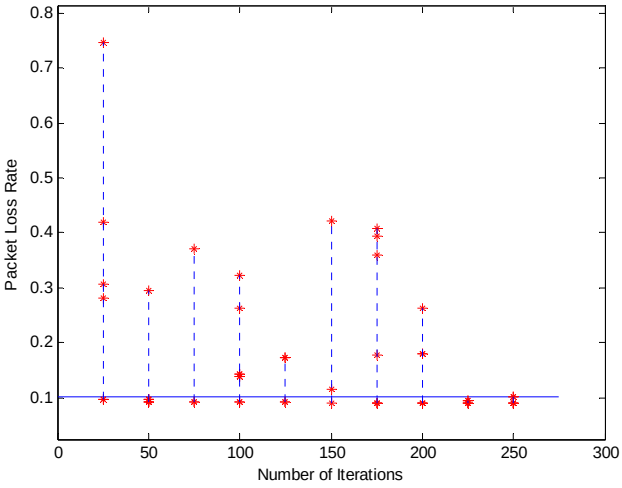

Figure 12. Pareto front of PLR in Model 2.

optimization, where the maximum end-to-end delay and average delay may be considered as related features. Maximum delay, average delay, maximum link utilization, cost of the tree are the four multi objective features considered by Crichigno *et al*. [22]; where the first two objectives belong to one feature. Fabregat *et al*. [4] considered a static network and they have optimized maximal link utilization, hop count, average delay, and bandwidth consumption parameters. Marwaha *et al*. [23] have considered end-to-end delay, packet delivery ratio, packet loss ratio, routing load and route failure as the optimization parameters for a mobile ad-hoc network with 900 seconds as the network pause time, where the packet delivery ratio and the packet loss ratio are related features. Whereas in our work, we have considered 5 distinct parameters such as bandwidth allocation, end-to-end delay, jitter, packet loss rate, and blocking probability as our multi-objective optimization criterion. Further the simulation environments considered by these researchers are not compatible to ours to make a meaningful performance comparison.

5. Conclusions

We have proposed a multi-objective multicast model for wireless ad-hoc network using GA. In this model we have considered five QoS parameters such as bandwidth, end-to-end delay, jitter, packet loss rate and blocking probability for multi-objective optimization. Simulation studies were carried out with a network of 100 nodes moving in a 3D space of volume: 5000 × 6000 × 300 cubic meters with the number of multicast destination nodes varying in the range 5 to 30. Our model established near optimal relationships among the QoS parameters to satisfy multi-objective optimization. Irrespective of increase in group size our model could optimize path length between any sources to its group members. Selection of min-cost paths from source to multiple destinations for multicasting is a NP-hard problem. Our approach could effectively obtain near optimal solution for QoS multicast applications in varying network conditions. As per our knowledge no relationships among the QoS parameters have so far been established. We propose a fuzzy-based parameter setting approach which establishes a Sigmoidal relationship among the parameters. Due to the dynamism of the network there is a possibility of sudden change of the network type and status of resources. The empirical results show superiority over the randomly selected resource values. As a future work, we plan to consider biological-inspired optimized techniques for estimation of multicast cost arising from queuing delays and propagation error.

6. References

[1] Y. He, I. Lee and L. Guan, "Optimized Video Multicasting Over Wireless Ad Hoc Networks Using Distributed Algorithm," *IEEE Transactions on Circuits and Systems for Video Technology*, Vol. 19, No. 6, June 2009, pp. 796-807.

[2] C. Fortuna, M. Mohorcic and B. Filipic, "Multi-objective Optimization of Service Delivery over a Heterogeneous Wireless Access System," *Proceeding of IEEE International Symposium on Wireless Communication Systems*, Reykjavik, 2008, pp. 133-137.

[3] W. X. Gu and X. F. Liu, "A New Algorithm for Probabilistic Planning Based on Multi-Objective Optimization," *Proceeding of IEEE International Conference on Machine Learing and Cybernetics*, Kunming, 12-15 July 2008, pp. 1812-1817.

[4] R. Fabregat, Y. Donoso, B. Baran, F. Solano and J. L. Marzo, "Multi-Objective Optimization Scheme for Multicast Flows: A Survey, a Model and a MOEA Solution," *Proceeding of 3rd International IFIP/ACM*

Copyright © 2010 SciRes.

Latin American Conference on Networking, New York, 2005, pp. 73-86.

[5] H. Juidette and H. Youlal, "Fuzzy Dynamic Path Planning Using Genetic Algorithms," *IEEE Electronics Letters*, Vol. 36, No. 4, February 2000, pp. 374-378.

[6] P. Chen and T. L. Dong, "A Fuzzy Genetic Algorithm for QoS Multicast Routing," *Journal of Computer Communication*, Vol. 26, No. 6, 2003, pp. 506-512.

[7] A. Khisti, U. Erez and G. W. Wornell, "Fundamental Limits and Scaling Behavior of Cooperative Multicasting in Wireless Networks," *IEEE Transactions on Information Theory*, Vol. 52, No. 6, June 2006, pp. 2762-2770.

[8] A. Striegel and G. Manimaran, "A Survey of QoS Multicasting Issues," *IEEE Communication Magazine*, Vol. 40, No. 6, June 2002, pp. 82-87.

[9] X. Cui, C. Lin and Y. Wei, "A Multi-objective Model for QoS Multicast Routing Based on Genetic Algorithm," *Proceeding of IEEE International Conference on Computer Networks and Mobile Computing* (*ICCNMC*), Shanghai, 2003, pp. 49-53.

[10] A. Dutta, J. Chennikara, W. Chen, O. Altintas and H. Schulzrinne, "Multicasting Streaming Media to Mobile Users," *IEEE Communications Magazine*, Vol. 41, No. 10, October 2003, pp. 81-89.

[11] C. Gomathy and S. Shanmugavel, "Supporting QoS in MANET by a Fuzzy Priority Scheduler and Performance Analysis with Multicast Routing Protocols," *EURASIP Journal on Wireless Communications and Networking*, Vol. 5, No. 3, 2005, pp. 426-436.

[12] A. Daid, V. Van and B. Gary, "Multi-Objective Evolutionary Algorithm: Analyzing the State-of-the-Art," *Evolutionary Computation*, Vol. 8, No. 2, 2000, pp. 125-147.

[13] J. Q. Wang, J. Qin and L. S. Kang, "A New QoS Multicast Routing Model and its Immune Optimization Algorithm," *Lecture Notes in Computer Science*, Vol. 4159, 2006, pp. 369-378.

[14] C. C. Palmer and A. Keshenbaum, "Representing Trees in Genetic Algorithms," *Proceeding of IEEE International Conference on Evolutionary Computation*, Orlando, Vol. 1, 1994, pp. 379-384.

[15] S. Sivavakeesar, G. Pavlou and A. Liotta "Stable Clustering through Mobility Prediction for Large-Scale Multiple Intelligent Ad-hoc Networks," *Proceeding of IEEE Wireless Communications and Networking Conference*, Atlanta, Vol. 3, March 2004, pp. 1488-1493.

[16] J. Yu, L. Chen and G. Chen, "A Fuzzy Grouping Mechanism for Distributed Interactive Simulation," *Proceeding of IEEE International Conference on Communication*, Seoul, 2005, pp. 881-885.

[17] G. M. B. Oliveira and P. T. Araujo, "Determining Multicast Routes with QoS and Traffic Engineering Requirements Based on Genetic Algorithm," *Proceeding of IEEE Conference on Cybernetics and Intelligent Systems*, Singapore, 1-3 December 2004, pp. 666-670.

[18] S. C. Rai, B. B. Mishra, A. K. Nayak, R. Mall and S. K. Pradhan, "A Multi-Objective Pareto Optimal Genetic Algorithm for QoS Multicasting," *Proceeding of IEEE International Advance Computing Conference*, Patiala, 2009, pp. 1303-1307.

[19] A. Roy and S. K. Das, "Optimizing QoS-Based Multicast Routing in Wireless Networks: A Mullti-objective Genetic Algorithmic Approach," *Proceedings of the* 2*nd International IFIP-TC*6 *Networking Conference on Networking Technologies*, *Services*, *and Protocols*, *Lecture Notes in Computer Science*, Berlin Heidelberg, Vol. 2345, Springer-Verlag, 2002, pp. 28-48.

[20] A. Roy, N. Banerjee and S. K. Das, "An Efficient Multi-Objective QoS-Routing Algorithm for Wireless Multicasting," *Proceeding of IEEE Vehicular Technology Conference*, San Diego, Vol. 3, 2002, pp. 1160-1164.

[21] D. Pinto and B. Baran, "Solving Multi-Objective Multicast Routing Problem with a New Ant Colony Optimization Approach," *Proceeding of* 3*rd International IFIP/ACM Latin American Conference on Networking*, New York, 2005, pp. 11-19.

[22] J. Crichigno and B. Baran, "Multi-Objective Multicast Routing Algorithm for Traffic Engineering," *Proceeding of* 13*th IEEE Inernational Conference on Computer Communications and Networks* (*ICCCN*), Chicago, 2004, pp. 301-306.

[23] S. Marwaha, D. Srinivasan, C. K. Tham and A. Vasilakos, "Evolutionary Fuzzy Multi-Objective Routing for Wireless Mobile Ad Hoc Networks," *Proceeding of Evolutionary Computation* (*CEC*'04), San Diego, Vol. 2, 2004, pp. 1964-1971.

Copyright © 2010 SciRes.

Int. J. Communications, Network and System Sciences, **2010, 3, 540-547**
doi:10.4236/ijcns.2010.36072 Published Online June 2010 (http://www.SciRP.org/journal/ijcns/).

Scientific Research

Uplink Performance Evaluation of CDMA Communication System with RAKE Receiver and Multiple Access Interference Cancellation

Ayodeji J. Bamisaye, Michael O. Kolawole
Department of Electrical and Electronics Engineering the Federal University of Technology, Akure, Nigeria
E-mail: *ayobamisaye@yahoo.com and kolawolm@yahoo.com*
Received January 26, 2010; *revised March* 2, 2010; *accepted April* 10, 2010

Abstract

In CDMA communication systems, all the subscribers share the common channel. The limitation factor on the system's capacity is not the bandwidth, but multiuser interference and the near far problem. This paper models CDMA system from the perspective of mobile radio channels corrupted by additive white noise generated by multipath and multiple access interferences. The system's receiver is assisted using different combining diversity techniques. Performance analysis of the system with these detection techniques is presented. The paper demonstrates that combining diversity techniques in the system's receivers markedly improve the performance of CDMA systems.

Keywords: CDMA, Multipath Diversity, Multiple Access Interference Cancellation, Rake Receiver, Parallel Interference Cancellation

1. Introduction

The mobile radio channel plays fundamental limitations on the performance of wireless communication systems. The transmission path between the transmitter and the receiver can vary from simple line-of-sight to one that is severely obstructed by buildings, mountains, and foliage. Unlike wired channels that are stationary and predictable, radio channels are extremely random and do not offer easy analysis. Even the speed of motion impacts how rapidly the signal level fades as mobile terminal moves in space. Modelling the radio channel has historically been one of the most difficult parts of mobile radio system design, and is typically done in a statistical fashion, based on measurements made specifically for intended communication system or spectrum allocation. Code Division Multiple Access (CDMA) is a multiple access technology that utilizes direct-sequence spread spectrum (DS-SS) techniques. With this technology comes a paradigm shift, including the use orthogonal or nearly orthogonal codes (so-called spreading sequences) to modulate the transmitted bits. Contrary to the conventional *frequency division multiple access* (FDMA) and *time division multiple access* (TDMA) systems where noise rejection deals, primarily with *out-of-band* noise, a CDMA system concerns mostly with *inband* noise. This noise may come from self-jamming (or self-noise), background noise, man-made noise, inter-modulation, or noise generated in the receiver [1,2]. If one can reduce the unwanted in-band noise, such reduction translates directly into improved performance. Undesired noise comes from many different sources. This noise may come from natural or human sources. Naturally occurring noise includes atmospheric disturbances, background noise, and thermal noise generated in the receiver itself. Through careful engineering, the effects of many unwanted signals can be reduced [3]. DS-CDMA is a multiple access system, where multiple users share a limited resource, the frequency. Conventional asynchronous DS-CDMA systems allow each user to transmit and receive independently. Each receiver performs a simple correlation between the received baseband signal and the corresponding user's spreading sequence. In a low-noise channel with orthogonal spreading sequence,this approach would be optimal. Due to the synchronicity of users and the need to support numerous users, such orthogonality is impossible, even on a hypothetical AWGN (additive white Gaussian noise) channel [4]. Thus, system performance rendered multiple-access interference (MAI) limited, and channel utilization is correspondingly low.

This paper models CDMA system from the perspective

Copyright © 2010 SciRes.

of mobile radio channels corrupted by additive white noise generated by multipath and multiple access interferences. The system's receiver is assisted using different combining diversity techniques. Performance analysis of the model with different detection techniques will be presented.

1.1. Mobile Radio Channel Model

Mobile radio channel is one of the most important elements in the mobile communication systems. When the signals are transmitted through Mobile radio channel, it is affected by shadow or large scale fading. Mobile communication is affected by multipath fading in addition to shadow fading. Multipath fading is caused by atmospheric, scattering, and reflection from building and other object. Multipath channel can be classified as discrete (consisting of resolvable multipath components) and diffuse (consisting of irresolvable multipath components) [5,6]. Consequently, the multipath fading could affect the transmitted signals in two ways: due to dispersion (also called time spreading or frequency selectivity), and due to time variant behaviour of the channel (due to motion of the receiver or changing environment such as of foliage or movement of reflectors and scatter). This means that the impulse response $h(t,\tau)$ of mobile radio channel is time variant [6,7], and if $h(t,\tau)$ has a zero mean, then the envelope $|h(t,\tau)|$ has a Rayleigh distribution with its probability density function described by

$$p(r)=\frac{r}{\sigma^2}\exp\left[-\frac{r^2}{2\sigma^2}\right] \tag{1}$$

where r is time dependent received signal (*i.e.*, $r(t)=|r|e^{-j\phi(t)}$, ϕ is its arbitrary phase) whose line of sight (LOS), specular, and diffuse components are assumed bounded in narrowband form, and σ^2 is the total power in the multipath signal. In this case the total power is considered to have zero-mean, amplitude fading. Otherwise, if the impulse response has a non-zero mean, then the envelope mobile radio channel would have a Rician distribution with its probability density function expressed as:

$$p(r)=\frac{r}{\sigma^2}\exp\left[\frac{-\left(r^2+s^2\right)}{2\sigma^2}\right]I_o\left(\frac{r^2}{\sigma^2}\right) \tag{2}$$

where s^2 is the power of the line-of-sight component, and I_o denotes the zeroth order Bessel function of the first kind argument (.). The Rayleigh distribution is a special case of Rician distribution when $s = 0$; *i.e.*, where the LOS component is negligible.

In most general case, the channel can be modelled as linear time-variant system [2] giving the response of the channel at time (t) to an impulse at time (t-τ). If $x(t)$ represents the transmitted (or emitted) signal through noiseless mobile radio channels, the received signal, $r(t)$ can be expressed as

$$r(t)=\int_{-\infty}^{\infty}h(t,\tau)x(t-\tau)\,d\tau \tag{3}$$

If the channel information is considered, its distributed channel impulse response may be expressed as

$$h(t,\tau)=\sum_{j=0}^{N-1}\beta_j(t)\delta(\tau-\tau_j) \tag{4}$$

In view of (4) in (3), we write modified channel received signal:

$$r(t)=\sum_{j=0}^{N-1}\beta_j(\tau_j)x(t-\tau_j) \tag{5}$$

$\beta_j(t)$ is complex amplitude, τ_j is the path delay, and N is the number of multipath components. In the wideband channel where the delay-line model had a large number of taps, not all the multipath components are likely to fade simultaneously. This may be used as a multipath diversity to improve the received signal SINR (carrier to interference plus noise ratio). Rake receiver, for instance, can be used to mitigate the effect of fading if the transmitted signal bandwidth is larger than the coherence bandwidth; a practical example is in the wideband-CDMA (WCDMA).

1.2. Rake Receiver

Conventional matched filters are single path detectors. In practice, when the transmitted signal passes through mobile radio channel, duplicates of the transmitted signal are generated by reflection, refraction, and diffraction, and the signal power is distributed in multipath. In CDMA system, the transmitted signal bandwidth is much larger than the coherent bandwidth of the channel, in which case the channel is frequency selective [4,8,9]. For the frequency-selective channels, the received signals are multiple copies of the transmitted signals with different channel delays and fading, combining the multipath components as multipath diversity. Thus, if one of the multipath components is attenuated by fading, some others may not be and the receiver could use unfaded components to make the decision. The idea behind the rake reception technique is that the signals propagating through different multipath are received in individual fingers of the rake receiver and the outputs from these fingers are then coherently combined to provide the input signal for the symbol decision. The received signal is chip matched and sampled at the chip rate. **Figure 1**, illustrates the structure of a typical rake receiver in which $s_k^*(i)$ and $c_{k,m}^*(i)$ (k = 1, 2, ..., K; m = 1, 2, ..., M) represent, respectively, the complex conjugate of chip-channel matched sampled signature sequence of the user

Copyright © 2009 SciRes.

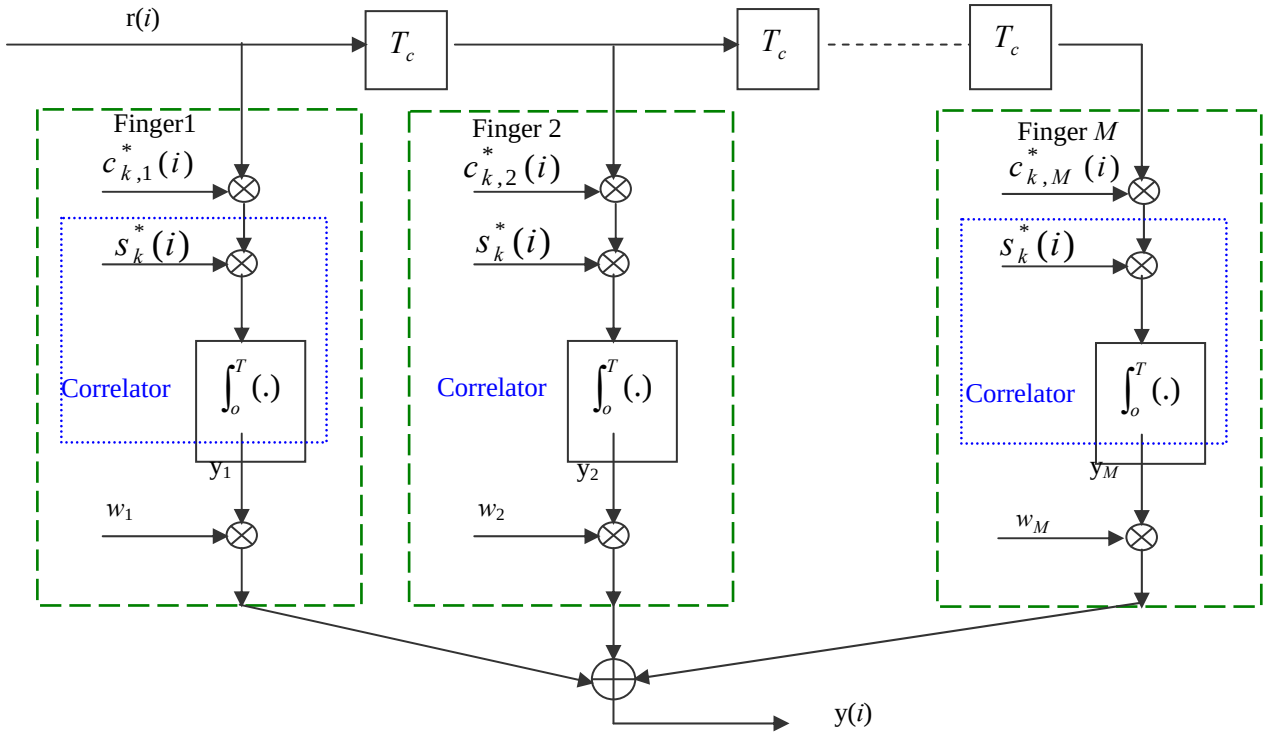

Figure 1. Rake Receiver with *M* fingers.

of interest and the complex conjugate estimate of the impulse response.

Then, the decision on the transmitted information bit is based on the sum of the individual correlator's outputs. In our study, the dimension of each correlator equals the system processing gain, and then the output of each finger $y(i)$ is given after channel is matched and correlating:

$$y(i)=\sum_{j=1}^{PG}\sum_{m=1}^{M}\sum_{k=1}^{K}c^*_{k,m}(i)s^*_{k,j}(i)r_k(i) \quad \text{for} \quad w_m=1$$
$$(\text{where} \quad m=1,2,\ldots,M) \qquad (6)$$

where *PG* is the processing gain, $c^*_{k,m}(i)$ is the complex conjugate estimate of the channel's impulse response, $s^*_{k,j}(i)$ is the complex conjugate of chip-matched sampled signature sequence of the users of interest.

1.2.1. Multistage Receivers

The input signal of a multiuser detector is the output of the matched filter bank, or *rake* receiver. Almost all modern multiuser detection techniques deal with the output of the matched filters bank and the cross-correlation information of all users in the system. Expressions (1) through (6) assumed noiseless cases, which is not valid in real life situation. If the time-dependent interference components, $n(t)$, are assumed additive, the output of the conventional matched filters receiver for single user *k* can be expressed as:

$$y_k(i)=\sum_{i=1}^{PG}c^*_k(i)s^*_k(i)r_k(i)+\sum_{i=1}^{PG}c^*_k(i)s^*_k(i)n(t) \qquad (7)$$

In the case of multiple K active users, the received signal in the receiver is

$$r(t)=\sum_{k=1}^{K}r_k(t)+n(t) \qquad (8)$$

So, the modified output of the conventional matched filter receiver y_k for the *k*th user is

$$y_k=\sum_{i=1}^{PG}r_k(i)c^*_k(i)s^*_k(i)$$
$$+\sum_{\substack{j=1\\ j\neq k}}^{K}\sum_{i=1}^{PG}r_j(i)c^*_k(i)s^*_k(i)+\sum_{i=1}^{PG}c^*_k(i)s^*_k(i)n(t) \qquad (9)$$

Expression (9) consists of three terms. The first term is the desired information which gives the signal of the information bit (which is exactly what is sought). The second term is the result of multiple access interference (MAI), and the last term is due to noise. The second term typically dominates the noise so that one would like to remove its influence. Its influence is felt through the cross-correlation between the chip sequences and the device-powers of users. If one knew the cross-correlations and the powers, then one would attempt to cancel the

Copyright © 2010 SciRes.

effect of one user upon another. This is, in fact, the intuitive motivation for interference cancellation scheme.

The difference between multistage receivers and successsive interference canceller (SIC) receivers is that instead of using previous bit decisions to cancel interfereence from desired user's signal as in SIC, tentative decisions on each user are used to improve signal quality [10]. Receiver structure is called multistage, since when decisions are made, they can be used to either make a final decision on data or to enhance the signal through cancellation. Reference signals are based on initial bit estimates, which are then subtracted from received signal to produce a cleaned spread signal for next stage. Since all signals are detected at each stage simultaneously, multistage receivers are also called parallel interference cancellers (PIC). A two-user multistage receiver is shown in **Figure 2**. The p-stage receiver outputs are $y_k^{p-1,p}(t)$, where $p = 1, 2, \ldots$.

Instead of a conventional (matched filter) receiver front end, a SIC receiver (or a decorrelator) can be used [11]. Performance of PIC is best when received signal powers are equal. Capacity of the system is limited by hardware.

1.3. Simulation and Results

Performance evaluations were performed for different scenarios using:

1) Conventional matched filters receiver with PIC (parallel interference cancellation);

2) Rake receiver with PIC;

3) Rake receiver with Decorrelating Detector and MMSE; and

4) Conventional matched filters receiver and rake receiver.

For each analysis, the number of users' symbols transmitted is clearly stated. It is assumed that the system uses unencoded BPSK signal, as well as no pulse-shaping filter. Each transmitted MS within each loop sends a block of data bits of known length. The input of MUD (multi user detection) is the soft decision of either rake receiver or conventional matched filters. In the simulation, the sub-optimum linear MUD decorrelating detector, linear minimum mean squared error (LMMSE) detector, and nonlinear sub-optimum PIC were built for the multishot model.

In relation to the decision operation, the hard decision output of received data is obtained by passing the soft decision output through the design circuit, which represents any sign function for BPSK. Also, we make the number of channel paths P equal the number of fingers M to make the rake receiver simpler in structure. In a less equivalent case, that is, when M < P or M > P, the system performance degrades. Therefore, the matched case provides the optimally achievable performance reference.

1.3.1. Performance of Conventional Matched Filters Receiver with PIC

Simulations were performed for 10 active users sending 10 symbols within each loop. The maximum loop equals to 100. The users send a total of 10000 symbols. The data are then spread by Walsh code and scrambled by Gold code with processing gain of 32. The channel parameters are updated randomly in each loop.

Simulation results are shown in **Figure 3**, which demonstrates progressive improvement in the system performance with diversity combining techniques in cancelling multiple access interferences.

1.3.2. Performance of Conventional Matched Filters Receiver and Rake Receiver

Similar parameters used in 1.3.1 are used in this analysis except the processing gain, PG, which is increased to 64. In addition, the channel parameters are updated randomly in each loop and the number of paths for each user changes randomly over (2-6). Two tests were carried out in this subsection: (i) to investigate the effect of rake receiver in the system for a single user and (ii) to investigate the effect of rake receiver and conventional (matched filter) receiver with a range of channel paths.

Figure 4 shows the performance with rake receiver and without rake receiver for a single user. In the receiver, 'equal gain combining' method is used in rake. The analysis demonstrates that lowering the SNR does not improve the system when SNR equals 20 dB, the BER is 10–2.9 and 10–1.9 respectively for conventional matched filter receiver and rake receiver. In contrast, improvement in system performance can be achieved by increasing SNR in both schemes.

In the case of test (ii), an AGWN is assumed in the channel paths. The number of users and the processing gain are decreased to 6 and 8 respectively, while other parameters are the same as previous simulations. The channel parameters are updated randomly in each loop, and the simulation computes for the different values of channel path, as shown in **Figure 5**.

Figure 5 shows the performance of the rake and conventional receivers for a number of multipath scenarios. In the case of one path, the system performance is the same for matched filter (MF) and rake receiver. But in the case of multipaths; for example, (4-path) the system performance with conventional matched filter degrades, whereas the system performance with rake receiver improves. Also, for the case of (7-path) the performance of MF becomes very poor, but improves markedly with rake receiver. As a result, the system performance can be deduced as increasing when diversity scheme is employed. Under Gaussian noise as interferer, the system performance improves with in creasing channel path with the rake receiver, which might not be optimal in real life situation.

Copyright © 2009 SciRes.

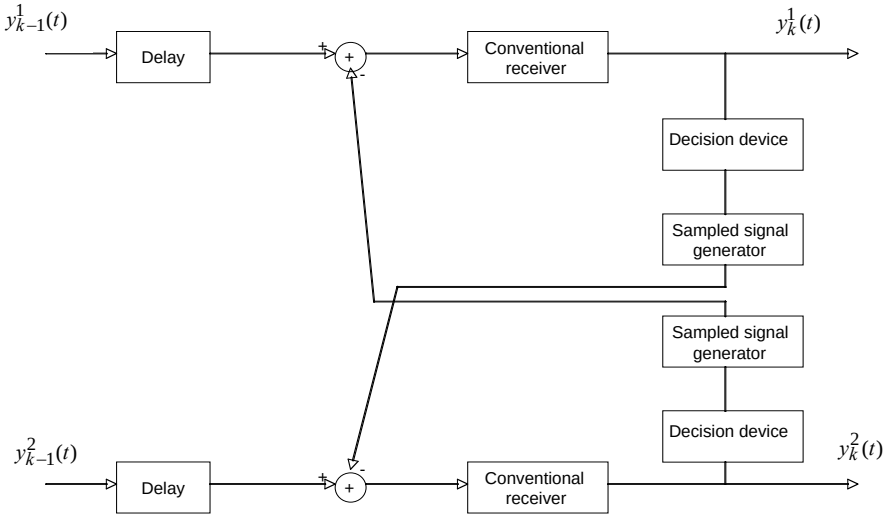

Figure 2. A two-user multistage receiver.

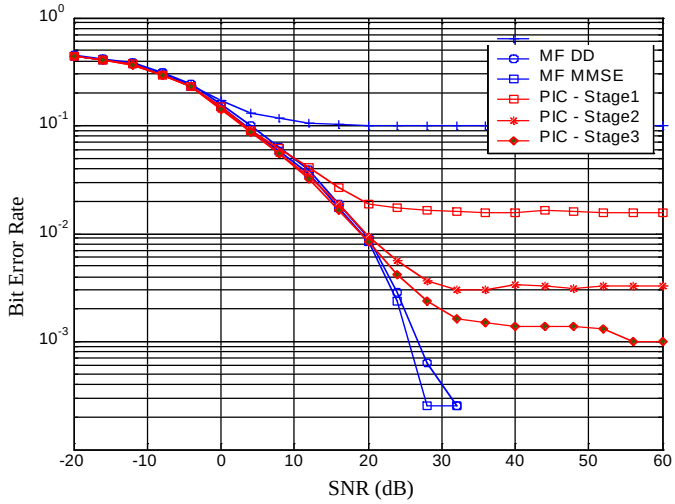

Figure 3. CDMA system performance evaluation using conventional matched filter (MF), with different diversity techniques: decorrelating detector (DD), minimum mean squared error (MMSE), and three-stage parallel interference cancellation (PIC).

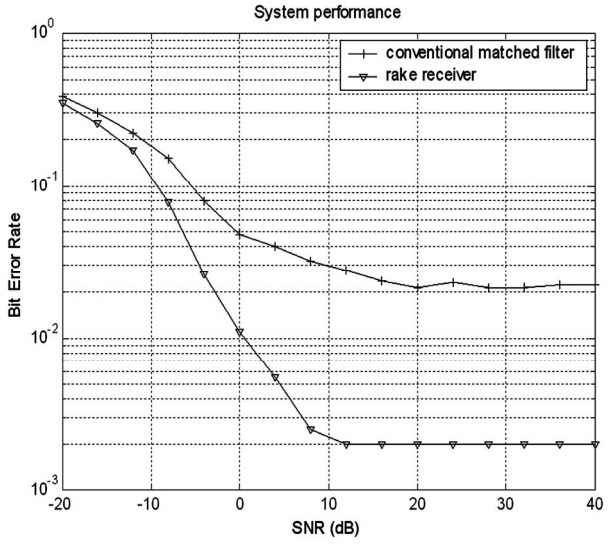

Figure 4. System performance of Rake receiver and conventional matched filters' receiver.

Copyright © 2010 SciRes.

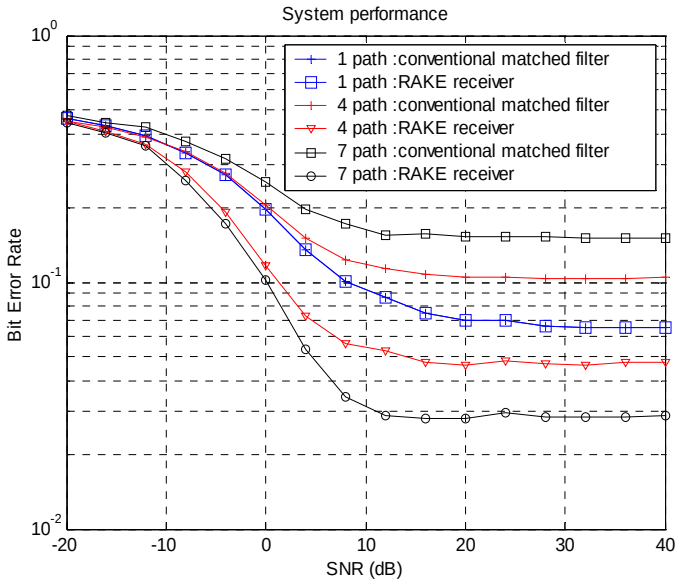

Figure 5. System performance of Rake receiver and conventional matched filters' receiver with different number of channel paths.

1.3.3. Performance of RAKE Receiver with Decorrelating Detector and MMSE

Similar parameters used in 1.3.1 are used in this analysis. In addition, the channel parameters are updated randomly in each loop, and the number of paths for each user changes randomly between 2 and 5. **Figure 6** clearly shows the importance of multiuser detection (MUD). The figure shows that for one path, marginal improve- ment in system performance is gained whether conventional matched filters receivers are used or in combination with decorrelating detector (DD) or with minimum mean squared error (MMSE) schemes. Note that the correlation matrix only contains the information of multiple access interferences in the first path and treated the other paths as AWGN. On the other hand, system performance improves markedly using rake receiver and MUD when taking the multipath into account; a finding consistent with that of [11].

1.3.4. Performance of RAKE Receiver with Parallel Interference Cancellation

For this simulation, 10 active users send 10 symbols respectively within each loop. The maximum loop is equal to 150, with a total of 15000 symbols sent. The data are then spread by Walsh code and scrambled by Gold code with performance gains, PGs, of 16 and 64. The channel parameters are updated randomly in each loop, and the number of channel path change randomly between 2 and 4. The received signal is processed with rake and conventional matched filter respectively. Three-stage parallel interference cancellation is employed to cancel the multiple access interference. As shown in **Figure 7**, the performance improved by using rake receiver instead of conventional matched filters.

1.3.5. Performance with Variable Processing Gain

In this simulation, 8 active users send 10 symbols respectively within each loop. The maximum loop is equal to 100, totalling 8000 symbols sent by the users. The data are then spread by Walsh code and scrambled by Gold code with performance gains of 16 and 64. The channel parameters are updated randomly in each loop, and the number of channel path change randomly between 2 and 4. The received signal is processed with rake and conventional matched filters respectively. Decorrelating detector is employed to cancel the multiple access interference. **Figure 8** indicates the processing gain influence to the system performance. The results demonstrate that large processing gains translate to high performance gain of the system.

1.4. Conclusions

This paper has modelled a CDMA system from the perspective of mobile radio channels corrupted by additive white noise generated by multipath and multiple access interferences. The system's receiver was assisted with different combining diversity schemes.The simulation is focused on the most important factors that will influence the performance of the CDMA systems using multi user detection method and interference cancellations scheme. Performance analysis of the system using the different detection techniques was presented. The paper estab-Lished that diversity-combining techniques markedly im-

Copyright © 2009 SciRes.

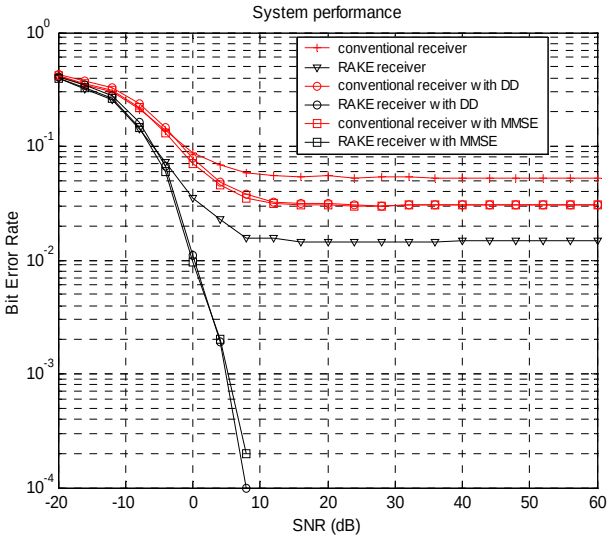

Figure 6. System performance of Rake receiver with decorrelating detector (DD) and minimum mean squared error (MMSE).

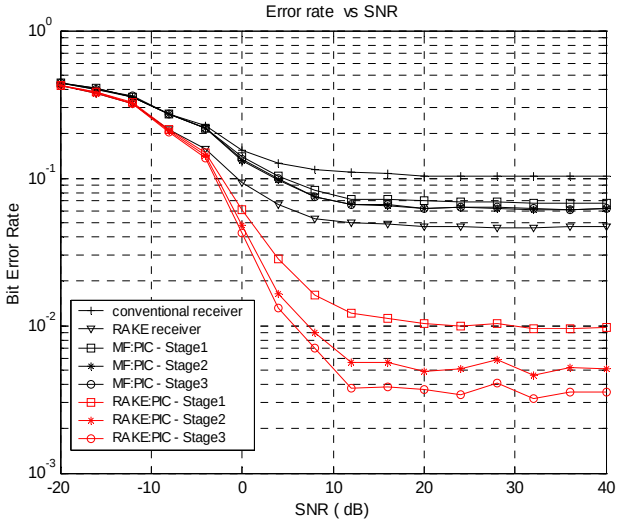

Figure 7. The system performance of RAKE receiver with three-stage parallel interference cancellation (PIC).

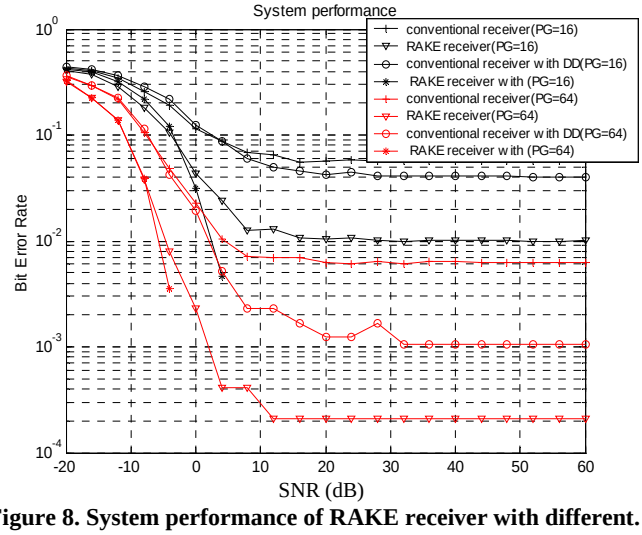

Figure 8. System performance of RAKE receiver with different.

Copyright © 2010 SciRes.

prove the performance of CDMA systems. Also, an important factor in reducing the multiple access interference, is the processing gain which the model employed.

2. References

[1] D. Torrieri, "Principle of Spread-Spectrum Communication Systems," Springer Science + Business Media, Boston, 2005.

[2] R. Prasad, "Universal Wireless Personal Communications," Artech House, 2000.

[3] S. C. Yang, "CDMA RF System Engineering," British Library Cataloguing in Publication Data, II. Series, TK5103.2.Y36, Irvine, California, 1998.

[4] A. J. Bamisaye, "Effect of Multiuser Interference on Subscriber Location in CDMA Network," M Eng Thesis, Department of Electrical and Electronics Engineering, the Federal University of Technology, Akure, 2009.

[5] A. J. Bamisaye and M. O. Kolawole, "Evaluation of Downlink Performance of a Multiple-Cell, Rake Receiver Assisted CDMA Mobile System," *Wireless Sensor Network Journals*, Vol. 2, No. 1, 2010, pp. 1-6.

[6] T. S. Rappaport, "Wireless Communications Principles & Practice," IEEE Press, New York, Prentice-Hall, 2002.

[7] M. Frikel, B. Targui, F. Hamon and M. M'Saad, "Adaptive Equalization Using Controlled Equal Gain Combining for Uplink/Downlink MC-CDMA Systems," *International Journal of Signal Processing*, Vol. 4, No. 3, 2008, pp. 230-237.

[8] A. Kansal, S. N. Batalama and D. A. Pados, "Adaptive Maximum SINR RAKE Filtering for DS-CDMA Multi-Path Fading Channels," *IEEE Journal on Selected Area in Communication*, Vol. 16, No. 9, 1998, pp. 1765-1773.

[9] T. Kim, K. Ko, Y. Kim and D. Hong, "Performance Evaluation of Uplink MC-CDMA Systems with Residual Frequency Offset," *IEICE Transactions on Communications*, Vol. E89-B, No. 4, 2006, pp. 1455-1458.

[10] K. Vardhe, D. Reynolds and M. C. Valenti, "The Performance of Multi-User Cooperative Diversity in an Asynchronous CDMA Uplink," *IEEE Transactions on Wireless Communications*, Vol. 7, No. 2, 2008, pp. 1930-1940.

[11] X. B. Yu, X. D. Zhang, D. Z. Xu and G. G. Bi, "Uplink Performance of CWP-MC-CDMA with Space Diversity Combining Technique over Rayleigh Fading Channel," *Journal of Electronics*, Vol. 23, No. 6, 2006, pp. 837-841.

Copyright © 2010 SciRes.

Int. J. Communications, Network and System Sciences, **2010, 3, 548-553**
doi:10.4236/ijcns.2010.36073 Published Online June 2010 (http://www.SciRP.org/journal/ijcns/).

Magnetization Performance of LDPC Reduced-Complexity Decoding Algorithms

Manel Abdelhedi[1], Omessaad Hamdi[2], Ammar Bouallegue[1]
[1]*SYSCOM Laboratory, ENIT, Tunis, Tunisia*
[2]*LaBRI Laboratory, University of Bordeaux, Bordeaux, France*
E-mail: *abdelhedi_manel@yahoo.fr, hamdi@univ-tln.fr, ammar.bouallegue@enit.rnu.tn*
Received March 20, 2010; *revised April* 21, 2010; *accepted May* 26, 2010

Abstract

Low-density parity-check (LDPC) codes are very efficient for communicating reliably through a noisy channel. N.Sourlas [1] showed that LDPC codes, which revolutionize the codes domain and used in many communications standards, can be mapped onto an Ising spin systems. Besides, it has been shown that the Belief-Propagation (BP) algorithm, the LDPC codes decoding algorithm, is equivalent to the Thouless-Anderson-Palmer (TAP) approach [2]. Unfortunately, no study has been made for the other decoding algorithms. In this paper, we develop the Log-Likelihood Ratios-Belief Propagation (LLR-BP) algorithm and its simplifications the BP-Based algorithm and the λ-min algorithm with the TAP approach. We present the performance of these decoding algorithms using statistical physics argument *i.e.*, we present the performance as function of the magnetization.

Keywords: LDPC Codes, Ising Spin, LLR-BP Algorithm, BP-Based Algorithm, λ-Min Algorithm, TAP Approach

1. Introduction

Low-density parity-check (LDPC) codes were first discovered by Gallager [3], in his thesis, in 1962 and have recently been rediscovered by Mackay and Neal [3,4]. These codes can get very close to the Shannon limit by mean of an iterative decoding algorithm called Belief-Propagation (BP) algorithm [5].

This performance combined with their relatively simple decoding algorithm makes these codes very attractive for the next generation of digital transmission systems. Indeed, these codes have been chosen as a standard for the second Satellite Digital Video Broadcasting normalization (DVB-S2). So, the search for efficient implementations of decoding algorithms is being a challenge.

The implementation of the BP algorithm is difficult. That's why different simplifications of this algorithm were discovered. The BP algorithm can be simplified using the BP-Based algorithm [6] and the λ-min algorithm [7].

N. Sourlas [1] has shown in 1989 that there is a mathematical equivalence of error-correcting codes to some theoretical spin-glass models. This analogy has contributed to the present proximity of the statistical physics and the information theory. Therefore, the methods of statistical physics developed in the study of disordered systems proved to be efficient for studying the properties of these codes. One of these methods is the Thouless-Anderson-Palmer (TAP) [2] approach which is shown equivalent to the BP algorithm by kabashima, *et al*. [8]. Unfortunately, no study has been made for the other decoding algorithms.

In this paper, we develop the Log-Likelihood Ratios-Belief Propagation (LLR-BP), the BP-Based and the λ-min decoding algorithms with the TAP approach. Their performance is evaluated as a function of a statistical physics parameter which is the magnetization.

This paper is organized as follows. Section 2 corresponds to a general description of the LDPC codes and their decoding algorithm. Section 3 describes the similarity between the BP algorithm and the TAP approach. In Section 4, we develop the LLR-BP algorithm and its simplifications the BP-Based algorithm and the λ-min algorithm with the TAP approach. Finally and before concluding, simulation results as function of the magnetization are presented in Section 5.

2. LDPC Codes and Decoding Algorithm

2.1. Low-Density Parity Check Codes

Binary LDPC codes, are linear block codes defined by a

Copyright © 2010 SciRes.

sparse parity check matrix $A(M \times N)$, where N denotes the codeword length and M the number of parity-check equations.

Using a notation similar to that in [4,6], let $L(\mu) = \{j / A_{\mu j} = 1\}$ denote the set of bit j that participate in check μ. Similarly, we define the set of checks in which bit j participates as $M(j) = \{\mu / A_{\mu j} = 1\}$. We denote a set $L(\mu)$ with bit j excluded by $L(\mu) \setminus j$, and a set $M(j)$ with parity check μ excluded by $M(j) \setminus \mu$. Finally, $s = (s_1,...,s_N)$ denotes the transmitted codeword.

2.2. Belief Propagation Algorithm

This section summarizes according to [4,5], the iterative decoding of LDPC codes based on the BP algorithm. The likelihood of s is given by $\prod_j f_j^a$, with $f_j^a = P(s_j = a)$.

Let $q_{\mu j}^a$ denotes the probability that bit j of s is a, given the information obtained via checks other than check μ. The quantity $r_{\mu j}^a$ is meant to be the probability of check μ is satisfied if bit j of s is considered fixed at a and the other bits have a separable distribution given by the probabilities $\{q_{\mu l} : l \in L(\mu) \setminus j\}$ [6].

The standard iterative decoding algorithm based on the BP approach consists on the following main steps.

- **Initialization:** The variables $q_{\mu j}^0$ and $q_{\mu j}^1$ are initialized to the values f_j^0 and f_j^1 respectively.
- **Iterative processing:**

1) Define $\delta q_{\mu j} = q_{\mu j}^0 - q_{\mu j}^1$ and for each μ, $j \in L(\mu)$, and for $a = \{0,1\}$, compute

$$\delta r_{\mu j} = \prod_{l \in L(\mu) \setminus j} \delta q_{\mu l}$$
$$r_{\mu j}^a = \frac{1}{2}\left(1 + (-1)^a \delta r_{\mu j}\right)$$

2) For each j and $\mu \in M(j)$, and for $a = \{0,1\}$ update

$$q_{\mu j}^a = \alpha_{\mu j} f_j^a \prod_{\nu \in M(j) \setminus \mu} r_{\nu j}^a$$
$$q_j^a = \alpha_j f_j^a \prod_{\mu \in M(j)} r_{\mu j}^a$$

where $\alpha_{\mu j}$ and α_j are chosen such that

$$q_{\mu j}^0 + q_{\mu j}^1 = 1 \text{ and } q_j^0 + q_j^1 = 1.$$

3) Create the word $\hat{s} = (\hat{s}_1 ... \hat{s}_N)$ the detection of the transmitted codeword such that:

$$\hat{s}_j = 0 \quad \text{if } \delta q_j > 0$$
$$\hat{s}_j = 1 \quad \text{if } \delta q_j \le 0$$

If $H.\hat{s}^T = 0$ the decoding process ends. Otherwise, we pass to another iteration of BP. A failure is declared and the decoding process ends if the number of iterations exceeds the maximum number of iterations and $\hat{s}$ is not a valid codeword.

3. Decoding Problem from Statistical Physics Point of View

3.1. Statistical Physics Analogy

In the previous section, we have described the LDPC codes using the additive Boolean group $(\{0,1\},+)$. However, in order to apply methods of statistical physics, it is convenient to introduce an equivalent group, the multiplicative binary group $(\{+1,-1\},\times)$ [1].

From a statistical physics point of view, the code can be regarded as a spin system. Each bit $S_j = (-1)^{s_j}$ is called a spin and takes values in $\{\pm 1\}$ and the word $S = ((-1)^{s_1},...,(-1)^{s_N})$ can be seen as a collection of N spins, called a configuration. The parity-check matrix gives rise to the interactions between the spins [1].

The decoding problem depends on posteriori like $P(S \setminus J)$ where J is the evidence (received message or syndrome vector). By applying Bayes' theorem this posteriori can be written in the form [1].

$$\begin{aligned} P(S \setminus J) &= \frac{P(J \setminus S)P(S)}{\sum_S P(J \setminus S)P(S)} \\ &= \frac{1}{Z}\exp\left[\ln P(J \setminus S) + \ln P(S)\right] \end{aligned} \quad (1)$$

In the statistical physics description, the probability (1) can be expressed as a Boltzmann distribution at the inverse temperature β [9].

$$P(S \setminus J) = \frac{1}{Z}\exp\left[-\beta H(S \setminus J)\right] \quad (2)$$

where $H(S \setminus J)$ is the Hamiltonian of the system.

In this Hamiltonian, we identify two components that are necessary for the analysis of LDPC codes.

- A term that guarantees that all parity checks are satisfied. It can be written with the Kronecker's delta δ [1].

$$P(J \setminus S) = \prod_{\mu=1}^{M} \delta\left[J_\mu, \prod_{j \in L(\mu)} S_j\right]$$

According [9], the δ 's can be replaced by a soft constraint.

$$P(J \setminus S) = const \exp\left[\beta \sum_{\mu=1}^{M} J_\mu \prod_{j \in L(\mu)} S_j\right]$$

Copyright © 2010 SciRes.

where $\beta \to \infty$.

- A prior term that provides some statistical information on the dynamical variables S. It can be represented by the prior distribution

$$P(S) = \frac{\exp\left(F \sum_{j=1}^{N} S_j \right)}{(2\cosh F)^N}$$

where F is the external field. It is determined by the flip rate f of channel noise as $F = \frac{1}{2}\ln\frac{1-f}{f}$.

So, the Hamiltonian $H(S \setminus J)$ is written as follows:

$$H(S \setminus J) = -\sum_{\mu=1}^{M} J_\mu \prod_{j \in L(\mu)} S_j - \frac{F}{\beta}\sum_{j=1}^{N} S_j$$

where J_μ is the muti-spin coupling.

3.2. Decoding in the Statistical Physics

The decoding process corresponds to finding local magnetization at the inverse temperature β, $m_j = \langle S_j \rangle_\beta$ and calculating estimates as [1].

$$\hat{S}_j = \operatorname{sign}(m_j) \tag{3}$$

The decoding performance in the statistical physics approach can be measured by the magnetization [1] defined by the overlap between the actual message and estimate:

$$m = \left\langle \frac{1}{N}\sum_{j=1}^{N} S_j \hat{S}_j \right\rangle$$

Here the overage $\langle ... \rangle$ is performed over the matrices A. This value provides information about the typical performance of the code.

The Magnetization is an order parameter which has a standard of judgment whether the whole system exhibits an ordered state or not.

- If $m = 1$ the system is in an ordered phase called ferromagnetic phase.
- If $m = 0$ the system is in a disordered phase called paramagnetic phase.

Two main methods can be employed for calculating the value of the magnetization: the replica method for diluted systems [9] and the TAP approach [8]. In this paper, we are interested only on the TAP approach.

3.3. TAP Approach

Kabashima, *et al*. [8] have shown the similarity between equations derived from the TAP [2] approach and those obtained from BP. The fields $q_{\mu j}^{a}$ correspond to the mean influence of sites other than the site j and the fields $r_{\mu j}^{a}$ represent the influence of j back over the system (reaction fields) [10].

The similarity can be exposed by observing that the likelihood $P(J_\mu \setminus S)$ is proportional to the Boltzmann weight [11]

$$\omega_B\left(J_\mu \setminus \{S_j : j \in L(\mu)\}\right) = \exp\left(-\beta J_\mu \prod_{j \in L(\mu)} S_j \right)$$

The conditional probability $r_{\mu j}^{S_j}$ can be seen as a normalized effective Boltzmann weight (effective Boltzmann probability) obtained by fixing the bit S_j [10]

$$\begin{aligned} r_{\mu j}^{S_j} &= \alpha_{\mu j}\omega_{eff}\left(J_\mu \setminus S_j\right) \\ &= \alpha_{\mu j}\sum_{S_l : l \in L(\mu)\setminus j} \omega_B\left(J_\mu \setminus \{S_l : l \in L(\mu)\}\right) \prod_{l \in L(\mu)\setminus j} q_{\mu l}^{(S_l)} \end{aligned}$$

Since spin variable S_j takes only two values ± 1, it is convenient to express the BP/TAP algorithm using spin averages $\sum_{S_j=\pm 1} S_j q_{\mu j}^{S_j}$ and $\sum_{S_j=\pm 1} S_j r_{\mu j}^{S_j}$ rather than the distributions $q_{\mu j}^{S_j}$ and $r_{\mu j}^{S_j}$ themselves. We use $\delta q_{\mu j} = m_{\mu_j}$ to denote $\sum_{S_j=\pm 1} S_j q_{\mu j}^{S_j}$. Similar notation $\delta r_{\mu j} = \hat{m}_{\mu_j}$ is used for $\sum_{S_j=\pm 1} S_j r_{\mu j}^{S_j}$. Additionally, it was shown in [10] that the following statements hold

$$\hat{m}_{\mu j} = \tanh(\beta J_\mu) \prod_{l \in L(\mu)\setminus j} m_{\mu l} \tag{5}$$

$$m_{\mu j} = \tanh\left(\sum_{\nu \in M(j)\setminus \mu} \tanh^{-1}(\hat{m}_{\nu j}) + \beta F \right) \tag{6}$$

The pseudo-posteriori can then be calculated

$$m_j = \tanh\left(\sum_{\mu \in M(l)} \tanh^{-1}(\hat{m}_{\mu j}) + \beta F \right) \tag{7}$$

This provides a way for computing the Bayes optimal decoding as follows:

$$\hat{S}_j = \operatorname{sign}(\delta q_j) = \operatorname{sign}(m_j) \tag{8}$$

The result that $\delta q_j = m_j$ is demonstrated as follows:

$$\begin{aligned} m_j &= \langle S_j \rangle_\beta \\ &= \frac{1}{Z}\sum_{S} S_j \exp[-\beta H(S \setminus J)] \\ &= \sum_{S} S_j P(S \setminus J) \\ &= \sum_{S_j} S_j \sum_{S \setminus S_j} P(S \setminus J) \\ &= \sum_{S_j} S_j P(S_j \setminus J) \\ &= \delta q_j \end{aligned} \tag{9}$$

Copyright © 2010 SciRes.

4. LLR-BP Algorithm and its Simplifications with TAP Approach

4.1. LLR-BP Algorithm with TAP Approach

In the LLR-BP algorithm instead of handling probabilities as in [3,5] we are going to deal with the LLRs. In practice, using LLRs as messages offers implementation advantages over using probabilities or likelihood ratios because multiplications are replaced by additions and the normalization step is eliminated [11].

In this section, we try to develop the LLR-BP with the TAP approach. Let $x_{\mu j}$ and $y_{\mu j}$ be the LLR of bit j which are sent from bit node j to check node μ and from the check node μ to bit node j, respectively. From the statistical physics definition, the LLR is defined as follows [12]:

$$x_{\mu j} = \frac{1}{2\beta}\ln\frac{q_{\mu j}^{+1}}{q_{\mu j}^{-1}} = \frac{x_{\mu j}^{'}}{2\beta} \tag{10}$$

And

$$y_{\mu j} = \frac{1}{2\beta}\ln\frac{r_{\mu j}^{+1}}{r_{\mu j}^{-1}} = \frac{y_{\mu j}^{'}}{2\beta} \tag{11}$$

We need also the following results

$$\begin{aligned}\tanh\left(\beta x_{\mu j}\right) &= \tanh\left(\frac{1}{2}\ln\left(\frac{q_{\mu j}^{+1}}{q_{\mu j}^{-1}}\right)\right)\\ &= \frac{q_{\mu j}^{+1}-q_{\mu j}^{-1}}{q_{\mu j}^{+1}+q_{\mu j}^{-1}}\\ &= q_{\mu j}^{+1}-q_{\mu j}^{-1}\\ &= m_{\mu j}\end{aligned} \tag{12}$$

Like in (12), the variable $\hat{m}_{\mu j}$ can be also written as:

$$\hat{m}_{\mu j} = \tanh\left(\beta y_{\mu j}\right) \tag{13}$$

So, from Equations (5), (12) and (13) we have

$$\begin{aligned}x_{\mu j} &= \frac{1}{\beta}\tanh^{-1}\tanh\left(\sum_{\nu\in M(j)\setminus\mu}\tanh^{-1}\left(\hat{m}_{\nu j}\right)+\beta F\right)\\ &= \sum_{\nu\in M(j)\setminus\mu} y_{\nu j} + F\end{aligned} \tag{14}$$

Also, $y_{\mu j}$ can be written as

$$\begin{aligned}y_{\mu j} &= \frac{1}{\beta}\tanh^{-1}\left(\hat{m}_{\mu j}\right)\\ &= \frac{1}{\beta}\tanh^{-1}\left(\tanh\left(\beta J_{\mu}\right)\prod_{l\in L(\mu)\setminus j}\tanh\left(\beta x_{\mu l}\right)\right)\end{aligned} \tag{15}$$

Finally, the posteriori LLR of bit S_j is

$$x_j = \sum_{\mu\in M(j)} y_{\mu j} + F \tag{16}$$

It's not easy to implement (15) which has the form of a product. Our idea is to decompose the check node update into sign and magnitude processing like in [13]. We have from (15)

$$\tanh\left(\beta y_{\mu j}\right) = \tanh\left(\beta J_{\mu}\right)\prod_{l\in L(\mu)\setminus j}\tanh\left(\beta x_{\mu l}\right) \tag{17}$$

Replacing $\left(\beta J_{\mu}\right)$ by $\operatorname{sign}\left(\beta J_{\mu}\right)\times\left|\beta J_{\mu}\right|$ and $\left(\beta x_{\mu l}\right)$ by $\operatorname{sign}\left(\beta x_{\mu l}\right)\times\left|\beta x_{\mu l}\right|$ in (17) yields

$$\begin{aligned}\operatorname{sign}\left(\beta y_{\mu j}\right) &= \prod_{l\in L(\mu)\setminus j}\operatorname{sign}\left(\beta^2 J_{\mu}x_{\mu l}\right)\\ &= \prod_{l\in L(\mu)\setminus j}\operatorname{sign}\left(J_{\mu}x_{\mu l}\right)\end{aligned} \tag{18}$$

$$\begin{aligned}\tanh\left|\beta y_{\mu j}\right| &= \tanh\left|\beta J_{\mu}\right|\prod_{l\in L(\mu)\setminus j}\tanh\left|\beta x_{\mu l}\right|\\ \tanh\left|\frac{y_{\mu j}^{'}}{2}\right| &= \tanh\left|2\frac{\beta J_{\mu}}{2}\right|\prod_{l\in L(\mu)\setminus j}\tanh\left|\frac{x_{\mu l}^{'}}{2}\right|\end{aligned} \tag{19}$$

Let $f(t)$ be defined by

$$f(t) = -\ln\left(\tanh\left(\frac{t}{2}\right)\right) = \ln\frac{e^t+1}{e^t-1} \tag{20}$$

Then, taking the logarithm of the inverse of both sides of (19) yields

$$\begin{aligned}-\ln\tanh\left|\frac{y_{\mu j}^{'}}{2}\right| &= -\ln\tanh\left|2\frac{\beta J_{\mu}}{2}\right| + \sum_{l\in L(\mu)\setminus j} -\ln\tanh\left|\frac{x_{\mu l}^{'}}{2}\right|\\ f\left(\left|y_{\mu j}^{'}\right|\right) &= f\left(\left|2\beta J_{\mu}\right|\right) + \sum_{l\in L(\mu)\setminus j} f\left(\left|x_{\mu l}^{'}\right|\right)\end{aligned} \tag{21}$$

The Equation (20) verifies

$$f\left(f(t)\right) = \ln\frac{\left(\frac{e^t+1}{e^t-1}\right)+1}{\left(\frac{e^t+1}{e^t-1}\right)-1} = t \tag{22}$$

So the Equation (21) can be written

$$\left|y_{\mu j}^{'}\right| = f\left(f\left(\left|2\beta J_{\mu}\right|\right) + \sum_{l\in L(\mu)\setminus j} f\left(\left|x_{\mu l}^{'}\right|\right)\right) \tag{23}$$

Using (10) and (11), the Equation (23) can be written as

$$\left|2\beta y_{\mu j}\right| = f\left(f\left(\left|2\beta J_{\mu}\right|\right) + \sum_{l\in L(\mu)\setminus j} f\left(\left|2\beta x_{\mu l}\right|\right)\right) \tag{24}$$

From (18) and (24), the check node processing in the statistical physics is denoted by

Copyright © 2010 SciRes.

$$y_{\mu j} = \prod_{l\in L(\mu)\setminus j} \operatorname{sign}\left(J_\mu x_{\mu l}\right)\times\frac{1}{2\beta}\times f\left(f\left(\left|2\beta J_\mu\right|\right)+\sum_{l\in L(\mu)\setminus j} f\left(\left|2\beta x_{\mu l}\right|\right)\right) \quad (25)$$

4.2. BP-Based with TAP Approach

In this section, we try to develop the approximation of the BP algorithm: the BP-Based [6] algorithm, with the TAP approach. The key idea of this algorithm is that $\sum_t f(t) \le f\left(\min_t t\right)$. The inequality is clear while depicting the function $f(t)$ on the **Figure 1**.

The Equation (24) is then approximated by

$$\begin{aligned}\left|2\beta y_{\mu j}\right| &= f\left(f\left(\left|2\beta J_\mu\right|\right)+\sum_{l\in L(\mu)\setminus j} f\left(\left|2\beta x_{\mu l}\right|\right)\right)\\ &\approx f\left(f\left(\min_{l\in L(\mu)\setminus j}\left(\left|2\beta J_\mu\right|,\left|2\beta x_{\mu l}\right|\right)\right)\right)\\ &= \min_{l\in L(\mu)\setminus j}\left(\left|2\beta J_\mu\right|,\left|2\beta x_{\mu l}\right|\right)\end{aligned} \quad (26)$$

So, the extrinsic information in the BP-Based algorithm written with the TAP equation is given by:

$$\begin{aligned}y_{\mu j} &= \prod_{l\in L(\mu)\setminus j}\operatorname{sign}\left(J_\mu x_{\mu l}\right)\times\frac{1}{2\beta}\times\min_{l\in L(\mu)\setminus j}\left(\left|2\beta J_\mu\right|,\left|2\beta x_{\mu l}\right|\right)\\ &= \prod_{l\in L(\mu)\setminus j}\operatorname{sign}\left(J_\mu x_{\mu l}\right)\times\min_{l\in L(\mu)\setminus j}\left(\left|J_\mu\right|,\left|x_{\mu l}\right|\right)\end{aligned} \quad (27)$$

Therefore, there is an important simplification in the BP-Based algorithm with TAP approach since the check node update is replaced by a selection of the minimum input value.

4.3. λ-min Algorithm with TAP Approach

In this section, we try to develop the λ-min algorithm [7] with the TAP approach. In the check node update of (25), the magnitude processing is run using the function defined by (20). While depicting this function on the **Figure 1**, it is clear that $\sum_t f(t)$ can be approximated by the maximal values of $f(t)$ which is obtained for the minimal values of $|t|$.

So, like Guilloud, *et al*. [7] we propose to compute (24) with only the λ bits that participate in check μ and which have the minimum magnitude.

$$\left|2\beta y_{\mu j}\right| = f\left(f\left(\left|2\beta J_\mu\right|\right)+\sum_{l\in L_\lambda(\mu)\setminus j} f\left(\left|2\beta x_{\mu l}\right|\right)\right) \quad (28)$$

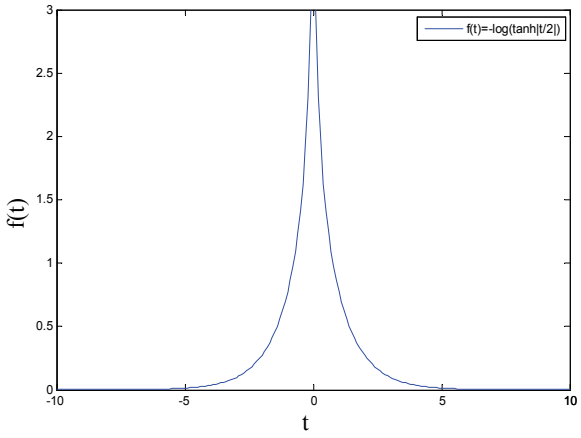

Figure 1. Shape of the function *f*.

With $L_\lambda(\mu)=\{j_0,...,j_{\lambda-1}\}$ be the subset of $L(\mu)$ which contains the λ bits that participate in check μ which $x_{\mu l}$ have the smallest magnitude.

The extrinsic information in the λ-min algorithm written with the TAP equation is given by (29)

$$y_{\mu j} = \prod_{l\in L(\mu)\setminus j}\operatorname{sign}\left(J_\mu x_{\mu l}\right)\times\frac{1}{2\beta}\times f\left(f\left(\left|2\beta J_\mu\right|\right)+\sum_{l\in L_\lambda(\mu)\setminus j} f\left(\left|2\beta x_{\mu l}\right|\right)\right) \quad (29)$$

Two cases will occur: if the bit j belongs to the subset $L_\lambda(\mu)$, then $y_{\mu j}$ are processed over $(\lambda-1)$ values of $L_\lambda(\mu)\setminus j$, otherwise $y_{\mu j}$ are processed over the λ values of $L_\lambda(\mu)$. Hence, for the second case, the computations have to be performed only once [13].

5. Simulation Results

Simulations have been performed using regular (3,6) LDPC code of length $N=1008$ and with 20 decoding iterations. We averaged the results over 10 codes. This ensemble of LDPC code is characterized by the same block length, the ones in each column and the ones in each row. For each run, a fixed code is used to generate 1008 bit codeword from 504 bit message. Corrupted versions of the codeword are then decoded using LLR-BP, BP-Based and λ-min decoding algorithms.

To observe the effect of the simplification in (27) and (29) on the performance from a statistical physics point of view, we have calculated the overlap between the actual message and the estimate (magnetization) for each fixed code and for each algorithm. After, we average the obtained results for the 10 different codes. **Figure 2** depicts the magnetization performance of the LLR-BP, BP-Based and the λ-min algorithms.

Copyright © 2010 SciRes.

According the results of **Figure 2**, we can conclude the effectiveness of the λ-min algorithm. At a magnetization of 0.9, the BP-Based algorithm introduces a degradation of 0.5 dB with 20 iterations. The 2-min algorithm introduces a degradation of 0.3 dB. The performance of the 3-min algorithm is slightly worse than that of the LLR-BP algorithm, the degradation is only 0.08 dB.

Another remark from **Figure 2** is that at high signal to noise ratio the magnetization is concentrate at the value $m = 1$. This value corresponds to the ferromagnetic state in the statistical physics and to the perfect decoding in the information theory.

The analogy between the Bit Error Rate (BER) performance and the magnetization performance can be examined in [14].

6. Conclusions

In this paper, we have been interested in the decoding of LDPC codes from a statistical physics approach. First, we have examined the correspondence between LDPC codes and Ising spin systems. The relation between the BP algorithm and TAP approach is investigated. Then, we showed that LLR-BP algorithm and its simplification *i.e.* the BP-Based algorithm and the λ-min algorithm can be obtained using the TAP approach of Ising spin systems in statistical physics. Besides, we have presented the performance of the decoding algorithms using a statistical physics parameter which is the magnetization.

Finally, we concluded that the BP-Based algorithm reduces the complexity for updating extrinsic information but there is degradation in performance compared to the LLR-BP algorithm. The λ-min algorithm reduces the complexity for updating extrinsic information without degradation in performance compared to the LLR-BP algorithm especially when λ increases. These results confirm with the results obtained in the information theory.

As a perspective of our work, we propose to study the replica method. This is a method from the statistical physics applied to find the magnetization. Besides, we propose to simplify the equations of this method by the same approximation in the BP-Based algorithm and the λ-min algorithm in order to compare the analytic results with the experimental ones.

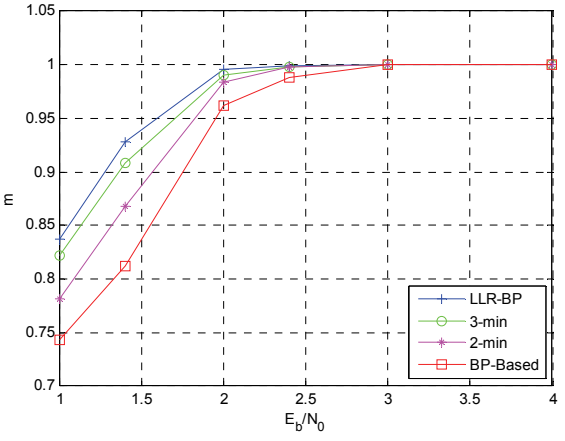

Figure 2. Magnetization performance of the LLR-BP, BP-Based and λ-min algorithms with λ = {2, 3}, for the (1008, 3, 6) LDPC code ensemble and with 20 decoding iterations.

7. References

[1] N. Sourlas, "Spin-Glass Models as Error-Correcting Codes," *Nature*, Vol. 339, No. 6227, 1989, pp.693-695.

[2] D. J. Thouless, P. W. Anderson and R. G. Palmer, "Solution of Solvable Model of A Spin Glass," *Philosophical Magazine*, Vol. 35, No. 3, 1977, pp. 593-601.

[3] R. G. Gallager, "Low-Density Parity-Check Codes," M.I.T. Press, Cambridge, Massachusetts, 1963.

[4] D. J. C. Mackay and R. M. Neal, "Near Shannon Limit Performance of Low Density Parity Check Codes," *Electronics Letters*, Vol. 32, No. 18, 1996, pp.1645-1646.

[5] D. J. C. Mackay, "Good Error-Correcting Codes Based on Very Sparse Matrices," *IEEE Transactions on Information Theory*, Vol. 45, No. 2, 1999, pp. 399-431.

[6] M. P. C. Fossorier, M. Mihaljevic and I. Imai, "Reduced Complexity Iterative Decoding of Low Density Parity Check Codes Based on Belief Propagation," *IEEE Transactions on Communications*, Vol. 47, No. 5, 1999, pp. 673-680.

[7] F. Guilloud, E. Boutillon and J. L. Danger, "λ-Min Decoding Algorithm of Regular and Irregular LDPC Codes," *Proceedings of 3rd International Symposium on Turbo Codes & Related Topics*, Brest, 2003, pp. 451-454.

[8] Y. Kabashima and D. Saad, "Belief Propagation vs. TAP for Decoding Corrupted Messages," *Europhysics Letters*, Vol. 44, No. 5, 1998, pp. 668-674.

[9] T. Murayama, Y. Kabashima, D. Saad and R. Vicente, "Statistical Physics of Regular Low-Density Parity-Check Error-Correcting Codes," *Physical Review E*, Vol. 62, No. 2, 2000, pp. 1577-1591.

[10] R. Vicente, D. Saad and Y. Kabashima, "Finite-Connectivity Systems as Error-Correcting Codes," *Physical Review E*, Vol. 60, No. 5, 1999, pp. 5352-5366.

[11] J. Chen, A. Dholakia, E. Eleftheriou, M. Fossorier and X. Y. Hu, "Reduced-Complexity Decoding of LDPC Codes," *IEEE Transactions on Communications*, Vol. 53, No. 8, 2005, pp. 1288-1299.

[12] M. Mezard and A. Montanari, "Information, Physics and Computation," Oxford University Press, Oxford, 2008.

[13] F. Guilloud, "Generic Architecture for LDPC Codes Decoding," PhD Thesis, ENST Paris, 2004.

[14] M. Abdelhedi, O. Hamdi and A. Bouallegue, "Magnetization Performance of LDPC Decoding Algorithms," *International Journal of Information and Coding Theory*, 18 March 2010.

Copyright © 2010 SciRes.

Int. J. Communications, Network and System Sciences, **2010, 3, 554-562**
doi:10.4236/ijcns.2010.36074 Published Online June 2010 (http://www.SciRP.org/journal/ijcns/).

Scientific Research

Performance of Multirate Multicast in Distributed Network

Soumen Kanrar, Mohammad Siraj
Department of Computer Engineering (*College of Computer and Information Sciences*),
King Saud University, Riyadh, Saudi Arabia
E-mail: {*sasit, siraj*}*@ksu.edu.sa*
Received March 11, 2010; *revised April* 19, 2010; *accepted May* 22, 2010

Abstract

The number of Internet users has increased very rapidly due to the scalability of the network. The users demand higher bandwidth and better throughput in the case of on demand video, or video conference or any real time distributed network system. Performance is a great issue in any distributed networks. In this paper we have shown the performance of the multicast groups or clusters in the distributed network system. In this paper we have shown the performance of different users or receivers belongs to the multicast group or cluster in the distributed network, transfer data from the source node with multirate multicast or unirate multicast by considering packet level forwarding procedure in different sessions. In this work we have shown that how the throughput was effected when the number of receiver increases. In this work we have considered the different types of queue such as RED, Fair queue at the junction node for maintaining the end to end packet transmission. In this work we have used various congestion control protocol at the sender nodes. This paper we have shown the performance of the distributed cluster network by multirate multicast.

Keywords: Throughput, Performance, Distributed Network, Cluster, Multicast, Session, Multirate Multicast, Queue

1. Introduction

The users *i.e.* the receivers are connected to the source for transferring data or exchanging information. Here the source and the receivers are forming a network, that network is scalable *i.e.*, in the network any new user or receiver can join. According to the real world scenario any number of existing user or receiver can leave from the cluster network can join different cluster or group. Each cluster be from a distributed network and well connected with other network. For any particular multicast group in the distributed network, the consist members of the group run different application program and required different packet size and data rate.

The performance of the distributed network in heterogeneous system, obtained by markovian model [1] and the queuing processing delay at the junction node.

Sending packets to the destination node with the minimum cost transmission delay, multicast session network coding techniques scheme used [2]. The end to end packet transmission in a set of active elastic sessions over a network, the session traffic [3] routed to the destination node through different path. The collision free broadcasting technique used [4] to minimize the latency and the number of transmissions in the broadcast network for end to end packet transmission in the distributed cluster network. The alternative ways for end to end packet forwarding used minimal congestion feed back signals from the router [5] and split the flow between each source destination pair. In end to end packet transmission, the random delay and TCP–congestion control [6] in the network is a issue. Receiver adjusts the rate based on the congestion level in Multicast Network [7] to reduce the congestion. In the real life scenario multicast traffic can cause more packet loss than uncast traffic for example in internet. The resource allocation by the Max –min fairness [8,9] and proportional fairness can reduce the traffic load in the network. The control multicast in the Network by using TCP [10,11] reduce the traffic load in the network. The inverted tree structure implemented in IP based network with the multicast session [12,13] to achieve better performance. The TCP congestion and the effect of that on the throughput of Multicast Group have greater impact in the system network [14]. Since the data

Copyright © 2010 SciRes.

packet be transferred between the source and receiver for end to end connection. The path between the source and receiver is not peer to peer, there be at least one junction node in between them .Due to limited bandwidth in the connecting paths, and queuing delay, data packet may be loss. The packet processing delay at the junction node (it is random service time) and the propagation time in the link be consider, the packet transmission delay at the junction node be negligible. The different receivers take data packet from the source node via the junction node (there may be more than one junction nodes in the source to receiver link). Now different receivers taken data packet with different rate in the multicast group of the distributed network in a multicast session. It is called the multirate multicast .If all the receiver node taken data packet with same rate it is called unirate multicast. Each multicast session is the collection of virtual session [15,16].

$S_j = \bigcup_{i=1}^{n} s_i^j$ where S_j is the *j*th multicast session, and n is the number of node (receiver) clearly, cardinality(S_j) $\leq$ n because in a particular session all receiver may not received data packet . s_i^j is the virtual session in the *j*-th multicast session for the *i*th receiver node in the multicast group. Different type of tree formed in the cluster of the distributed network like the **Figures 1**,**2**,**3**.

In **Figure 1** there is one multicast group and one junction node, In **Figure 2** there are two multicast group and two junction node In **Figure 3** three multicast group and three junction node. The receiver node takes data packet from the source node via the junction node through the source to receiver link path. The different types of queue like RED, FQ, SFQ attach at the junction node to capture the packet loss and measure the delay for the multicast group in the multirate multicast session. **Figure 4** represent the junction node [17].

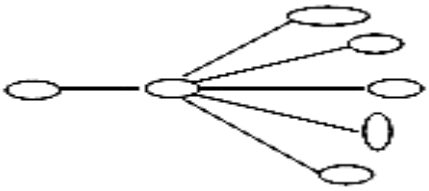

Figure 1. One multicast group.

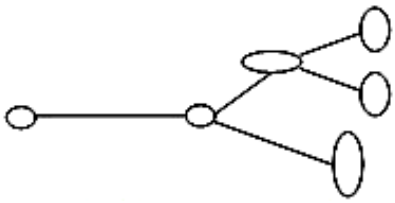

Figure 2. Two multicast group.

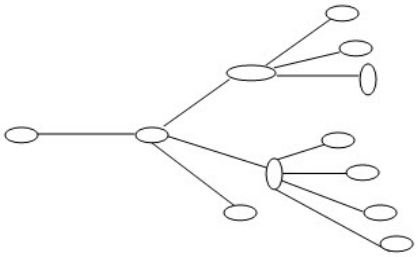

Figure 3. Three multicast group.

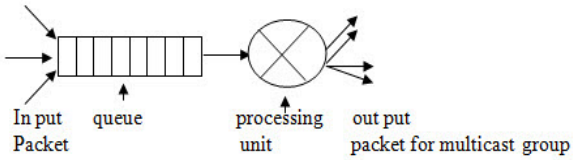

Figure 4. Junction node.

Figure 4 represents the junction node of the network. The packets approach the junction node randomly and the queue stored the packets. The packets stored into the queue in the order *n* + 1, *n*, *n* – 1… *i.e.*, the $(n-1)th$ packet be forwarded to the processing unit after that the $(n)th$ and $(n+1)th$ be forwarded to the processing unit. In side the queue there be waiting time for each packet and each packet have random service time or processing time according to the size of the packet and the destination multicast group. By using the packet level simulation we check how the throughput, delay, packet loss how the throughput be effected by increasing the number of receiver in the multicast group. The paper is structured as follows Section 1 is introduction, Section 2 presents Proposed model Section 3 presents the algorithms for the mathematical models, Section 4 and 5 represents simulation results and the conclusion.

2. Proposed Model for Multirate Multicast Virtual Session

2.1. Assumption 1

Let L be the set of links and $l \in L$ be a particular link path. The maximum capacity of the link l is l_c. Let ^{+}S be the set of all session, such that $s \in S_l$ be the a particular session through link l, where S_l be the set of session passing through the link l . Clearly $^{+}S = \bigcup_l S_l$ and R_s be the set of receiver at the particular session s for the multicast group.

V_s be the set of virtual session that using the link l at the session s. If $p_{sr}(t)$ be the rate at which the data be transferred at session s to the receiver r at the time (t).

Then, $Max_{s \in S_l}\{p_{sr}\} \leq l_c$ briefly we can write

Copyright © 2010 SciRes.

$Max\{p_{sr} \mid s \in S_l\} \le l_c$ means we consider the maximum flow through the link path l for the set of session S_l within the threshold limit of the link capacity l_c. According to the **Figure 5**, There were the two sessions for sending data packet from the source node A to the receiver node C and the source node D to the receiver node C . Now the maximum data packet be transferred through the junction node B to the receiver node C be within the capacity of the link for the set of sessions.

In the 1^{st} session data packet be transferred like A->B->C and A->B->D and in the 2^{nd} session data packet be transferred like D->B->C. Here nodes {D,B,C} forming a multicast group for the network of nodes { A,B,C,D}.

Our objective is to maximize the flow within the congestion threshold window size at the source end by consider the multirate multicast. The basic objective goes to maximize the data flow from the source to the multicast group in presence of queue size and random service at the junction node or the random processing time at the junction node.

2.2. Assumption 2

Let $S_l^- \subseteq S_l$. Where S_l^- be the set of all session passing through the link l at time (*t*). here S_l a countable finite is set and S_l^- is the finite subset of S_l.

The total flow through the link l at time t be

$$\sum_{s \in S_l^-} \{p_{sr} : R^{\ge o} -> R^{\ge 0} \mid (r \in R_s)(s \in S_l)[Max\{p_{sr}(t)]\}$$

The above expression is the sum of the set of values for all session through link l at time *t*. where p_{sr} be a real valued function from the time domain to the real valued data rate where the suffix *r* and *s* are belongs to the set of receivers of the multicast group and s is the session through *l* link such that *r* and *s* belongs to sets R_s and S_l.

Here we consider only the maximum data rate at different session at time *t* for the receiver *r*.

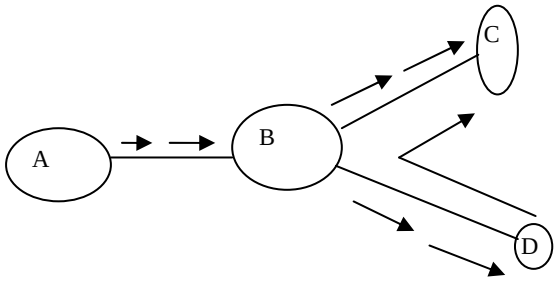

Figure 5. Distributed nodes.

3. Proposed Algorithm for the Packet Level Forwarding

It is possible to store information of all packet for all the multirate multicast session through the link path (source to receiver).

Here the proposed algorithms for selected single packet forwarding time computation from source to a receiver (that belongs to multicast group) per session that belongs to multirate multicast session.

Algorithm:

// $s \in S_p$, S_p be the set of all session passing through path p (source to receiver)
// k = cardinality (S_p)
// m be any selected packet for any session
// n be the number of nodes required for the link path source to receiver r.
// n $\le$ dimension of network
// S_m^i be the random service or processing time for the m^{th} packet at the i^{th} junction
// node.
// $S_m^i \in A[1..k,1\ldots n]$ in 2D space
// X_m^i be the forwarding time for the m^{th} packet at the i^{th} junction node
// $X_m^i \in B[1..k,1..n]$ in 2D space.
// t_m^i be the propagation time of the m^{th} packet between the junction nodes (i – 1) and (i)
// $t_m^i \in C[1..k,1..n]$ in 2D space.

Var
S_m^i, X_m^i, t_m^i : float
Var
T_p, T: integer // T_p be total propagation time one selected packet per session,

// source to receiver $T_p \in D[1..k,1]$. k
// numbers of rows and 1 column.
// T be the total time one packet per session // $T \in E[1..k,1]$
Var
sum = 0 : integer
2sum = 0 : integer

function : f (float a, float b)
{ if ABS(a) > ABS(b)
// ABS(a) is || a || in normed space
return (a)
if ABS(a) < ABS(b)

Copyright © 2010 SciRes.

```
                    return(b)
              if    ABS(a) = = ABS(b)
                    return(a)
            }

for   i = 1   to k do begin
for   j = 1   to n do begin
              A[i, j] = 0
              B[i, j] = 0
              C[i, j] =0
                                  end        // loop 1
                                  end        // loop 2
for   j=1 to n do begin
              D[j, 1] = 0;
              E[j, 1] = 0;
      end // loop for j
begin
for j = 1 to k do begin

 // repeat the process one packet per session
 //    selected  m^th  packet for the  j^th  session
for i=1 to n do begin
//    n be node index for the  r^th  receiver for a session

if ( i = = 1 )        // i = 1 is the source node

  X^1_m  =  X^1_{m-1}  +  S^1_m ;
// value of   X^1_{m-1}  is B[j–1,1] and B[1,1] is the // starting
clock time

B[j, 1] =  X^1_m  ;
    if ( i > 1 &&   i < r )
 //    r is the receiver node index
     {
X^i_m = f ( X^i_{m-1}  ,  X^{i-1}_m ) + S^i_m ;
// forwarding time of  (m-1)^th  packet at  i^th
// junction node and
//  m^th  packet at  (i-1)^th  junction node
 B[j, I] =  X^i_m ;
t^i_m  =  X^i_m  –  X^{i-1}_m  –  s^i_m ;        // where   t^1_m  =0
sum = sum +  t^i_m ;
      }  // end if block
if ( i = = n )
       {
X^r_m  =    X^{r-1}_m  + t^n_m ;
// r is the sink node, no further forward is
// required.  X^{r-1}_m   = B [j, r–1]
B[ j, r]   =  X^r_m ;
 // Approximate value of  t^n_m  is  1/(n-2) Σ_{j=2}^{n-1} t^j_m  as
// the sample mean of size (n – 2)

          } // end if block
sum = sum +  t^n_m
end       // loop for i
 sum = D[j, 1]
2sum = 0
for   i = 1 to n do begin
2sum = 2sum + B [j, i]
end   // loop for i
2sum = E [j, 1]
end        //   loop for   j
end       // Algorithm
```

By solving the number of computation of the proposed algorithm, the time complexity of the proposed algorithms belongs to $O(n^2)$.

4. Experimental Result and Discussion

The **Figure 6** shows the result corresponding to the diagram **Figure 1** where the data transferred from the source node through the junction node in a session. The receivers build a single cluster with a cluster head. The cluster has n–numbers of receiver nodes. The cluster members gradually connected to the source node *i.e*. it is gradually expands from the time 0.25 second (in a session) and gradually release resources *i.e.* the size of the cluster reduce from the 0.32 second (in other session). It shown from the **Figure 6** that when the number of nodes (receivers) increase in the cluster, the throughput decreases as in the receiver side, the packet loss increase *i.e*. packet delay increase. When the number of nodes in cluster decrease, *i.e.*, the member node leaves the group, the packet receive rate increase. As well as the throughput increases for the group as it is indicated in between the time (0.32, 0.35).

The **Figure 7** shows the result corresponds to the diagram **Figure 2**, initially the Network have two cluster of two different size. In a session up to 0.31 second member connected to the source node via the junction nodes and the receive packets After 0.31 second in the new session one group leave from the network, *i.e*. release the resources the **Figure 7** shows the effect that on the throughput.

In **Figure 8** and **Figure 9** the effect on the overall throughput when the one cluster leaves the network (smaller in number of nodes) and a comparatively bigger cluster connect to the network in other session. **Figure 10** and **Figure 11** represent how the load increased in junction nodes that connected to the two clusters. **Figure 12** and **Figure 13** represent the traffic pattern that pass through the two junction nodes that connected to the two different clusters.

Copyright © 2010 SciRes.

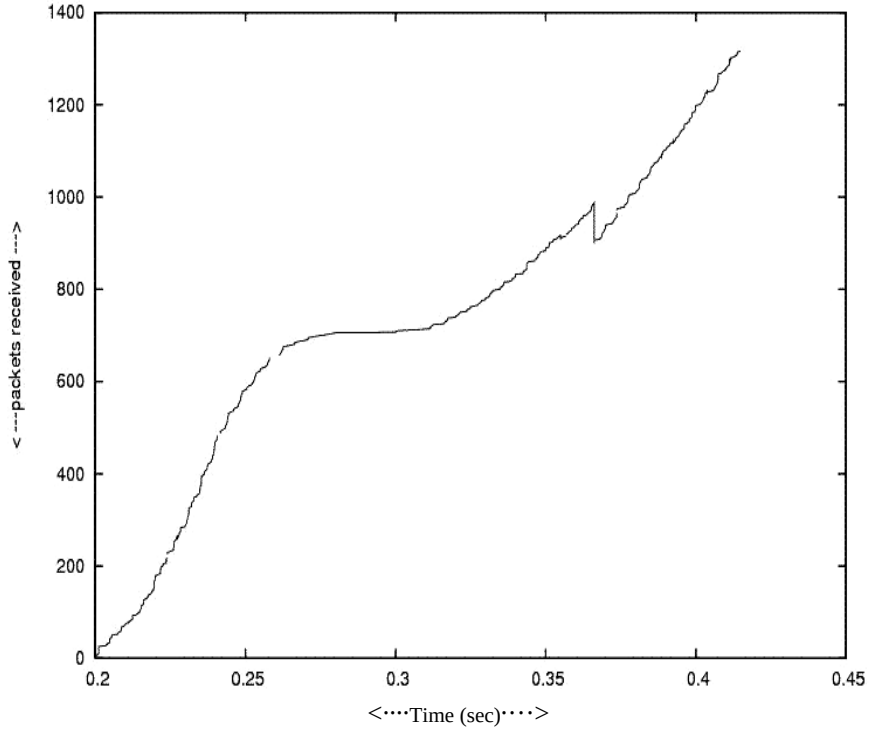

Figure 6. Packet received—Time.

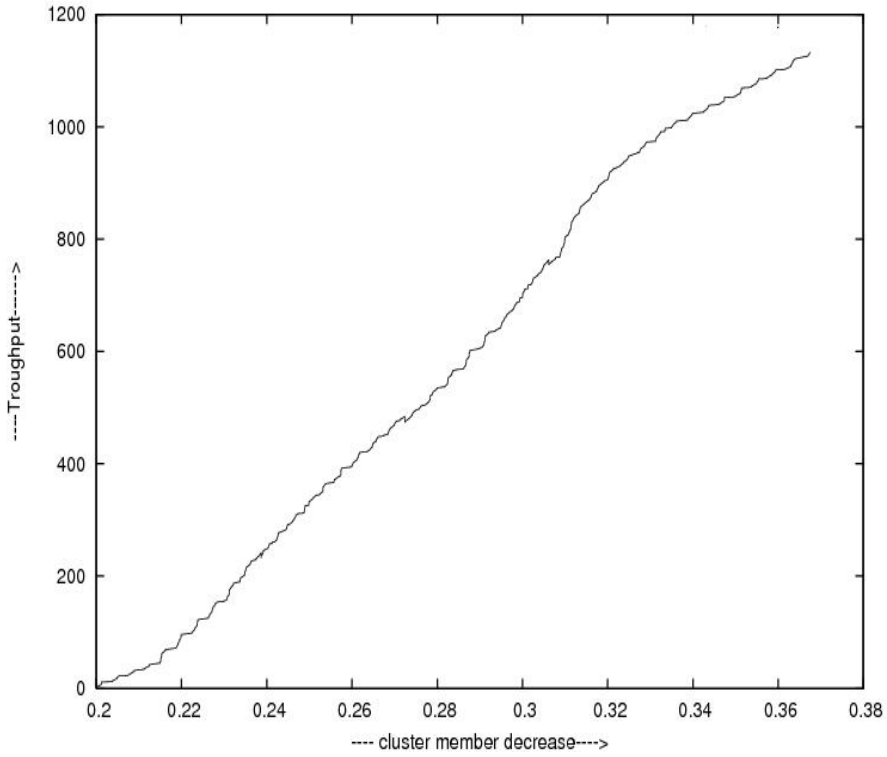

Figure 7. Throughput—Decrease cluster number time.

Copyright © 2010 SciRes.

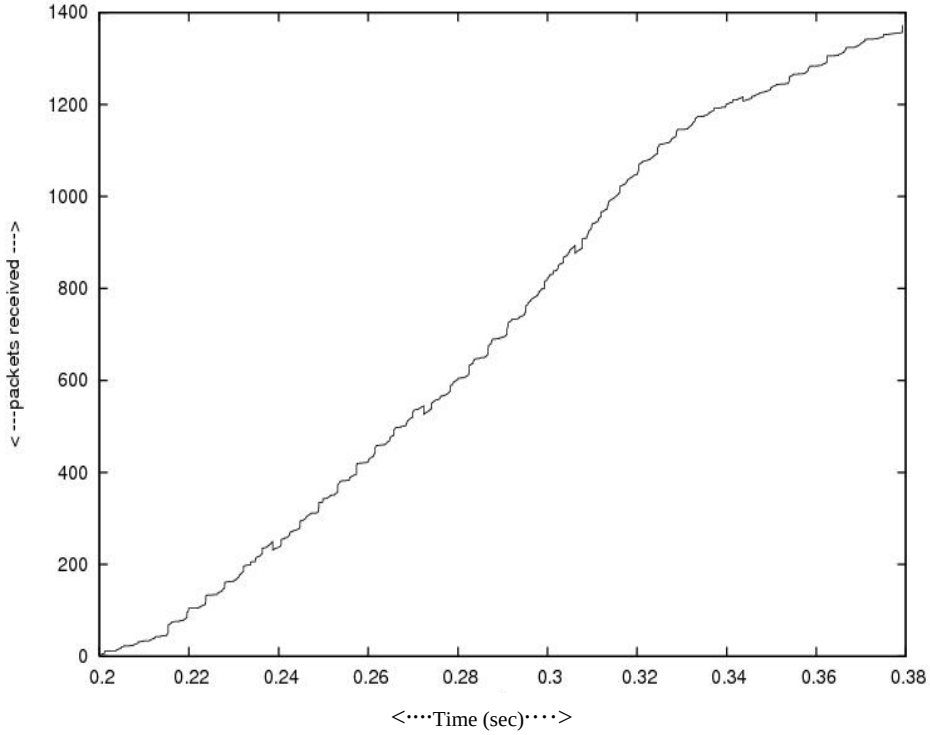

Figure 8. Packet receive.

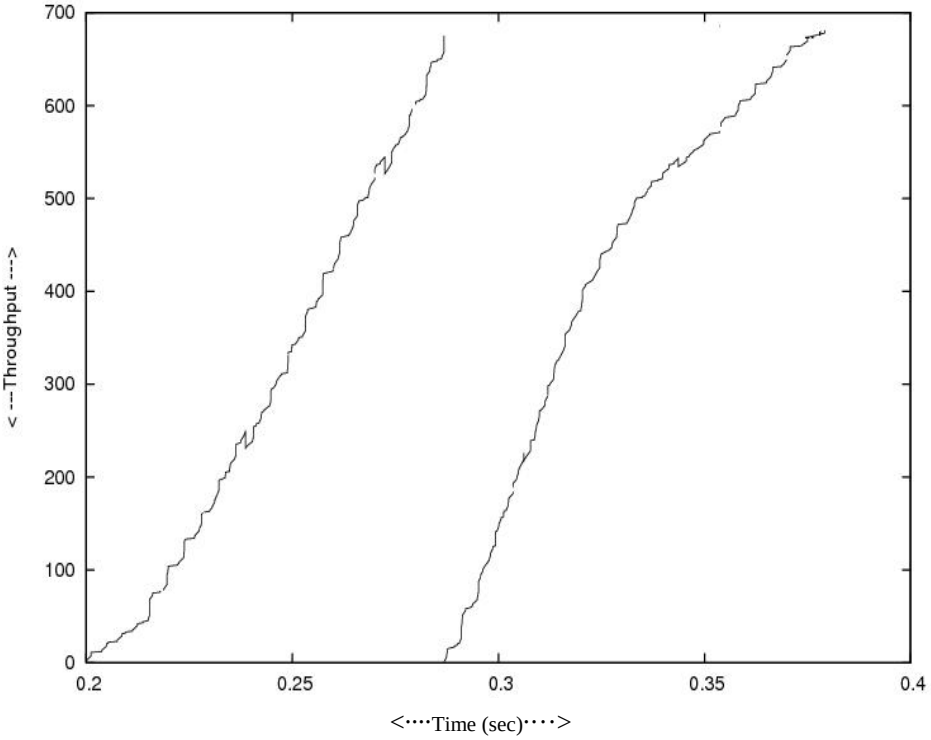

Figure 9. Throughput two different size clusters.

Copyright © 2010 SciRes.

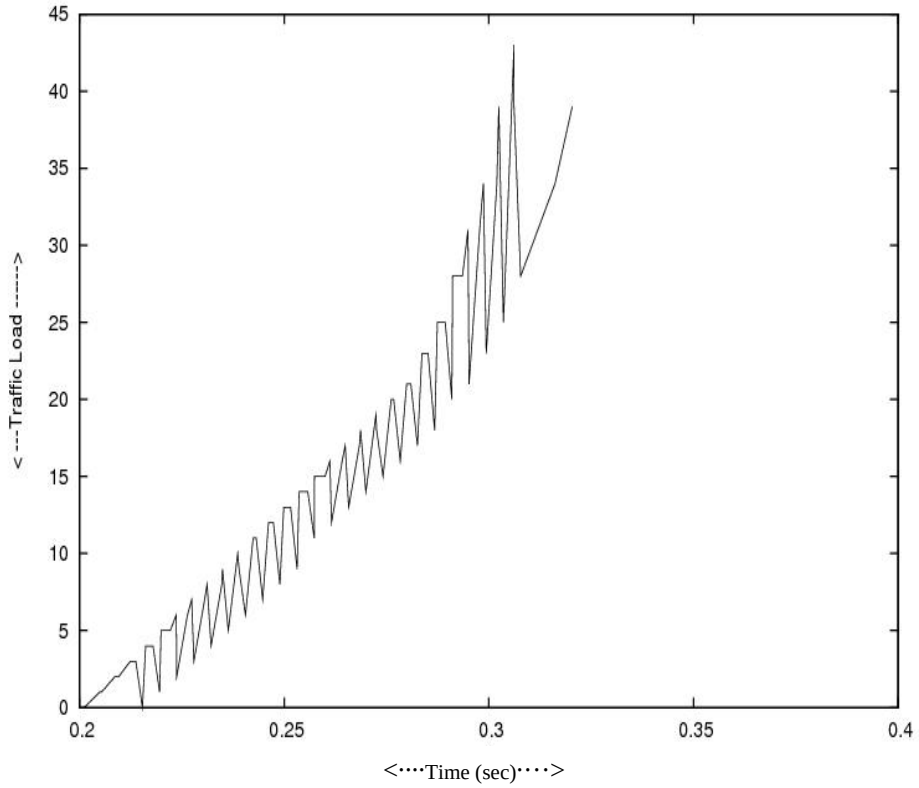

Figure 10. Traffic load in side the small cluster.

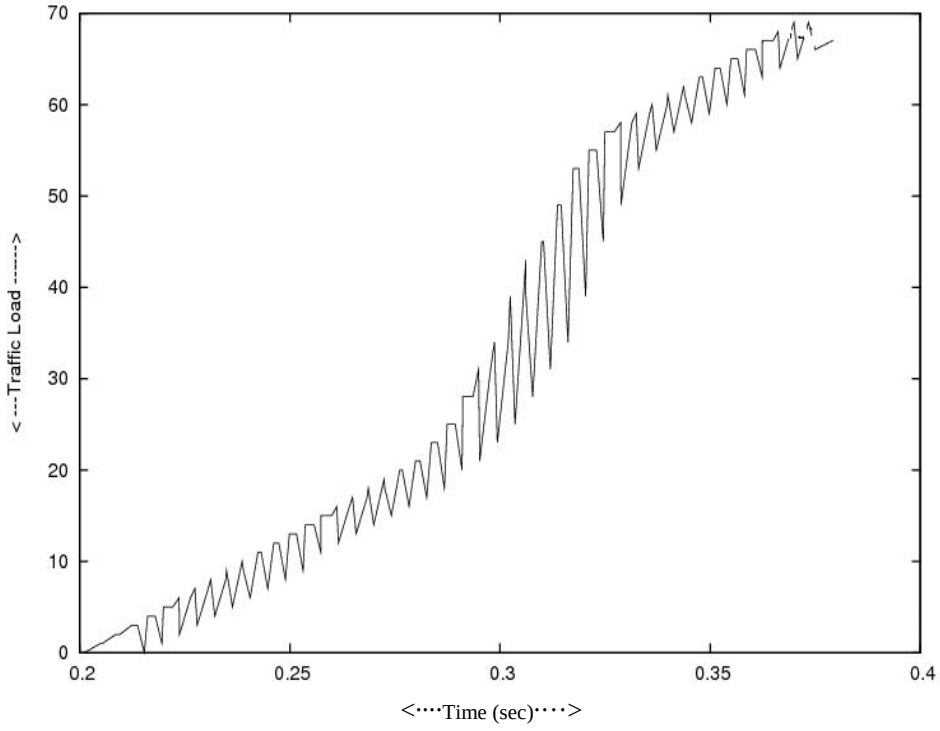

Figure 11. Traffic load in side big cluster.

Copyright © 2010 SciRes.

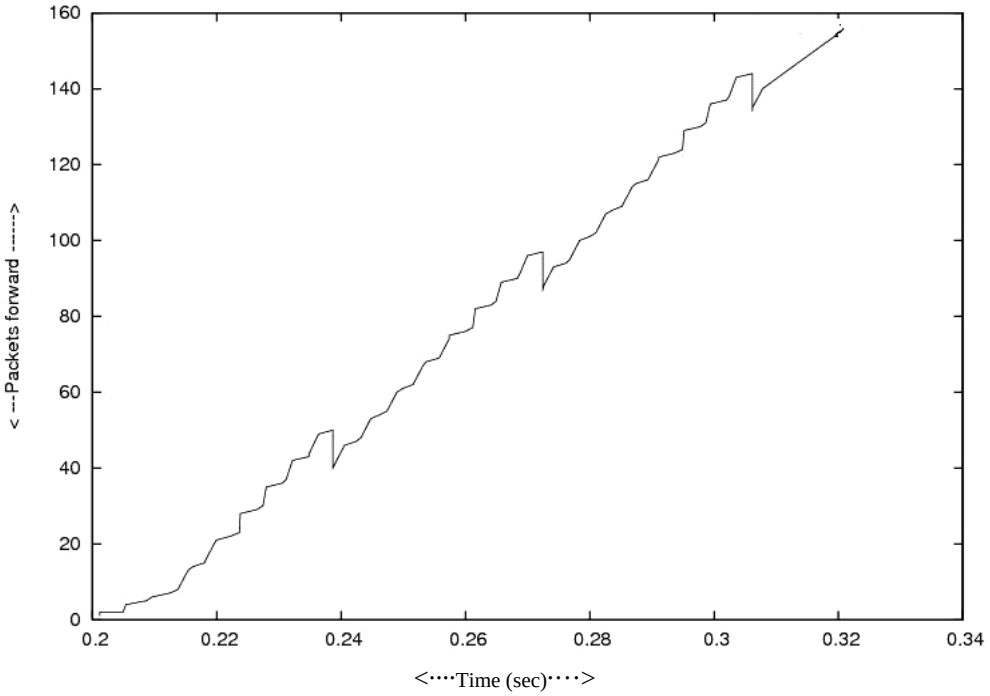

Figure 12. Packet received at receiver small cluster.

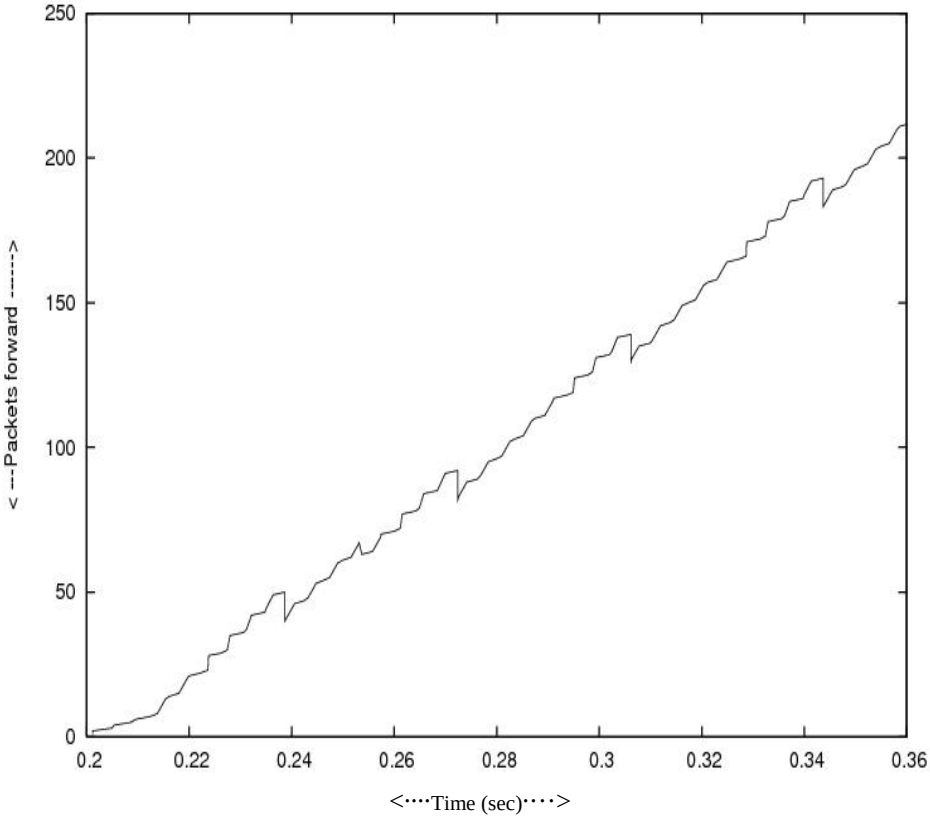

Figure 13. Packet received at receiver big cluster.

Copyright © 2010 SciRes.

5. Concluding Remarks

In this paper we develop the novel algorithms, the packet level forwarding in multicast session and on the basis of that we simulate the real problem in the lab environment. When the cluster size increases the throughput decreases. We consider a single cluster that expands in a session and reduces in other session as some nodes join in the cluster in a session and some node leaves as in other session.

We also study when the network is composed of multiple cluster and some cluster expands in number and some cluster reduces in number in different sessions. We experiment that with respect to real scenarios.

The work can be further extended for the problem arise in the next generation Network (NGN). In the case of IP based video on demand problem. In that case in spite of bandwidth limited constraint the number of receiver connected to the main video server as getting the clips Video –on-demand as IP data packets (datagram), the receiver forms single or more than one multicast groups .The receiver get the data packet as in the multicast session to the receiver as for the views particular (channel) that is related channel to a particular frequency.

6. References

[1] S. Kanrar and M. Siraj, "Performance of Heterogeneous Network," *International Journal of Computer Science and Network Security*, Vol. 9, No. 8, 2009, pp. 255-261.

[2] Y. F. Xi and E. M. Yeh, "Distributed Algorithms for Minimum Cost Multicast with Network Coding," *IEEE/ ACM Transaction on Networking*, Vol. 18, No. 2, 2009, pp. 379-392.

[3] J. Nair and D. Manjunath, "Distributed Iterative Optimal Resource Allocation with Concurrent Updates of Routing and Flow Control Variables," *IEEE/ACM Transaction on Networking*, Vol. 17, No. 4, 2009, pp. 1312-1325.

[4] R. Gandhi, A. Mishra and S. Parthasarathy, "Minimizing Broadcast Latency and Redundancy in Ad Hoc Networks," *IEEE/ACM Transaction on Networking*, Vol. 16 No. 4, 2008, pp. 840-851.

[5] H. Han, S. Shakkottai, C. V. Hollot, R. Srikant and D. Towsley, "Multi-Path TCP: A Joint Congestion Control and Routing Scheme to Exploit Path Diversity in the Internet," *IEEE/ACM Transaction on Networking*, Vol. 14, No. 6, 2006, pp. 1260-1271.

[6] S. J. Golestani and K. K. Sabanani, "Fundamental Observations on Multicast Congestation Control in The Internet," *Proceedings of IEEE INFOCOM*, New York, Vol. 2, March 1999, pp. 990-1000.

[7] X. Li, S. Paul and M. Ammar, "Layered Video Multicast with Retransmission (LVMR): Evaluation of Hierarchical Rate Control," *Proceedings of IEEE INFOCOM*, San Francisco, Vol. 3, June 1998, pp. 1062-1072.

[8] A. Mankin, A. Romanow, S. Bradner and V. Paxon, "IETF Criteria for Evaluating Reliable Multicast Transport and Application Protocols," Networking Working Group, Internet Draft, RFC 2357, 1998.

[9] J. Mo and J. Walrand, "Fair End to End Windows Based Congestion Control," *IEEE/ACM Transaction on Networking*, Vol. 8, No. 5, October 2000, pp. 556-557.

[10] F. P. Kelly, "Charging and Rate Control for Elastic Traffic," *European Transactions on Telecommunications*, Vol. 8, No. 1, 1998, pp. 33-37.

[11] M. Handley and S. Floyd, "Strawman Congestion Control Specifications," Internet Research Task Force (IRTF), Reliable Multicast Research Group (RMRG), 1998. http:// www.aciri.org/mjh/rmcc.ps.gz

[12] L. Rizzo, L. Vicisano and J. Crowcroft, "TCP Like Congestion Control for Layered Multicast Data Transfer," *Proceedings of IEEE INFOCOM*, San Francisco, Vol. 3, March 1998, pp. 996-1003.

[13] I. Stoica, T. S. E. Ng and H. Zhang, "REUNITE: A Recursive Unicast Approach to Multicast," *Proceedings of IEEE INFOCOM*, Tel Aviv, Vol. 3 March 2000, pp. 1644-1653.

[14] S. Bhattacharyya, D. Towslay and J. Kurose, "The Loss Path Multiplicity Problem in Multicast Congestion Control," *Proceedings of IEEE INFOCOM*, New York, Vol. 2, March 1999, pp. 856-863.

[15] A. Chaintreau, F. Baccelli and C. Doit, "Impact of TCP-Like Congestion Control on the Throughput of Multicast Grouph," *IEEE/ACM Transaction on Networking*, Vol. 10, No. 4, 2002, pp. 500-512.

[16] S. Deb and R. Srikant "Congestion Control for Fair Resource Allocation in Networks with Multicast Flow," *IEEE/ACM Transaction on Networking*, Vol. 12, No. 2, 2004, pp. 274-285.

[17] R. C. Chalmers and K. C. Almeroth, "Modeling the Branching Characteristics and Efficiency Gains of Global Multicast Tree," *Proceedings of IEEE INFOCOM*, Anchorage, Vol. 1, April 2001, pp. 449-458.

Copyright © 2010 SciRes.

Int. J. Communications, Network and System Sciences, **2010, 3, 563-568**
doi:10.4236/ijcns.2010.36075 Published Online June 2010 (http://www.SciRP.org/journal/ijcns/).

Design and Simulation of Intelligent Optical WDM Switching Node Based on Erlang Traffic Model

Manoj Kumar Dutta, Vinod Kumar Chaubey
Electrical and Electronics Engineering Department, Birla Institute of Technology & Science, Pilani Rajasthan, India
E-mail: *mkdutta*13*@gmail.com, vkc@bits-pilani.ac.in*
Received February 6, 2010; *revised March* 17, 2010; *accepted April* 25, 2010

Abstract

In this paper we propose a new architectural switching nodes consisting of two processing nodes that follow Erlang B and Erlang C traffic respectively. The developed model is used to best utilize the given number of output channels to achieve the least blocking probability. An appropriate mathematical model has been further devised and its call blocking probability has been enunciated. Performance of the model has been evaluated for different values of blocking probabilities. It has been observed that the performance of the network is satisfying for different design parameters.

Keywords: WDM Networks, Erlang Traffic, Optical Node, Blocking Probability, Traffic Fraction

1. Introduction

Wavelength division multiplexing (WDM) is a promising technology which, in conjunction with wavelength routing, enables the optical networks to provide a throughput of the order of Gbs/sec and to handle hundreds of nodes simultaneously. This is possible because of all optical wavelength routed networks exploit wavelength reuse and removes the electro-optic bottleneck from the networks [1-3]. Tremendous traffic demand in all optical networks needs an appropriate optical control layer supported with configurability, restorability, bandwidth utilization and node accessibility [4-8]. Various application based traffic to support quality of service in the wavelength division-multiplexed (WDM) system needs effective control protocols and efficient algorithms [9-10]. Several approaches have been proposed to manage the optical traffic through WDM network involving optical circuit switching, optical packet switching or optical burst switching with appropriate routing algorithms [11-13]. WDM technology along with optical packet switching has changed the static usage of WDM network into an intelligent optical network capable of efficient routing and switching [14-15]. The performance of packet switched optical networks is characterized by evaluating the blocking probability and optimum management of available channels. This traffic management requires optical logic processing and data buffering [16]. In optical wavelength-division multiplexing (WDM) networks, traffic can be very bursty in nature. The instantaneous characterization of such traffic shows that the irregular oscillation of the traffic load and the occurrence of blockings in a light-loaded network are highly correlated. Specifically, most blockings occur concentratively at the peaks of the instantaneous load. In some other time, network resources may not be sufficiently utilized. To make better utilization of network resources, a novel and intelligent channel assignment scheme is necessary. By releasing a portion of available channel resources under light loading and recapturing them when the load goes up, a number of blockings brought by the irregular oscillation of the traffic load can be reduced [17].

In the present paper we propose an appropriate model of WDM optical switch having two processing nodes (node B, node C) with fixed number of output channels. In the node architectural design the processing node B is assumed to follow Erlang B traffic model while the node C serves with Erlang C traffic model. Further it is also assumed Poisson arrivals of traffic from the source to the intermediate router which then arbitrarily routes the incoming traffic to the nodes. The flow of traffic to node B and node C is highly irregular *i.e.*, at any instant of time one node may be heavily loaded and other one is lightly loaded. This may cause a rise in blocking probability of the heavily loaded node to increase beyond the desired value but at the same time other node may be left with some unused channels and thus the available channels of the nodes are not always best utilized. Here we have introduced one controller unit which will reallocate (reserve or release) the available output channels of the nodes depending on the traffic load of the respective

Copyright © 2010 SciRes.

node. In the present model if the traffic flows to a particular node becomes high then the traffic flow through the other node falls due to sharing of the incoming traffic by the two nodes. In this situation the heavily loaded node will not be able to maintain the desired blocking probability with its own output channels where as the lightly loaded node has unused channels which can be shared by the busy node and vice-versa. Traffic flow through the nodes are purely random but can be measured. From this measured value of traffic the controller unit with the help of some empirical formula will continuously calculate the number of output channels required to meeting the desired blocking probability and hence the necessary action will be taken.

Evaluation of these channel shifting properties and the corresponding blocking probability is of utmost importance and in this paper an attempt has been made to develop a simple analytical model and mathematical expressions for an optical switching network capable to implement different blocking probabilities and to provide best channels utilization. The performance of the switch has been evaluated to show their qualitative proximity with existing result.

2. Modeling of Optical Network

Here we have assumed that source is generating maximum ρ amount of traffic and sending them to the traffic router. The traffic router will route a fraction 'k' of the incoming traffic to node B, Erlang B traffic and the rest of the traffic *i.e.*, $(1 - k)$ fraction to node C, Erlang C traffic. The value of traffic fraction 'k' may vary from zero to one. Value of k equal to zero means the entire incoming traffic is routed to node C and k equal to one means the entire traffic is routed to node B. **Figure 1** depicts the switch architecture showing N and M output channels for node B and node C respectively, to support a critical value of traffic fraction k to be processed through B for a particular blocking probability at the node. If the value of 'k' goes beyond that value then blocking probability in Node B will start to increase and that in Node C will decrease and vice-versa. In the next section a mathematical model has been developed to estimate the critical value of 'k' to ensure a desired blocking probability. The traffic router will continuously check the value of 'k' and will send a corresponding control signal to the channel shifter as shown in the **Figure 1**. Here the function of the channel shifter is to shift some channels between node B and node C as and when required. The number of channels required to be shifted (n) to keep the blocking probability unchanged has also been developed through the simulation results in the next section. If required number of channels to meet the desired blocking probability is not available for the other lightly loaded node, then the shifter may shift the instantaneous available free channels to reduce the blocking probability of the heavily loaded node to some extent. Three different types of control signals will be generated by the traffic router and will be transmitted to the channel shifter so that it can take proper actions, viz. no action is necessary, shift maximum 'n' number of channels from node C to node B or reverse. This proposed model may be used to best utilize the given number of output channels for least blocking probability. The complete functional behavior of the proposed switching network has been described by the flowchart as shown in the **Figure 2**.

3. Mathematical Model

In order to evaluate the performance of the proposed WDM optical network we need to derive the probabilistic evaluation of Node B and Node C. The Node B and Node C of the present WDM network contain N and M number of output channels respectively. The well known Erlang B formula is derived from the assumption that node B has no queue so an arriving call is either served or rejected. Blocking probability of Erlang B formula is

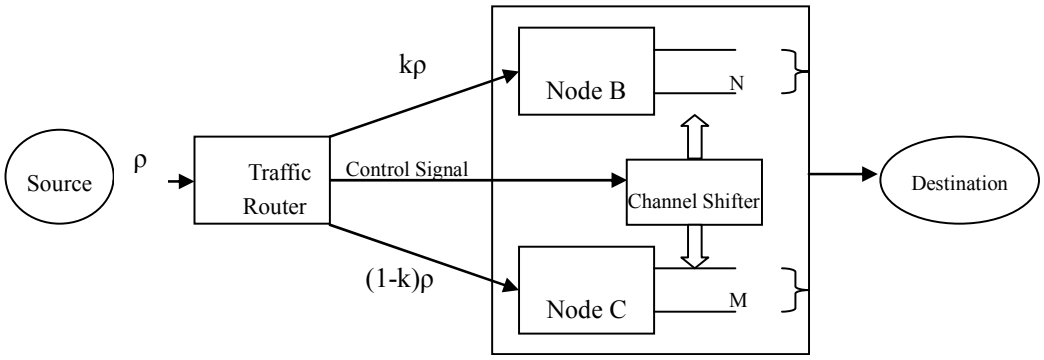

Figure 1. Node Architecture.

Copyright © 2010 SciRes.

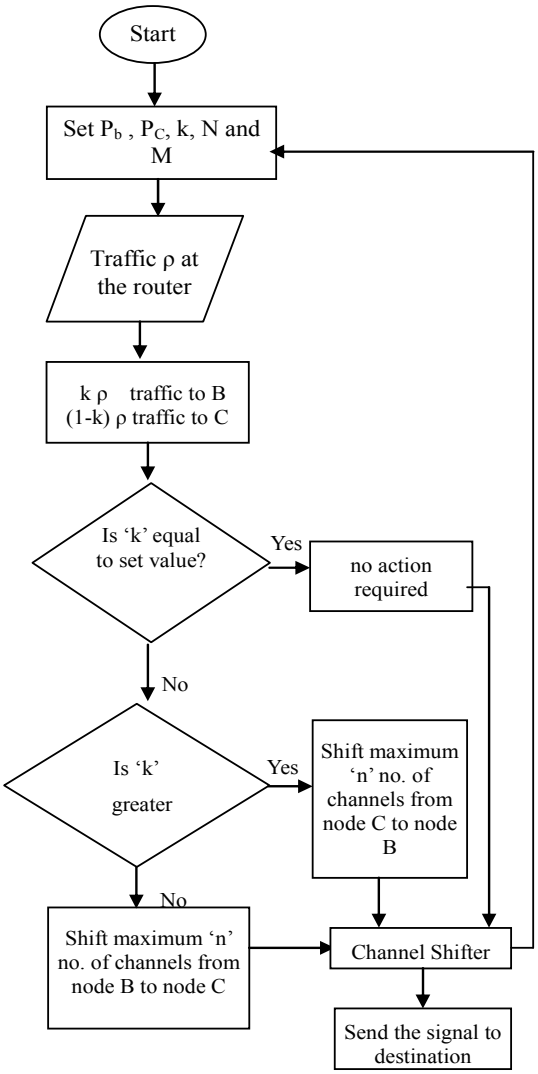

Figure 2. Flow chart of the proposed switching node.

given by

$$P_B = \frac{\frac{\rho^N}{N!}}{\sum_{i=0}^{N}\frac{\rho^N}{i!}} \quad (1)$$

where, ρ is the incoming traffic. In our model the traffic through the nodes are purely random in nature. The traffic router will route 'ρ k' amount of the incoming traffic to node B, and ρ (1 – k) amount of traffic to node C. So in this case the above Erlang B blocking probability will be modified and

$$P_B = \frac{\frac{(k\rho)^N}{N!}}{\sum_{i=0}^{N}\frac{(k\rho)^N}{i!}} \quad (2)$$

Erlang C formula is derived from assumption that a queue is used a queue is used to hold all request calls which cannot be immediately assigned a channel. The Erlang C formula is given by

$$P_c[CalDelayed] = \frac{\rho^M}{\rho^M + M!(1-\frac{\rho}{M})\sum_{i=0}^{M}\frac{\rho^i}{i!}} \quad (3)$$

and the blocking probability is given by

$$P_C = \frac{\rho^M}{\rho^M + M!(1-\frac{\rho}{M})\sum_{i=0}^{M}\frac{\rho^i}{i!}} * \exp\frac{-(M-\rho)}{H}t \quad (4)$$

where, t is the delay time and H is the average duration of the call. But in our network the equation will be modified and

$$P_C = \frac{\{(1-k)\rho\}^M}{\{(1-k)\rho\}^M + M!(1-\frac{\{(1-k)\rho\}}{M})\sum_{i=0}^{M}\frac{\{(1-k)\rho\}^i}{i!}} * \exp\frac{-[M-\{(1-k)\rho\}]}{H}t \quad (5)$$

The above equations have been used to find out the critical value of 'k' to ensure a desired blocking probability and the result is shown in the table below. From the simulation results which have been listed in **Table 1**, the following empirical formula has been developed to find out the required number of output channels to maintain the desired blocking probability for different values of traffic fraction 'k'. n = [a (1.6^k) – N], where 'a' is some constant and whose value will depend on node parameters.

These equations have been used in blocking probability calculation in the MATLAB environment under the appropriate node and traffic assumptions.

Table 1. Call blocking probability for various traffic fraction.

	k=.1	k=.15	k=.2	k=.25	k=.3	k=.35	k=.4	k=.45	k=.5	k=.55	k=.6	k=.65	k==.7	k=.75	k=.8	k=.85
No de B	6.0×10^{-8}	1.25×10^{-6}	$.9\times10^{-5}$	4.1×10^{-5}	1.4×10^{-4}	4×10^{-4}	$.8\times10^{-3}$	1.75×10^{-3}	3×10^{-3}	5.1×10^{-3}	.008	.0125	1.75×10^{-2}	.024	.03	.04
No de C	2.1×10^{-4}	1.25×10^{-4}	7×10^{-5}	4×10^{-5}	2.1×10^{-5}	1.2×10^{-5}	6×10^{-6}	3×10^{-6}	1.4×10^{-6}	6×10^{-7}	2.5×10^{-7}	0.9×10^{-7}	2.8×10^{-8}	7×10^{-9}	1.4×10^{-9}	1.7×10^{-10}

Copyright © 2010 SciRes.

4. Simulation and Results

The simulations are carried out for the proposed optical switching node for a generic traffic with variable traffic routing factor. Case 1 presents the dependence of routed incoming traffic on the required number of output channels at processing nodes for different blocking probabilities considering ρ as 5 Earlang. In case 2 the dependency of blocking probability on the number of output channels for three different values of incoming traffic fraction have been evaluated and the corresponding curves have been drawn in **Figures 5** and **6**.

It is inferred from **Figures 3** and **4** that a higher traffic needs a larger number of output channels to maintain a required value of blocking probability. Similarly it is also clear from the graph that, addition of output channels decreases the blocking probability for both types of nodes. It is found from the figures that the number of channels required to maintain same blocking probability is significantly higher in case of node B as compared to node C for the same circumstances. It may also be noted that to maintain a blocking of 4.1×10^{-5} at 4.5 Erlang load,

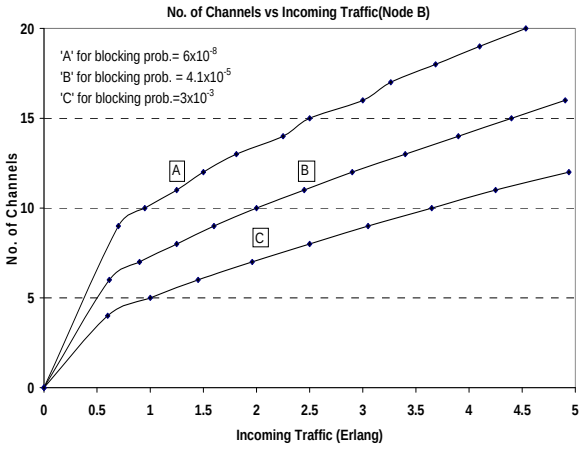

Figure 3. No of channels vs incoming traffic for different.

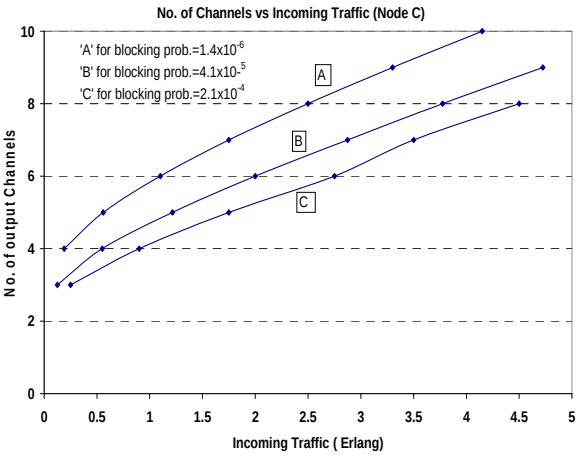

Figure 4. No of channels vs incoming traffic for different.

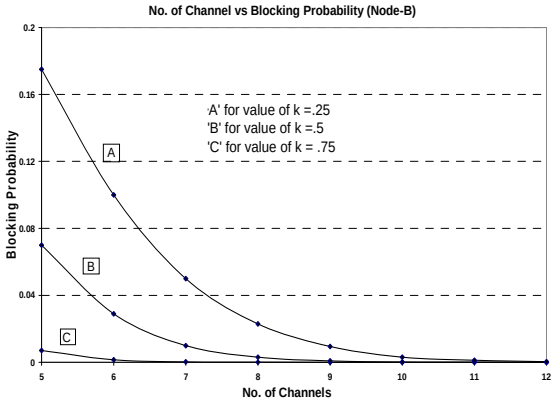

Figure 5. Blocking probability vs no of channels for different values of traffic fraction in nod B.

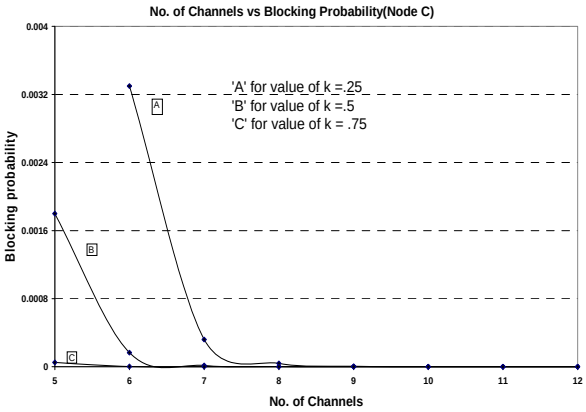

Figure 6. Blocking probability vs no of channels for different values of traffic fraction in node C.

the desired output channels for node B to process alone will be 15, however this number get reduced to 9 in case of traffic to be processed by node C alone. This observation is quite obvious due to different traffic handling capacities of the nodes. For a given number of available output channels Erlang C model is superior to Erlang B model but implementation of previous adds cost and the network complexity. Therefore in our proposed switching node we have used the combination of both types of traffic models. This approach may lead to a compromise between cost and complexity with the node throughput.

Figure 3, curve 'A' indicates that, for 8 available output channels node B can process upto 0.5 Erlang of incoming traffic to maintain a blocking probability of 6×10^{-8}. Similarly the channel requirement graph for a larger allowed blocking probability has been depicted by curves B and C, showing a lower channel requirement implying a compromise with the throughput. The channel requirement increases almost linearly with the amount incoming traffic for a fixed blocking probability but the slope of curve becomes steeper to yield low blocking probability. On the other hand the node C with 8 output channels can process upto 2.5 Erlang of traffic even after

Copyright © 2010 SciRes.

maintaining blocking probabilities of 1.4×10^{-5} as is evident by curve 'A' in **Figure 4**. Node C shows the similar behavior as in case of node B, but with smaller quantitative difference. It is interesting to note that as the incoming traffic is distributed between the two nodes unevenly, one of the nodes gets highly loaded leaving the other with a lesser load. At this condition the lightly loaded node is left with few unused channels but the highly loaded node suffers from scarcity of output channels, leading to poor performance. In this situation if the unused channels of lightly loaded node are available to the heavily loaded node then blocking probability of the entire switching node will improve significantly.

The variation of blocking probability with number of output channels has shown in **Figures 5** and **6** for both the cases. Three different values of incoming traffic fraction 'k' have been considered to execute the blocking probability with the number of output channels for both of the processing nodes. It can be inferred from the curves of **Figures 5** and **6** that blocking probability reduces as the number of output channel increases for both types of nodes. This change is more prominent in node C; showing a significant improvement in the blocking probability. This improvement may be attributed to the efficient traffic model applicable to node C.

These observations can be used to employ channel shifting property of the proposed node architecture to obtain a satisfactory reduction in blocking probability at high traffic flow. Thus present analysis is useful for the node designer to optimize the available channels for the minimum blocking probability through switching node utilizing channel shifter effectively.

5. Conclusions

This paper presents an analytical approach to investigate the performance of an optical WDM switching node under variable Erlang traffic condition. A new architectural model with two different types of processing nodes has been proposed for the switching action. Mathematical model also been developed to evaluate the blocking probability of the switching node for variable incoming traffic. The proposed architecture may be used to utilize the given number of output channels for least blocking probability. The approach adopted is quite simple and involves basic node system behavior but still provides a well acceptable performance. The results are validated by MATLAB simulations and show a distinct influence of the incoming traffic over usable channel and blocking probability of the switching node as well.

6. References

[1] A. Sridharan and K. N. Sivarajan, "Blocking in All-Optical Networks," *IEEE/ACM Transactions on Networking*, Vol. 12, No. 2, 2004, pp. 384-397.

[2] M. K. Dutta and V. K. Chaubey, "Priority Based Wavelength Routed WDM Networks: A Queueing Theory Approach," *International Journal of Recent Trends in Engineering* (*Electrical & Electronics*), Vol. 1, No. 3, 2009, pp. 253-256.

[3] M. De Leenheer, C. Develder, F. De Truck, B. Dhoedt and P. Demeester, "Erlang Reduced Load Model for Optical Burst Switched Grids," Erlang-gobs, 2007.

[4] Y. L. Hsue, M. S. Rogge, S. Yamamoto and L. G. Kazovsky, "A Highly Flexible and Efficient Passive Optical Network Employing Dynamic Wavelength Allocation," *IEEE/OSA Journal of Lightwave Technology*, Vol .23, No. 1, 2005, pp. 277-286.

[5] A. A. Saleh and J. M. Simmons, "Evolution towards the next Generation Core Optical Network," *IEEE/OSA Journal of Lightwave Technology*, Vol. 24, No. 1, 2006, pp. 3303-3320.

[6] L. Guo, J. Cao, H. Yu and L. Li, "Path Based Routing Provisioning with Mixed Shared Protection in WDM Mesh Networks," *IEEE/OSA Journal of Lightwave Technology*, Vol. 24, No. 3, 2006, pp. 1129-1141.

[7] Y.-L. Hsue, J. Kim, C.-F. Su, R. Rabbat, T. Hamada, C. Tian and L.G. Kazovsky, "Traffic Grooming on WDM Ring Using Optical Burst Transport", *IEEE/OSA Journal of Lightwave Technology*, Vol. 24, No. 1, 2006, pp. 44-52.

[8] V. K. Chaubey and K. Divakar, "Modeling and Simulation of WDM Optical Netwroks under Traffic Control Protocols," *Optical Fiber Technology*, Vol. 15, No. 2, 2009, pp. 95-99.

[9] M. K. Dutta and V. K. Chaubey, "Optical Network Traffic Control Algorithm under Variable Loop Delay: A Simulation Approach," *International Journal of Communication, Network and System Sciences*, Vol. 7, 2009, pp. 651-655.

[10] G. S. Zervas, M. D. Leenheer, *et al*., "Multi Granular Optical Cross-Connect Design, Analysis and Demonstration," *Journal of optical communication Netwroking*, Vol. 1, No. 1, 2009, pp. 69-84.

[11] B. Wen, R. Shenai and K. Sivalingam, "Routing, Wavelength and Time-Slot-Assignment Algorithms for Wavelength-Routed Optical," *IEEE/OSA Journal of Lightwave Technology*, Vol. 23, No. 9, 2005, pp. 2598-2609.

[12] A. Mukherjee, S. P. Singh and V. K. Chaubey, "Wavelength Conversion Algorithm in an Intelligent WDM Network," *Optics Communications*, Vol. 230, 2004, pp. 59-65.

[13] R. Kundu and V. K. Chaubey, "Analysis of Optical WDM Network Topologies with Application of LRWC under Symmetric Erlang-C Traffic, Novel Algorithms and Techniques in Telecommunication, Automation and Industrial Electronics," Springer Science, 2008, pp. 468-473.

[14] F. C. G. Corazza and C. Raffaelli, "An Optical Packet switch with a Multi-Stage Buffer for IP traffic, Optical Networking," A. Banoni, Ed., Springer, 1999, pp. 300-311.

Copyright © 2010 SciRes.

[15] F. Masetti, *et al*., "High Speed, High Capacity ATM Optical Switches for Future Telecommunication Transport Networks," *IEEE Journal on Selected Areas in Communications*, Vol. 14, No. 5, 1996, pp. 979-999.

[16] J. Y. Wei, C. D. Lie, S. Y. Park, K. M. Liu, R. S. Ramamurthy, H. Kim and M. W. Marda, "Network Control and Management for Next Generation Internet," *IIEICE Transactions on Communications*, Vol. E83-B, No. 10, 2000, pp. 2191-2209.

[17] N. Hua, X. P. Zheng, H. Y. Zhang and B. K. Zhou, "A Wavelength-Buffering Scheme for Dynamic Traffic in Optical Wavelength-Division Multiplexing Networks," *Photonic Network Communications*, Vol. 16, 2008, pp. 43-51.

[18] J. C. Bellamy, "Digital Telephony," 3rd Edition, John Wiley & Sons, New York, 2002.

Copyright © 2010 SciRes.

Int. J. Communications, Network and System Sciences, **2010, 3, 569-577**
doi:10.4236/ijcns.2010.36076 Published Online June 2010 (http://www.SciRP.org/journal/ijcns/).

Scientific Research

Flocking Control of a Group of Agents Using a Fuzzy-Logic-Based Attractive/Repulsive Function

Hui Yu, Jigui Jian, Yanjun Shen
Institute of Nonlinear and Complex Systems, China Three Gorges University, Yichang, China
E-mail: {*yuhui, jiguijian, Shenyj*}*@ctgu.edu.cn*
Received March 5, 2010; *revised April* 7, 2010; *accepted May* 17, 2010

Abstract

In this study, a novel procedure is presented for control and analysis of a group of autonomous agents with point mass dynamics achieving flocking motion by using a fuzzy-logic-based attractive/repulsive function. Two cooperative control laws are proposed for a group of autonomous agents to achieve flocking formations related to two different centers (mass center and geometric center) of the flock. The first one is designed for flocking motion guided at mass center and the other for geometric center. A virtual agent is introduced to represent a group objective for tracking purposes. Smooth graph Laplacian is introduced to overcome the difficulties in theoretical analysis. A new fuzzy-logic-based attractive/repulsive function is proposed for separation and cohesion control among agents. The theoretical results are presented to indicate the stability (separation, collision avoidance and velocity matching) of the control systems. Finally, simulation example is demonstrated to validate the theoretical results.

Keywords: Flocking, Cooperative Control, Multi-Agent System, Fuzzy Logic

1. Introduction

A special behavior of large number of interacting dynamic agents called "flocking" has attracted many researchers from diverse fields of scientific and engineering disciplines. Examples of this behavior in the nature include flocks of birds, schools of fish, herds of animals, and colonies of bacteria.

In 1986, Reynolds introduced three heuristic rules that leads to the creation of the first computer animation model of flocking [1]. It should be noticed that these rules are also known as cohesion, separation, and alignment rules respectively in the literature. Similar problems have become a major thrust in systems and control theory, in the context of cooperative control, distributed control of multiple vehicles and formation control. A research field which is tightly related to the theme of this paper is that of consensus seeking of autonomous multi-agent. In this case, multi-agent achieve consensus if their associated state variables converge to a common value [2-5]. In the meantime, an important progression has been achieved on synchronous and/or asynchronous swarm stability analysis [6-8]. Pioneering works [9-11] on flocking motion of particle systems have properly explained the heuristic rules embedded in Reynolds model. One of the important works in [9-11] is the design of attractive/repulsive potential function. In [12], Gu and Hu proposed a flocking control algorithm for fixed and switching network of multi-agent respectively, in which the attractive/repulsive potential was designed using fuzzy logic. Stability is analyzed using the classical Lyapunov theory in fixed network and non-smooth analysis in dynamical network, respectively.

In this study, the flocking behaviors of multi-agent systems with point mass dynamics and dynamical network topology are investigated. The major difference or contribution compared with previous works, for example [9-12], can be outlined as follows. First of all, the new results are based on more general particle model and the flocking motion is centered at different centers, e.g., mass center and geometric center. Secondly, two new cooperative control laws are proposed such that desired collective behaviors (separation, collision avoidance and velocity matching) can be achieved. Finally, smooth graph Laplacian and smooth attractive/repulsive potential based on fuzzy logic are proposed to overcome the difficulties in theoretical analysis and for separation and cohesion control between agents, respectively. In contrast to [12], owing to the design of smooth attractive/repulsive potential based on fuzzy logic and application of smooth graph Laplacian, stability analysis both in fixed and dynamical networks can easily conducted using classical Lyapunov theory.

The rest of the paper is organized as follows. In Section

Copyright © 2010 SciRes.

2, the problems are formulated based on algebraic graph theory, preliminaries about smooth collective potential function and fuzzy control function are provided. In Section 3, two flocking control laws based on fuzzy logic are proposed. Stability analysis is given in Section 4. Simulation results are provided in Section 5. Finally, concluding remarks are made in Section 6.

2. Problem Formulation and Preliminaries

2.1. System Dynamics

Consider a group of N agents (or particles) moving in an n-dimensional Euclidean space, each has point mass dynamics described by

$$\begin{cases} \dot{x}_i = v_i \\ m_i \dot{v}_i = u_i - k_i v_i, i = 1,2,\mathbf{L},N \end{cases} \tag{1}$$

where $x_i = (x_i^1, x_i^2, \mathbf{L}, x_i^n)^T \in \mathbb{R}^n$ is the position vector of agent i, $v_i = (v_i^1, v_i^2, \mathbf{L}, v_i^n)^T \in \mathbb{R}^n$ is its velocity vector, $m_i > 0$ is its mass, $u_i = (u_i^1, u_i^2, \mathbf{L}, u_i^n)^T \in \mathbb{R}^n$ is the control input acting on agent i, $k_i > 0$ is the velocity damping gain, and $-k_i v_i$ is the velocity damping term.

For flocking motion of a group of agents, the control objectives are to design flocking control laws such that:

a) The distances $\| x_j - x_i \|$ between any two neighbor agents are asymptotically convergent to a desired constant value d;

b) The velocity vectors v_i reach consensus, *i.e.*, $v_1 = v_2 = \mathbf{L} = v_N = v_c = v_r$, where v_c is the velocity vector of the center of a group of agents and v_r is the velocity vector of a virtual agent;

c) No collision between agents occurs during the flocking.

The theoretical framework presented in this paper for creation of flocking behavior relies on a number of fundamental concepts in algebraic graph theory [13] that are described below.

A weighted undirected graph will be used to model the interaction topology among agents. An undirected graph G consists of a set of vertices $\mathrm{V} = \{1, 2, \mathbf{L}, N\}$ and a set of edges $\mathrm{E} = V \times V$, where an edge is an unordered pair of distinct vertices in V. In graph G, the ith node represents agent i and a edge denoted as e_{ij} or (i, j) represents an information exchange link between agent i and j. The adjacency matrix $\mathrm{A(G)} = [a_{ij}]$ of a graph G is a matrix with nonzero elements satisfying the property $a_{ij} \neq 0 \Leftrightarrow (i, j) \in \mathrm{E}$. Throughout the paper, for simplicity of notation, we assume $a_{ii} = 0$ for all i (or the graphs have no loops). The graph is called weighted whenever the elements of its adjacency matrix are other than just $0-1$ elements. Here, weighted undirected graph is used in this paper. The degree matrix of G is a diagonal matrix $\Delta(\mathrm{G})$ with diagonal elements $\Sigma_{j=1}^{N} a_{ij}$ that are row-sums of $\mathrm{A(G)}$. The graph Laplacian is defined as $\mathrm{L(G)} = \Delta(\mathrm{G}) - \mathrm{A(G)}$. The Laplacian matrix $\mathrm{L(G)}$ always has a right eigenvector $1_N = (1, 1, \mathbf{L}, 1)^T$ associated with eigenvalue $l_1 = 0$. A graph G is called undirected if and only if the adjacency matrix $\mathrm{A(G)}$ is symmetric. The set of neighbors of node i is defined by

$$\mathrm{N}_i = \{ j \in \mathrm{V} : a_{ij} \neq 0 \} = \{ j \in \mathrm{V} : (i, j) \in \mathrm{E} \} \tag{2}$$

In fixed network topology, agent i can range or communication with a fixed set of neighbors. Therefore, the set N_i is time invariant. However, in dynamical or switching network topology, the set of neighbors of agent i is time-varying due to limited communication.

2.2. Smooth Collective Potential Function

Smooth collective potential function is originally proposed in [11]. The following is a brief introduction about it. For more detailed information, the reader is referred to [11].

In order to construct smooth collective potential function, a map $\|\cdot\|_s : \mathbb{R}^n \to \mathbb{R}_{\geq 0}$ is defined as

$$\| z \|_s = \frac{1}{e} \left(\sqrt{1 + e \| z \|^2} - 1 \right)$$

with a parameter $e > 0$. Note that $\| z \|_s$ is differentiable everywhere, but $\| z \|$ is not differentiable at $z = 0$.

Smooth adjacency matrix elements are constructed by using a scalar function $r_h(z)$ that smoothly varies between 0 and 1. One possible choice is as follows:

$$r_h(z) = \begin{cases} 1 & z \in [0, h) \\ \frac{1}{2}\left[1 + \cos\left(p \, \frac{z - h}{1 - h} \right) \right] & z \in [h, 1] \\ 0 & otherwise \end{cases} \tag{3}$$

where $h \in (0,1)$. Using this function, a position-dependent adjacency matrix $\mathrm{A}(x)$ can be defined as $\mathrm{A}(x) = [a_{ij}(x)]$ with

$$a_{ij}(x) = r_h(\| x_j - x_i \|_s / r_s) \in [0,1], j \neq i \tag{4}$$

and position-dependent Laplacian matrix as $\mathrm{L}(x) = \Delta(\mathrm{A}(x)) - \mathrm{A}(x)$, where $x = (x_1^T, x_2^T, \mathbf{L}, x_N^T)^T$, $r_s = \| r \|_s$,

Copyright © 2010 SciRes.

$r > 0$ denote the interaction range between two agents.

The set of neighbors of agent i is defined by

$$\mathrm{N}_i(x) = \{ j \in \mathrm{V} : \| x_j - x_i \| < r \} .$$

By the definition of $\| z \|_s$, the control objective (1) can be expressed as following algebraic constraint:

$$\| x_j - x_i \|_s = d_s , \forall j \in \mathrm{N}_i(x) \tag{5}$$

where $d_s = \| d \|_s$.

Given a interaction range $r > 0$, a neighboring graph $\mathrm{G}(x)$ can be specified by V and the set of edges $\mathrm{E}(x) = \{(i, j) \in \mathrm{V} \times \mathrm{V} : \| x_j - x_i \| < r, j \neq i\}$, that clearly depends on x.

A smooth collective potential function has the form:

$$V_1(x) = \frac{1}{2} \sum_i \sum_{j \neq i} y (\| x_j - x_i \|_s)$$

where $y(z)$ is a smooth pairwise attractive/repulsive potential with a finite cut-off at $z = r_s$ and a global minimum at $z = d_s$. In order to construct a smooth potential function $y(z)$, denote $f(z) = \nabla_z y(z)$ and define this function as:

$$f(z) = \nabla_z y(z) = r_h(z / r_s) j(z) \tag{6}$$

where $j(z)$ is some function to be designed. Obviously, function $f(z)$ should vanish for all $z \geq r_s$.

In the next section, the function $f(z)$ is implemented using fuzzy logic.

2.3. Preliminaries of Fuzzy Control Function

To the best of our knowledge, for flocking control, [12] is the first paper in which attractive/repulsive function is designed using fuzzy logic. In this section, we provide a brief introduction about fuzzy control function [12].

A set of fuzzy logic rules performs a mapping from an input $z \in R^P$ to a deterministic control $g(z)$, *i.e.*, fuzzy control function. For the *k*th dimension state $x_i^k (k = 1, 2, \mathbf{L}, n; i = 1, 2, \mathbf{L}, N)$, agent i uses states (x_i, x_j) to build a P-dimension vector $z = (z_1, z_2, \mathbf{L}, z_P)$ as fuzzy input. The corresponding fuzzy input set is $F_1, F_2, \mathbf{L}, F_P$. A fuzzy rule between agent i and agent j can be expressed as:

$$R^l : \text{IF } z_1 \text{ is } F_I^l \text{ AND, L, AND } z_P \text{ is } F_P^l,$$
$$\text{THEN } g_{ij}^{k,l} = q_O^l + \sum_{P=1}^{P} q_P^l z_P$$

where $k = 1, 2, \mathbf{L}, n; l = 1, 2, \mathbf{L}, L$, L is the number of fuzzy rules.

Use the Gaussian function to define the membership function of fuzzy set F_p^l: $m_{F_p^l} = \exp[-\frac{z_p - a_p^l}{2(s_p^l)^2}]$, where $a_p^l, s_p^l (p = 1, 2, \mathbf{L}, P)$ are the mean and variance, respectively. The activation degree of rule R^l is calculated by product operation:

$$x^l = \prod_{p=1}^{P} \exp[-\sum_{p=1}^{P} \frac{z_p - a_p^l}{2(s_p^l)^2}].$$

The crisp output $g_{ij}^k(z), k = 1, 2, \mathbf{L}, n,$ is calculated by center of area method:

$$g_{ij}^k(z) = \sum_{l=1}^{L} x^l g_{ij}^{k,l} \Big/ \sum_{l=1}^{L} x^l .$$

3. Flocking Motion Guided at Mass Center and/or Geometric Center

In this section, two cooperative control algorithms are developed for flocking guided at mass center and geometric center respectively. In flocking motion, each agent applies a control input that consists of four terms:

$$u_i = u_i^f + u_i^c + u_i^g + k_i v_i \tag{7}$$

where $u_i^f = -\nabla_{x_i} V_1(x)$ is a gradient-based term and will be designed using fuzzy logic, u_i^c is a velocity consensus/alignment term, u_i^g is a navigation term due to a group objective and $k_i v_i$ is the velocity damping term.

Similar to [9-11], the velocity consensus/alignment term u_i^c is in the form

$$u_i^c = \sum_{j \in N_i(x)} a_{ij}(x)(v_j - v_i) \tag{8}$$

and

$$u_i^c = \sum_{j \in N_i(x)} m_i a_{ij}(x)(v_j - v_i) \tag{9}$$

for flocking motion guided at mass center and geometric center, respectively. The navigation term u_i^g is designed in the following form

$$\begin{aligned} u_i^g &= -k_1 m_i (x_i - x_r) - k_2 m_i (v_i - v_r) \\ &+ \frac{m_i}{m_r} f(x_r, v_r), k_1, k_2 > 0. \end{aligned} \tag{10}$$

The pair $(x_r, v_r) \in \mathbf{¡}^n \times \mathbf{¡}^n$ is the desired state vector of the group center (mass center or geometric center). The desired state of the group center can be described by

$$\begin{cases} \dot{x}_r = v_r \\ m_r \dot{v}_r = f(x_r, v_r) \end{cases} \tag{11}$$

Copyright © 2010 SciRes.

3.1. Fuzzy Attractive/Repulsive Control

For state vector x_i, the fuzzy input z consists of $\| x_j - x_i \|_s - d_s$, $j \in \mathrm{N}(x)$ and $a_{ij}(x) n_{ij}^k$, $j \in \mathrm{N}(x)$, where $n_{ij}^k = \frac{x_j^k - x_i^k}{\sqrt{1+e\| x_j - x_i \|^2}}$, *i.e.*, $P = 2$ and $z = (z_1, z_2) = (\| x_j - x_i \|_s - d_s, a_{ij}(x) n_{ij}^k)$. The fuzzy output is defined as

$$g_{ij}^{k,l} = q_2^l a_{ij}(x) n_{ij}^k, k = 1, 2, \mathbf{L}, n.$$

which implies $q_0^l = q_1^l = 0$. A fuzzy rule R^l is then defined as:

IF $\left\| x_j - x_i \right\|_s - d_s$ is F_I^l THEN $g_{ij}^{k,l} = q_2^l a_{ij}(x) n_{ij}^k$

Therefore,

$$g_{ij}^k(z) = a_{ij}(x) \frac{\sum_{l=1}^{L} x^l q_2^l}{\sum_{m=1}^{M} x^l} n_{ij}^k.$$

The fuzzy output vector between agent i and j is

$$g_{ij}(z) = (g_{ij}^1, g_{ij}^2, \mathbf{L}, g_{ij}^n)^{\mathrm{T}} = a_{ij}(x) \frac{\sum_{l=1}^{L} x^l q_2^l}{\sum_{m=1}^{M} x^l} n_{ij},$$

where $n_{ij} = (n_{ij}^1, n_{ij}^2, \mathbf{L}, n_{ij}^n)^{\mathrm{T}} = \frac{x_j - x_i}{\sqrt{1 + e\| x_j - x_i \|^2}}$.

Denote the gradient of the attractive/repulsive potential $y(\| x_j - x_i \|_s)$ as:

$$\nabla_{z_1} y(\| x_j - x_i \|_s) = a_{ij}(x) \frac{\sum_{l=1}^{L} x^l q_2^l}{\sum_{l=1}^{L} x^l}$$

and denote $j(\| x_j - x_i \|_s) = \frac{\sum_{l=1}^{L} x^l q_2^l}{\sum_{l=1}^{L} x^l}$, we have

$$\begin{aligned} g_{ij}(z) &= a_{ij}(x) j(\| x_j - x_i \|_s) n_{ij} \\ &= \nabla_{z_1} y(\| x_j - x_i \|_s) n_{ij} \\ &= -\nabla_{z_1} y(\| x_j - x_i \|) \nabla_{x_i} z_1 \\ &= -\nabla_{x_i} y(\| x_j - x_i \|_s) \end{aligned} \tag{12}$$

Therefore, gradient-based control term can be designed as

$$\begin{aligned} u_i^f &= -\sum_{j \in \mathrm{N}_i(x)} \nabla_{x_i} y(\| x_j - x_i \|_s) = \sum_{j \in \mathrm{N}_i(x)} g_{ij}(z) \\ &= \sum_{j \in \mathrm{N}_i(x)} a_{ij}(x) j(\| x_j - x_i \|_s) n_{ij} \end{aligned} \tag{1}$$

3.2. Flocking Control guided at Group Centers

Consider the multi-agent motion relative to the group center x_c (the mass center x_{mc} or geometric center x_{gc}). The position and velocity vectors of agent i relative to x_c is denoted by $\tilde{x}_i = x_i - x_c$ and $\tilde{v}_i = v_i - v_c$, the collective state vectors of all agents relative to x_c by $\tilde{x} = x - 1_N \otimes x_c$ and $\tilde{v} = v - 1_N \otimes v_c$, where $x_c = x_{mc}$ or x_{gc}, $v_c = \tilde{x}_c$, $\otimes$ is kronecker product.

The mass center of all agents is defined as

$$x_{mc} = \sum_{i=1}^{N} m_i x_i \Big/ \sum_{i=1}^{N} m_i \tag{14}$$

Note that

$$\begin{aligned} u_i^g &= -k_1 m_i (x_i - x_r) - k_2 m_i (v_i - v_r) + \frac{m_i}{m_r} f(x_r, v_r) \\ &= -k_1 m_i \tilde{x}_i - k_2 m_i \tilde{v}_i - k_1 m_i (x_{mc} - x_r) \\ &\quad - k_2 m_i (v_{mc} - v_r) + \frac{m_i}{m_r} f(x_r, v_r) \end{aligned} \tag{15}$$

and due to $\sum_{i=1}^{N} u_i^f = 0, \sum_{i=1}^{N} u_i^c = 0$, $\sum_{i=1}^{N} m_i \tilde{x}_i = 0$, $\sum_{i=1}^{N} m_i \tilde{v}_i = 0$, we have

$$\begin{aligned} \tilde{v}_{mc} &= \sum_{i=1}^{N} m_i \tilde{v}_i \Big/ \sum_{i=1}^{N} m_i \\ &= -k_1 (x_{mc} - x_r) - k_2 (v_{mc} - v_r) + \frac{1}{m_r} f(x_r, v_r) \end{aligned}$$

Then, the dynamic of mass center is given by

$$\begin{cases} \dot{\tilde{x}}_{mc} = v_{mc} \\ \dot{\tilde{v}}_{mc} = -k_1 (x_{mc} - x_r) - k_2 (v_{mc} - v_r) + \frac{1}{m_r} f(x_r, v_r) \end{cases} \tag{16}$$

Denote $e_{mc} = (x_{mc}^T - x_r^T, v_{mc}^T - v_r^T)^T$, the relative dynamic of center of mass is given by

$$\dot{e}_{mc} = \tilde{K} e_{mc} \tag{17}$$

where $\tilde{K} = K \otimes I_n, K = \begin{pmatrix} 0 & 1 \\ -k_1 & -k_2 \end{pmatrix}$.

We can choose proper control parameters $k_1 > 0$ and $k_2 > 0$ such that matrix K is Hurwitz stable, and from Lyapunov theory, for given positive matrix $Q \in \mathbf{¡}^{2\times 2}$, there exists a positive definite matrix $P \in \mathbf{¡}^{2\times 2}$, such that:

$$K^T P + PK = -Q. \tag{18}$$

For creation of flocking motion relative to mass center, we propose following control laws:

Copyright © 2010 SciRes.

$$
\begin{aligned}
u_i &= u_i^{mc} \\
&= \sum_{j\in \mathrm{N}_i(x)} a_{ij}(x) j(\| x_j - x_i \|_s) n_{ij} \\
&\quad + \sum_{j\in \mathrm{N}_i(x)} a_{ij}(x)(v_j - v_i) k_1 m_i (x_i - x_r) \\
&\quad - k_2 m_i (v_i - v_r) + \frac{m_i}{m_r} f(x_r, v_r) + k_i v_i
\end{aligned} \tag{19}
$$

where $j(\| x_j - x_i \|_s) = \sum_{m=1}^{M} x_{ij}^m q_i^{m,2} \Big/ \sum_{m=1}^{M} x_{ij}^m$.

The geometric center of all agents is defined as

$$
x_{gc} = \mathrm{ave}(x) = \frac{1}{N}\sum_{i=1}^{N} x_i \tag{20}
$$

Similarly, for geometric center, we propose following control law:

$$
\begin{aligned}
u_i &= u_i^{gc} \\
&= \sum_{j\in \mathrm{N}_i(x)} a_{ij}(x) m_i j(\| x_j - x_i \|_s) n_{ij} \\
&\quad + \sum_{j\in \mathrm{N}_i(x)} a_{ij}(x) m_i (v_j - v_i) \\
&\quad - k_1 m_i (x_i - x_r) - k_2 m_i (v_i - v_r) + \frac{m_i}{m_r} f(x_r, v_r) + k_i v_i
\end{aligned} \tag{21}
$$

4. Analysis of Stability

In this section, we present our main results for flocking in multi-agent networks with dynamical topology, and conduct stability analysis based on classical Lyapunov theory and LaSalle's invariance principle. In [12], owing to the discontinuity of collective potential function in the case of dynamical topology, stability analysis is done using classical Lyapunov theory in fixed networks and nonsmooth analysis theory, which is difficult to understand for engineers in real applications, in dynamical networks, respectively. In our paper, due to the design of smooth collective potential function, in both cases of fixed network and dynamical network, stability analysis can be conducted based on classical Lyapunov theory and LaSalle's invariance principle.

For the collective motion relative to mass center x_{mc}, define energy function

$$
V(x,v) = V_1(x) + V_2(x) + V_3(v) + V_4(x,v) \tag{22}
$$

where,

$$
\begin{aligned}
V_1(x) &= \frac{1}{2}\sum_i \sum_{j\neq i} y(\| x_j - x_i \|_s) \\
&= \frac{1}{2}\sum_i \sum_{j\neq i} y(\| \tilde{x}_j - \tilde{x}_i \|_s), \\
V_2(x) &= \frac{1}{2} k_1 \sum_{i=1}^{N} m_i \tilde{x}_i^T \tilde{x}_i, V_3(v) = \frac{1}{2}\sum_{i=1}^{N} m_i \tilde{v}_i^T \tilde{v}_i, \\
V_4(x,v) &= e_{mc}^T (P \otimes I_n) e_{mc},
\end{aligned}
$$

$k_1 > 0$ is the parameter of the navigation term.

Applying control law (19) to system (1), following theorem is held to explain the emergence of flocking behaviors of agents guided at center of mass x_{mc}.

Theorem 1 Consider a group of agents applying control law (19) with proper selected parameters $k_1, k_2 > 0$ satisfying (18) to system (1). Assume that the initial value $V(x(0), v(0))$ is finite. Then, the following statements hold.

(i) The solution of system (1) asymptotically converges to an equilibrium point (x^*, v_{mc}) where x^* a local minima of is $V_1(x) + V_2(x)$.

(ii) The velocities of all agents asymptotically converge to the velocity of mass center v_{mc}, and the velocity of mass center v_{mc} asymptotically converge to the desired velocity v_r, *i.e.*, $v_i \to v_{mc}, i = 1, 2, \mathbf{L}, N, v_{mc} \to v_r$.

(iii) No collision between agents occurs during the flocking.

Proof: First of all, we explain the fact that the energy function $V(x,v)$ is positive definite.

Obviously, $V_2(x), V_3(v)$ and $V_4(x,v)$ is positive. Therefore, the positive definiteness of energy function $V(x,v)$ is equivalent to that of $V_1(x)$. By similar analysis to theorem 1 of [12], $y(\| \tilde{x}_j - \tilde{x}_i \|_s)$ can be designed positive definite by using proper fuzzy rules, *i.e.*, $V_1(x)$ can be designed positive definite.

Secondly, the derivative of the energy function $V(x,v)$ is seminegative definite.

$$
\dot{V}_1(x) = \sum_{i=1}^{N} \sum_{j\in N_i(x)} v_i^T \nabla_{x_i} y(\| x_j - x_i \|_s) = -\sum_{i=1}^{N} v_i^T u_i^f \tag{23}
$$

$$
\dot{V}_2(x) = k_1 \sum_{i=1}^{N} m_i \tilde{v}_i^T \tilde{x}_i \tag{24}
$$

Due to $\sum_{i=1}^{N} m_i \tilde{v}_i = 0$, we have

$$
\dot{V}_3(v) = -\dot{V}_1(x) - \tilde{v}^T (\mathrm{L} \otimes I_n)\tilde{v} + \sum_{i=1}^{N} \tilde{v}_i^T u_i^g .
$$

From (15) and note that

$$
\begin{aligned}
&\sum_{i=1}^{N} \tilde{v}_i^T [-k_1 m_i (x_{mc} - x_r) - k_2 m_i (v_{mc} - v_r) \\
&\quad + \frac{m_i}{m_r} f(x_r, v_r)] = 0,
\end{aligned}
$$

We have

$$
\sum_{i=1}^{N} \tilde{v}_i^T u_i^g = -k_1 \sum_{i=1}^{N} m_i \tilde{v}_i^T \tilde{x}_i - k_2 \sum_{i=1}^{N} m_i \tilde{v}_i^T \tilde{v}_i .
$$

Then,

Copyright © 2010 SciRes.

$$\begin{aligned}\dot{V}_3(v) &= -\dot{V}_1(x) - \dot{v}^T(\mathrm{L}\otimes I_n)\dot{v} \\ &\quad -\dot{V}_2(x) - k_2\dot{v}^T(M\otimes I_n)\dot{v}\end{aligned} \tag{25}$$

where $M = diag(m_1, m_2, \mathbf{L}, m_N)$.

From (17), we have

$$\dot{V}_4(x,v) = -e_{mc}^T(Q\otimes I_n)e_{mc} \tag{26}$$

From (23) to (26), we have

$$\begin{aligned}\dot{V}(x,v) &= V_1(x)+V_2(x)+V_3(v)+V_4(x,v) \\ &= -\dot{v}^T(\mathrm{L}\otimes I_n)\dot{v} - k_2\dot{v}^T(M\otimes I_n)\dot{v} \\ &\quad - e_{mc}^T(Q\otimes I_n)e_{mc} \le 0.\end{aligned} \tag{27}$$

Part (i) and part (ii) follow from LaSalle's invariance principle. As $\dot{V}(x,v)$ is seminegative definite, given $\Omega_c = \{(x,v): V(x,v) \le c\}$, Ω_c is an invariant set. From $V(x,v) \le c$, we have $\| e_{mc}\|^2 \le c / l_{\min}(P\otimes I_n)$. Therefore, both $\| x_{mc} - x_r\|$ and $\| v_{mc} - v_r\|$ are bounded. Given the desired state (x_r, v_r) is bounded and from the definition of x_{mc} and v_{mc}, we know (x,v) is bounded.

From LaSalle's invariance principle, all states starting in Ω_c converge to the largest invariant set $S = \{(x,v) \in \Omega_c : \dot{V}(x,v) = 0\}$. Hence, all states converge to the largest invariant set $S = \{(x,v) \in \Omega_c : v_i = v_{mc} = v_r, x_{mc} = x_r\}$ asymptotically, *i.e.*, all agent velocities v_i converge to the velocity of center of mass, v_{mc}, and the position and velocity vectors of center of mass, x_{mc}, v_{mc}, converge to the desired states, x_r, v_r, asymptotically.

Furthermore, in stable state, $V(x,v) \to V_1(x) + V_2(x)$. There is a equilibrium point at (x^*, v_{mc}) where x^* is a local minima of $V_1(x) + V_2(x)$.

Finally, we prove part (iii) by contradiction. Assume there exists a time $t = t_1 > 0$ when two distinct agents k, l collide, *i.e.*, $x_k(t_1) = x_l(t_1)$. For all $t > 0$, we have

$$\begin{aligned}V_1(x(t)) &= \frac{1}{2}\sum_i \sum_{j\ne i} y(\| x_j - x_i\|_s) \\ &= y(\| x_k(t) - x_l(t)\|_s) \\ &\quad + \frac{1}{2}\sum\nolimits_{i\in \mathrm{V}\setminus\{k,l\}} \sum\nolimits_{j\in \mathrm{V}\setminus\{i,k,l\}} y(\| x_j - x_i\|_s) \\ &\ge y(\| x_k(t) - x_l(t)\|_s)\end{aligned}$$

At $t = t_1$, defining $y(0)$ larger than c leads to $V_1(x(t_1)) \ge c$, which is in contradiction with the invariant set Ω_c. Therefore, no two agents collide at any time $t \ge 0$.

Remark: From theorem 1, control objective a) and b) are achieved, but the geometric characterization of local minima x^* of $V_1(x) + V_2(x)$ is not possible satisfying the algebraic constraint (5). In [11], the authors pose two conjectures that establish the close relationship between geometric and graph theoretic properties of any local minima of $V_1(x) + V_2(x)$ and features of flocks. Based on the conjectures in [11], we can conclude that the local minima x^* of $V_1(x) + V_2(x)$ is a so-called *quasi- a -lattice* [11], *i.e.*, $-d \le \| x_j - x_i\|_s - d \le d$, $0 \le d = d_s, \forall (i,j) \in \mathrm{E}(x)$. Obviously, it is very close to the conformation satisfying algebraic constraint (5).

When control laws (21) applied to system (1), similar theorem is established to explain the emergence of flocking behavior of agents guided at geometric center.

For the collective motion relative to geometric center x_{gc}, define energy function

$$U(x,v) = V_1(x) + U_2(x) + U_3(v) + V_4(x,v)$$

Where

$$V_1(x) = \frac{1}{2}\sum_i \sum_{j\ne i} y(\| x_j - x_i\|_s), U_2(x) = \frac{1}{2}k_1\sum_{i=1}^N x_i^T x_i,$$

$U_3(v) = \frac{1}{2}\sum_{i=1}^N v_i^T v_i, V_4(x,v) = e_{gc}^T(P\otimes I_n)e_{gc}$, $k_1 > 0$ is the parameter of the navigation term, $e_{gc} = (x_{gc}^T - x_r^T, v_{gc}^T - v_r^T)^T$.

We have following theorem.

Theorem 2 Consider a group of agents applying control law (21) with proper selected parameters $k_1, k_2 > 0$ satisfying (18) to system (1). Assume that the initial value $U(x(0), v(0))$ is finite. Then, the following statements hold.

1) The solution of system (1) asymptotically converges to an equilibrium point (x^*, v_{gc}) where x^* a local minima of is $V_1(x) + U_2(x)$.

2) The velocities of all agents asymptotically converge to the velocity of geometric center v_{gc}, and the velocity of geometric center v_{gc} asymptotically converge to the desired velocity v_r, *i.e.*, $v_i \to v_{gc}$, $i = 1, 2, \mathbf{L}, N$, $v_{gc} \to v_r$.

3) No collision between agents occurs during the flocking.

Proof: The proof of this theorem is similar to that of theorem 1.

5. Simulation

In this section, mass center guided flocking motion is

Copyright © 2010 SciRes.

simulated in 2-dimentional space. The following parameters were fixed throughout the simulation: $d=2, r=1.2d, e=0.5$, and $h=0.3$ for $r_h(z)$. Eight fuzzy sets are designed for the fuzzy control input $\| x_j - x_i \| - d_s$. They are LN, N, SN, Z, SP, P, LP, and PP as shown in **Figure 1**. Eight fuzzy rules are designed as follows:

IF $\| x_j - x_i \|_s - d_s$ is LN THEN

$g_{ij}^{k,1} = -90\, r_h(\| x_j - x_i \|_s / r_s) n_{ij}^k$;

IF $\| x_j - x_i \|_s - d_s$ is N THEN

$g_{ij}^{k,2} = -80\, r_h(\| x_j - x_i \|_s / r_s) n_{ij}^k$;

IF $\| x_j - x_i \|_s - d_s$ is SN THEN

$g_{ij}^{k,3} = -50\, r_h(\| x_j - x_i \|_s / r_s) n_{ij}^k$;

IF $\| x_j - x_i \|_s - d_s$ is Z THEN $g_{ij}^{k,4} = 0$;

IF $\| x_j - x_i \|_s - d_s$ is SP THEN

$g_{ij}^{k,5} = 0.5\, r_h(\| x_j - x_i \|_s / r_s) n_{ij}^k$;

IF $\| x_j - x_i \|_s - d_s$ is P THEN

$g_{ij}^{k,6} = r_h(\| x_j - x_i \|_s / r_s) n_{ij}^k$;

IF $\| x_j - x_i \|_s - d_s$ is LP THEN

$g_{ij}^{k,7} = 1.5\, r_h(\| x_j - x_i \|_s / r_s) n_{ij}^k$;

IF $\| x_j - x_i \|_s - d_s$ is PP THEN

$g_{ij}^{k,8} = 2\, r_h(\| x_j - x_i \|_s / r_s) n_{ij}^k$.

Control parameters k_1, k_2 are selected to be $k_1 = k_2 = 1$. The two eigenvalues of matrix $K = \begin{pmatrix} 0 & 1 \\ -1 & -1 \end{pmatrix}$ are $-05000 + 08660i$ and $-05000 - 08660i$. Therefore, matrix K is Hurwitzstable. Let $Q = I_2$, using Matlab command *lyap*(*K*,*Q*), we obtain positive definite matrix $P = \begin{pmatrix} 1.5 & -0.5 \\ -0.5 & 1 \end{pmatrix}$.

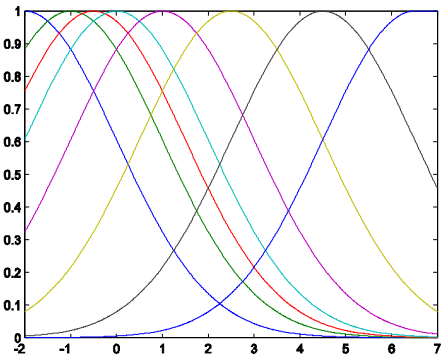

Figure 1. Fuzzy membership function.

Simulation is calculated within 20 seconds time by using Matlab Simulink. In addition, the position of each agent is marked with a right triangle sign.

Figures 2 to **5** show the simulation results within 2-D flocking using control law (19) for 50 agents. **Figures 2** to **4** show snapshots of 2-D flocking at time $t = 0, 4.3495$, and 20 (sec). The initial position and initial velocity coordinates were uniformly chosen in the random domain of $[0,3]\times[0,3]$ and $[0,1]\times[0,1]$, respectively. The mass of each agent was also uniformly chosen in a random domain of [0.5, 1.5]. A steady configuration was formed

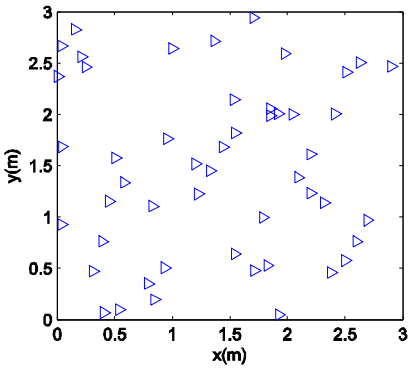

Figure 2. Initial positions of 50 agents.

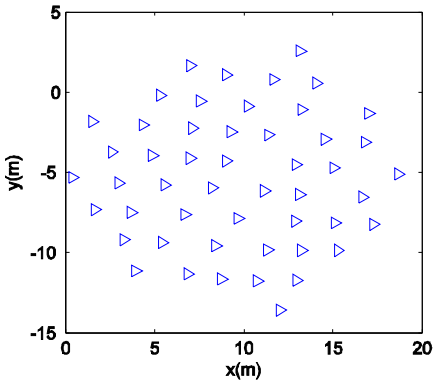

Figure 3. Configuration of 50 agents at t = 4.3495 (sec).

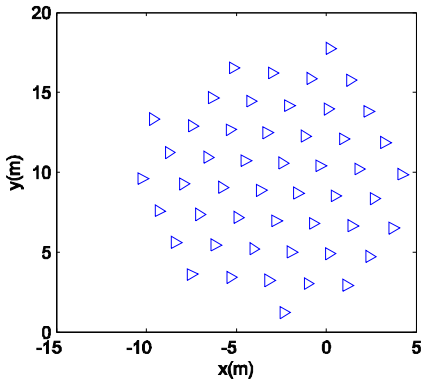

Figure 4. Final configuration of 50 agents at t = 20 (sec).

Copyright © 2010 SciRes.

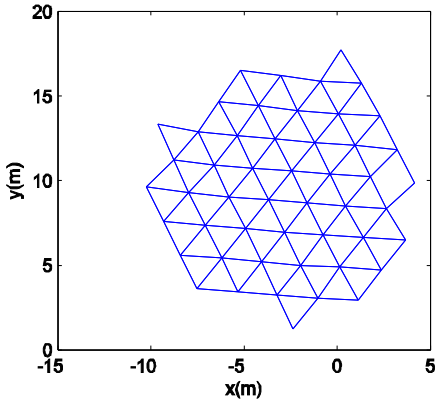

Figure 5. Position-dependent neighboring graph at t = 20 (sec).

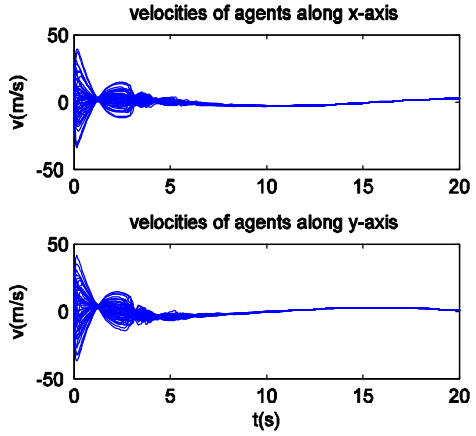

Figure 6. Velocities of 50 agents along x-axis and y-axis respectively.

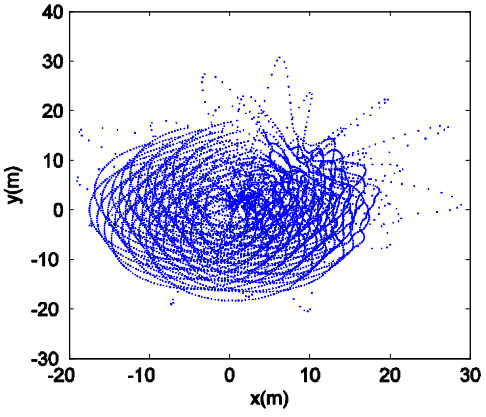

Figure 7. Trajectories of all agents within 20 (sec) time.

as shown in **Figure 4** and maintained thereafter. A virtual agent

$$x_r(t) = (10\sin(03t), 10\cos(03t))^T,$$
$$v_r(t) = (3\cos(03t), -3\sin(03t))^T$$

was used for this example. For highly disconnected neighboring graph $G(x)$ in initial state, **Figure 5** shows the connected neighboring graph $G(x)$ corresponding to the final configuration. **Figure 6** shows velocity matching is achieved along x-axis and y-axis respectively. **Figure 7** shows the trajectories of all agents within 20(sec) simulation time and the cohesive behaviors. The simulation demonstration with control law (21) was similar to that conducted by control laws (19), and therefore is not necessarily repeated here.

6. Conclusions

This paper establishes a theoretical framework for design and analysis of flocking control algorithms using a fuzzy-logic-based attractive/repulsive potential function for multiple agent networks with dynamical topology. Two cooperative control laws have been proposed for a group of autonomous agents to achieve flocking motion relative to different centers (mass center and geometric center). A virtual agent is introduced to represent a group objective for tracking purposes. Smooth Laplacian and smooth fuzzy-logic-based attractive/repulsive potential are proposed to overcome the difficulties in stability analysis. Simulation results validated the theoretical results.

7. Acknowledgements

This paper is supported in part by Hubei Provincial Natural Science Foundation under the grant 2008CDB316, Natural Science Research Project of Hubei Provincial Department of Education under the grant D20101201, and Scientific Innovation Team Project of Hubei Provincial College under the grant T200809.

8. References

[1] C. W. Reynolds, "Flocks, Herds, and Schools: A Distributed Behavioral Model," *Computer Graphics* (*ACM SIGGRAPH '87 Conference Proceedings*), Vol. 21, No. 4, 1987, pp. 25-34.

[2] R. Olfati-Saber and R. M. Murray, "Consensus Problems in Networks of Agents with Switching Topology and Time-Delays," *IEEE Transactions on Automatic Control*, Vol. 49, No. 9, September 2004, pp. 101-115.

[3] A. Jadbabaie, J. Lin and S. A. Morse, "Coordination of Groups of Mobile Agents Using Nearest Neighbor Rules," *IEEE Transactions on Automatic Control*, Vol. 48, No. 6, June 2003, pp. 988-1001.

[4] W. Ren and R. Beard, "Consensus Seeking in Multi-Agent Systems Using Dynamically Changing Interaction Topologies," *IEEE Transactions on Automatic Control*, Vol. 50, No. 5, May 2005, pp. 655-661.

[5] L. Moreau, "Stability of Multiagent Systems with

Copyright © 2010 SciRes.

Time-Dependent Communication Links," *IEEE Transactions On Automatic Control*, Vol. 50, No. 2, February 2005, pp. 169-182.

[6] Y. Liu, K. M. Passino and M. M. Polycarpou, "Stability analysis of M-dimensional Asynchronous Swarms with a Fixed Communication Topology," *IEEE Transactions on Automatic Control*, Vol. 48, No. 1, Juanary 2003, pp.76-95.

[7] Y. Liu, K. M. Passino and M. M. Polycarpou, "Stability Analysis of One-Dimensional Asynchronous Swarms," *IEEE Transactions on Automatic Control*, Vol. 48, No. 10, October 2003, pp. 1848-1854.

[8] V. Gazi and K. M. Passino, "Stability Analysis of Swarms," *IEEE Transactions on Automatic Control*, Vol. 48, No. 4, April 2003, pp. 692-697.

[9] H. G. Tanner, A. Jadbabaie and G. J. Pappas, "Stable Flocking of Mobile Agents, Part I: Fixed Topology," *The* 42*nd IEEE Conference on Decision and Control*, Maui, December 2003, pp. 2010-2015.

[10] H. G. Tanner, A. Jadbabaie and G. J. Pappas, "Stable Flocking of Mobile Agents, Part II: Dynamic Topology," *The* 42*nd IEEE Conference on Decision and Control*, Maui, December 2003, pp. 2016-2021.

[11] R. Olfati-Saber, "Flocking for Multi-Agent Dynamic Systems: Algorithms and Theory," *IEEE Transactions on Automatic Control*, Vol. 51, No. 3, March 2006, pp. 401-420.

[12] D. Gu and H. Hu, "Using Fuzzy Logic to Design Separation Function in Flocking Algorithms," *IEEE Transactions on Fuzzy Systems*, Vol. 16, No. 4, August 2008, pp. 826-838.

[13] C. Godsil and G. Royle, "Algebraic Graph Theory," Springer, New York, 2001.

Copyright © 2010 SciRes.

Call for Papers

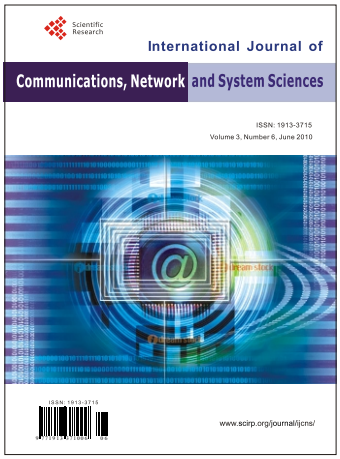

International Journal of

Communications, Network and System Sciences (IJCNS)

ISSN 1913-3715 (Print) ISSN 1913-3723 (Online)

http://www.scirp.org/journal/ijcns/

IJCNS is an international refereed journal dedicated to the latest advancement of communications and network technologies. The goal of this journal is to keep a record of the state-of-the-art research and promote the research work in these fast moving areas.

Editors-in-Chief

Prof. Huaibei Zhou	Wuhan University, China
Prof. Tom Hou	Virginia Tech, USA

Subject Coverage

This journal invites original research and review papers that address the following issues in wireless communications and networks. Topics of interest include, but are not limited to:

MIMO and OFDM technologies	Sensor networks
UWB technologies	Ad Hoc and mesh networks
Wave propagation and antenna design	Network protocol, QoS and congestion control
Signal processing and channel modeling	Efficient MAC and resource management protocols
Coding, detection and modulation	Simulation and optimization tools
3G and 4G technologies	Network security

We are also interested in:

- Short reports—Discussion corner of the journal:
  2-5 page papers where an author can either present an idea with theoretical background but has not yet completed the research needed for a complete paper or preliminary data.
- Book reviews—Comments and critiques.

Notes for Intending Authors

Submitted papers should not have been previously published nor be currently under consideration for publication elsewhere. Paper submission will be handled electronically through the website. All papers are refereed through a peer review process. For more details about the submissions, please access the website.

Website and E-Mail

http://www.scirp.org/journal/ijcns ijcns@scirp.org

Int. J. Communications, Network and System Sciences, **2010, 3, 495-577**
Published Online June 2010 in SciRes (http://www.SciRP.org/journal/ijcns/).

TABLE OF CONTENTS

Volume 3 Number 6 **June 2010**

Performances of Chaos Coded Modulation Schemes Based on Mod-MAP Mapping and High Dimensional LDPC Based Mod-MAP Mapping with Belief Propagation Decoding
N. Khodor, J. P. Cances, V. Meghdadi, R. Quere..... 495

Efficiency Improvement of Space Time Block Codes
Z. A. Baloch, M. U. Baloch, N. Hussain..... 507

An Empirical Examination of Routing Protocols in Mobile Ad Hoc Networks
K. Sahadevaiah, O. B. V. Ramanaiah..... 511

Nonlinear Blind Equalizers: NCMA and NMCMA
D. Wang, S. Chandana..... 523

A Multi-objective QoS Optimization with Fuzzy Based Parameter Setting for Real-Time Multicasting
S. C. Rai, B. B. Misra, A. K. Nayak, R. Mall, Sateesh Kumar Pradhan..... 530

Uplink Performance Evaluation of CDMA Communication System with RAKE Receiver and Multiple Access Interference Cancellation
A. J. Bamisaye, M. O. Kolawole..... 540

Magnetization Performance of LDPC Reduced-Complexity Decoding Algorithms
M. Abdelhedi, O. Hamdi, A. Bouallegue..... 548

Performance of Multirate Multicast in Distributed Network
S. Kanrar, M. Siraj..... 554

Design and Simulation of Intelligent Optical WDM Switching Node Based on Erlang Traffic Model
M. K. Dutta, V. K. Chaubey..... 563

Flocking Control of a Group of Agents Using a Fuzzy-Logic-Based Attractive/Repulsive Function
H. Yu, J. G. Jian, Y. J. Shen..... 569

Copyright©2010 SciRes.